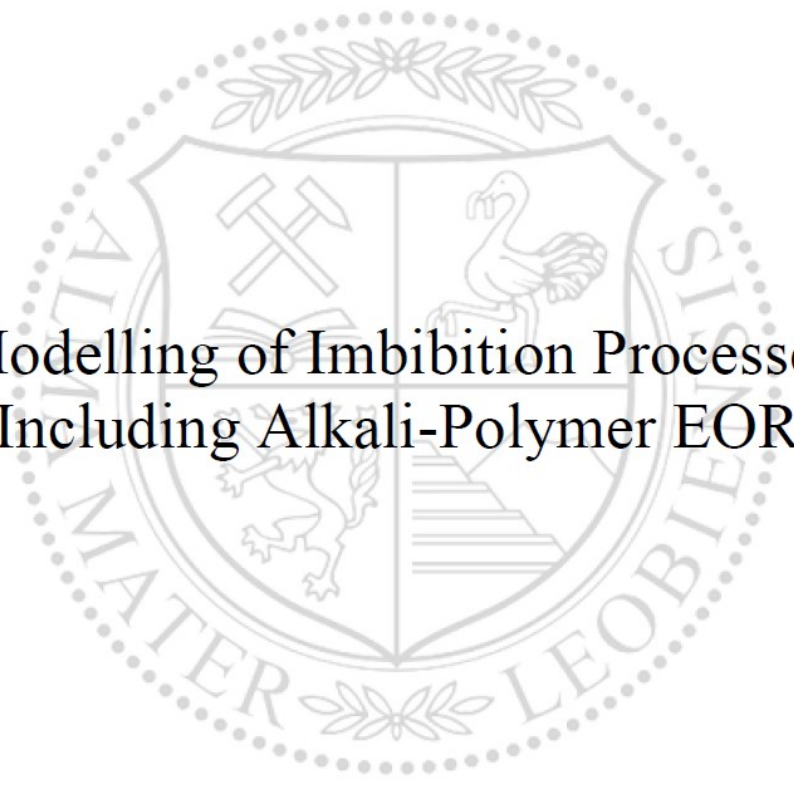




Chair of Reservoir Engineering

Master's Thesis



Modelling of Imbibition Processes
Including Alkali-Polymer EOR

Leisan Mukhametshina

November 2020



MONTANUNIVERSITÄT LEOBEN

www.unileoben.ac.at

EIDESSTATTLICHE ERKLÄRUNG

I declare on oath that I wrote this thesis independently, did not use other than the specified sources and aids, and did not otherwise use any unauthorized aids.

I declare that I have read, understood, and complied with the guidelines of the senate of the Montanuniversität Leoben for "Good Scientific Practice".

Furthermore, I declare that the electronic and printed version of the submitted thesis are identical, both, formally and with regard to content.

Datum 25.11.2020

Signature Author
Leisan Mukhametshina

Acknowledgements

Firstly, I would like to thank my supervisor, Prof. Holger Ott, for giving me the opportunity to work on this thesis.

I would like to thank OMV Exploration & Production GmbH for providing me with this great chance to pursue my master studies in MUL, and for sponsoring me in the past two years. I sincerely thank Dr. Torsten Clemens for being my supervisor in this thesis, and for his insights that helped me develop the work of this thesis. Special thanks go to my co-supervisor, Gisela Vanegas Cabas, for her immense support to me during my work on this thesis, her encouragement, insightful discussions, and feedback. I also would like to thank Bettina Schumi for her valuable comments.

Last but not least, I would like to thank my loving mother, Svetlana Mukhametshina, without whom I would not have been able to finish this work. I am grateful for her moral encouragement, her faith in me, and comforting that helped me to go through the rough days.

Abstract

The thesis provides a simulation model for a spontaneous imbibition process on a sandstone plug sample with different chemical solutions, including alkali/polymer EOR. The input data, e.g. porosity, absolute permeability, fluid saturations, density and viscosity of fluids, are taken from laboratory experiments performed by OMV Upstream.

The model was built using tNavigator [version 19.4], which is an integrated static and dynamic modelling tool. A spontaneous imbibition experiment with an Amott cell was used as a base for the structure and the shape of the model. Two main regions were defined in the model: the rock saturated by oil and water, and the Amott cell itself containing the displacing fluid (water or the chemical solution). Spontaneous imbibition laboratory experiments were conducted upfront with prepared test water, alkali, polymer and alkali-polymer solutions. The results of those experiments were used to history match the simulation model.

The oil production is mostly affected by the capillary pressure and relative permeability curves for the water-oil case, and also the capillary desaturation curve (CDC) for the chemical cases. These three major parameters were unknown before the creation of the simulation model. Therefore, they were used as variables in the history match of the model.

In the first part of the work, a simulation of the base experiment with test-water was done. The impact of both capillary and gravitational forces was investigated. The relationship of these forces was controlled by the vertical to horizontal permeability ratio (kv/kh). In the second part of the thesis, the models for alkali and alkali-polymer experiments were simulated. The reduction of interfacial tension (IFT) caused by alkali decreases the capillary pressure. IFT was used as one of parameters for the history matching.

In the previously performed laboratory experiment, wettability alteration was studied using aged and non-aged core plugs. However, within this thesis, only the modelling of the water-wet sample was performed. Hence, the influence of alkali on wettability change is out of the scope of the thesis.

The provided simulation model helps understand the physical processes that are taking place during spontaneous imbibition and gives a visualization of the saturation profile in the core. However, the models did not completely match the oil production in the laboratory

experiments. The results of this work can be used to reduce the uncertainty in the IFT, and capillary desaturation curves used to forecast the incremental recovery from chemical EOR.

Zusammenfassung

Diese Arbeit liefert ein Simulationsmodell einer spontanen Imbibition auf einem Sandsteinbohrkern mit verschiedenen chemischen Lösungen, einschließlich Alkali- und Polymer-EOR. Die Eingabeparameter wie die Porosität, die absolute Permeabilität, die Flüssigkeitssättigung, die Dichte und die Viskosität von den Flüssigkeiten wurden aus Labortests von OMV Upstream entnommen.

Das Modell wurde mit tNavigator erstellt, einer integrierten statischen und dynamischen Modellierungssoftware. Das spontane Imbibitionsexperiment mittels des Amott-Tests wurde als Grundlage für die Struktur und die Form des Modells verwendet. Im Modell wurden zwei Regionen definiert: das mit Öl und Wasser gesättigte Gestein, und die Zelle, die die Verdrängungsflüssigkeit enthält (Wasser oder eine chemische Lösung). Spontane Imbibitionsexperimente wurden in einer Arbeit zuvor mit vorbereiteten Testwasser-, Alkali-, Polymer- und Alkalipolymerlösungen durchgeführt. Die Ergebnisse dieser Experimente wurden im Historymatch des Simulationsmodells verwendet.

Die empfindlichsten Parameter sind der Kapillardruck und die relativen Permeabilitäten für den Wasser-Öl-Fall sowie die Kapillarentsättigungskurve (CDC) für die chemischen Fälle. Diese drei Hauptparameter waren vor der Erstellung des Simulationsmodells unbekannt. Daher wurden sie als Variablen im Historymatch des Modells verwendet.

Im ersten Teil der Arbeit wurde eine Simulation des Experiments mit Testwasser durchgeführt. Der Einfluss der Kapillar- und Gravitationskräfte wurde untersucht, und die Beziehung zwischen diesen Kräften wurde durch das Verhältnis der vertikalen zur horizontalen Permeabilität (k_v / k_h) gesteuert. Im zweiten Teil der Arbeit wurden die Modelle für die Alkali- und Alkalipolymer-Experimente simuliert. Die Verringerung der Grenzflächenspannung (IFT) durch Alkali verringert den Kapillardruck. Die Grenzflächenspannung wurde als einer der Parameter für den Historymatch verwendet.

Im Laborexperiment wurde die Veränderung der Benetzbarkeit unter Verwendung von gealterten und nicht gealterten (aged and non-aged) Bohrkernen untersucht. Im Rahmen dieser Arbeit wurde jedoch nur die Modellierung der wasserbenetzenden Probe durchgeführt. Der Einfluss von Alkali auf die Veränderung der Benetzbarkeit liegt außerhalb des Rahmens der Arbeit.

Das Simulationsmodell hilft beim Verständnis der physikalischen Prozesse, die während der spontanen Imbibition stattfinden, und bietet eine Visualisierung des Sättigungsprofils im Bohrkern. Die Modelle haben jedoch nicht vollständig mit der Ölproduktion in den Laborexperimenten übereingestimmt. Der Hauptbeitrag dieser Arbeit ist die Verringerung der Unsicherheit in der Grenzflächenspannung (IFT)- und Kapillarentsättigungskurven, die zur besseren Prognose der inkrementellen Entölung durch die chemischen EOR verwendet werden können.

Table of Contents

Acknowledgements	iii
Abstract.....	v
Zusammenfassung	vii
Table of Contents	ix
List of Figures	xi
List of Tables	xv
Abbreviations	xvii
Chapter 1	19
Chapter 2.....	23
2.1 Alkaline EOR.....	23
2.1.1 Alkali Reaction with Oil	24
2.1.1 Alkaline Interaction with Water	25
2.1.2 Alkali Interaction with Rock	25
2.1.3 Recovery Mechanisms	26
2.2 Polymer EOR	27
2.2.1 Types of Polymers	27
2.2.2 Polymer Retention	28
2.2.3 Inaccessible Pore Volume	29
2.2.4 Permeability Reduction.....	29
2.2.5 Polymer Degradation	30
2.3 Alkali-Polymer EOR	30
2.4 Spontaneous Imbibition	31
2.4.1 Driving Forces	33
2.4.2 Flow Regimes of Spontaneous Imbibition	33
Chapter 3	37
3.1 The Amott Cell for the Laboratory Experiment	37
3.2 Geological Model.....	38
3.3 Simulation Model Initialization.....	42
3.3.1 Grid Coarsening.....	42
3.3.2 Fluid Characterization.....	43
3.3.3 Pressure Distribution.....	44
3.3.4 Rock Characterization.....	45
3.3.5 Insertion of Chemical Solutions in Simulation Model.....	45
Chapter 4	48
4.1 Description of the History Matching	49
4.1.1 Capillary Pressure Curve.....	52
4.1.2 Relative Permeability Curves	53

4.1.3	Vertical to Horizontal Permeability Ratio	56
4.1.4	Interfacial Tension Between Oil and Water.....	57
4.1.5	Capillary Number.....	58
4.1.6	Polymer Adsorption.....	59
4.1.7	Polymer Retention and Inaccessible Pore Volume.....	60
4.2	History Match Results	60
4.2.1	Simulation Model for the Test Water Experiment	60
4.2.2	Simulation Model for the Alkali Experiment.....	79
4.2.3	Simulation Model for the Alkali-Polymer Experiment	89
Chapter 5	93
5.1	Summary	93
5.1.1	Test-Water Model Results	93
5.1.2	Alkali Model Results	94
5.1.3	Alkali-Polymer Model Results.....	95
5.2	Evaluation.....	95
5.3	Future Work.....	96
Chapter 6	97
Appendix A	A-1
Appendix B	3
Appendix C	7

List of Figures

Figure 1 – Aging of Cores under Reservoir Temperature in the Oven (Arekhov, 2019).....	21
Figure 2 – Cumulative Oil Production for the Test-Water, Alkali and Alkali-Polymer Spontaneous Imbibition Experiment.....	22
Figure 3 – Schematic of Anionic Surfactant Creation During Alkaline Flooding (deZabala, et al., 1982).....	24
Figure 4 – Schematic Representation of the Polymer Retention Mechanisms (Sorbie, 2013).28	
Figure 5 – Illustration of Forced and Spontaneous Imbibition and Drainage Capillary Pressure Curve (Morrow & Mason, 2001).....	32
Figure 6 – Schematic of Counter-Current and Co-Current Flow Regimes in Vertically Situated Cylindrical Core (Babadagli, 2005).....	34
Figure 7 – Spontaneous Imbibition in a Long (a) and a Short (b) Core with All Faces Open. 35	
Figure 8 – Scheme of the Amott Cell (Arekhov, 2019).....	37
Figure 9 – Proportions of the Amott Cell.....	38
Figure 10 – Polygon for the Plug Region inside of the Amott Cell (white contour). Model Cross-Section (view from the top).....	39
Figure 11 – Fluid in Place Regions in the Model. Region of the Displacing is Blue, and the Plug Region is Brown. The Cross-Section is in Z-Direction.....	40
Figure 12 – Saturation Regions in the Model. Region of the Displacing is Blue, and the Plug Region is Brown. The Cross-Section in X-Direction (the Scale is 1:2 in Z).....	41
Figure 13 – Comparison of the Dynamic Model Grid (Left) and the Static Model Grid (Right). A Side View. Aspect Ratio is 2:5.	42
Figure 14 – Example of Cumulative Oil Production for the Laboratory Experiment and Simulation Model	48
Figure 15 – An Example of "Coreywo" Keyword, used in the Simulation Model for the Relative Permeability and the Capillary Pressure Curves.A Description for Each Saturation Region..	55
Figure 16 – Schematic of the Relative Permeabilities for a Water-Oil System (tNavigator 19.4, 2020).....	55
Figure 17 – IFT Measurements for the Test-Water, Polymer, Alkali and Alkali-polymer Experiments (Arekhov, 2019).	57
Figure 18 – An Example of the Capillary Desaturation Curve for the Keyword "Surfcap" in tNavigator.....	59
Figure 19 – Cumulative Oil Production for the Sensitivity Study of the Influence of kv/kh and Pc on the Test-Water Simulation Model.	61

Figure 20 – Pearson Correlation Coefficients Between the Variables (Capillary Pressure @ Irreducible Water Saturation and k_v/k_h) and the Cumulative Oil Production as the Functions of Time.....	63
Figure 21 – The Range of the Cumulative Production of Oil for the Test Water Experiment. Blue lines Indicate Created during History Match Models, and Red Dots Represent Laboratory Data.	64
Figure 22 – Distribution of Cumulative Oil Production after 25 hours for History Matching Simulation Models for the Test-Water Experiment.	65
Figure 23 – Cumulative Oil Production as a Function of Time for the Laboratory Experiment and Three Simulation Cases (P90, P50, P10). The Red Dotted Line represents Laboratory Data.	65
Figure 24 – Cumulative Distribution Function for the Oil Recovery According to the 45 Chosen Cases from the History Match on the Left Axis and Cumulative Frequency for the Bar Charts on the Right Axis.....	66
Figure 25 – Relative Permeabilities and Capillary Pressure Curve for P50 Simulation Case.	67
Figure 26 – Distributions of the Variables Used in History Match for 45 Chosen Simulation Models, where the Red Lines Correspond to P90, P50 and P90 Cases of the Cumulative Oil Production.....	68
Figure 27 – The Oil Saturation Profile after 25 Hours (Z Cross-Section) for the Test Water Simulation Model. Oil Saturation Scale is from 0.3 to 0.4. X:Y is 1:1.	69
Figure 28 – The Oil Saturation Profile after 25 Hours (X Cross-Section) for the Test Water Simulation Model. Color range is from 0.3 to 0.4. L:Z is 1:3.....	70
Figure 29 – Schematic of the Water Profile during Spontaneous Imbibition (Hamad, 2019).	71
Figure 30 – 3D Oil Saturation Profile after 25 Hours for the History-Matched Test-Water Simulation Model. X:Y:Z is 1:1:3.....	72
Figure 31 – Capillary Pressure Distribution for the Central X Cross-Section for the History-Matched Test-Water Simulation Model after 15 minutes. Picture Scale 2:3.....	73
Figure 32 – Cross-Plots for the Variables Used in the History Match for the Test-Water Model and Cumulative Oil Production at 25 Hours. Red dots represent P90, P50, P10 Simulation Cases.....	74
Figure 33 – Pearson Correlation Coefficient as the Function of Time for the Variables (n_{pw} , P_{cow} , S_{owcr} , k_v/k_h) Used in the History Match for the Test-Water Simulation Model.....	75
Figure 34 – Pearson Correlation Coefficient as the Function of Time for the Variables (k_{rowr} , k_{rwr} , n_{ow} , n_w) Used in the History Match for the Test-Water Simulation Model.	75
Figure 35 – The Cross-Section in X-Direction for the Test-Water Model: a Coarsened Regular GRID (Left) and a Tartan GRID (Right). Scale 2:5.	76
Figure 36 – The Cross-Section in Z-Direction for the Tartan GRID of the Test-Water Model. Scale 1:1.	77

Figure 37 – Oil Saturation Profile after 25 Hours (X Cross-Section) for the Tartan GRID of the Test Water Simulation Model. Oil Saturation Scale is 0.35-0.42. Scale 2:3.....	78
Figure 38 – The Cumulative Oil Production for the History Match Probability Cases for the Regular (in red) and the Tartan GRID (in blue) of the Test-Water Model.....	79
Figure 39 – The Cumulative Oil Production for the History Matched Test-Water Model and the Alkali Model with the same Values for Variables and Initial Values for the Surfactant Keywords.	80
Figure 40 – The Cumulative Oil Production for the History Match of the Alkali Simulation Model. kv/kh is Fixed and Equal to 0.63. Blue lines Indicate Created during History Match Models, and Red Dots Correspond to the Laboratory Data.....	81
Figure 41 – The Cumulative Oil Production for the Best Achieved Simulation Cases of the History Match for the Alkali Simulation Model. Red Dots Correspond to the Laboratory Data.	82
Figure 42 – The Capillary Desaturation Curve as a Function of Miscibility Factor (Top) and Residual Oil Saturation (Bottom). The Orange Line is for the Case 1, and the Blue Line is for the Case 2 of the History Match.	84
Figure 43 – Oil Saturation Profile for the Central X Cross-Section for the History-Matched Alkali Simulation Model after 1 Hour. Oil Saturation Scale is 0.0-0.5. Picture Scale 2:3.....	85
Figure 44 – A Simplified Example of The Water Saturation Profile for the Case of an Oil Bank Creation. No Smearing Effects Influenced by Capillary Pressure Diffusion are Included.	86
Figure 45 – The Oil Saturation Profile after 25 Hours (X Cross-Section) for the Alkali Simulation Model. Oil Saturation Scale is from 0.13 to 0.4. L:Z is 1:3.....	88
Figure 46 – The Oil Saturation Profile after 25 Hours (Z Cross-Section) for the Alkali Simulation Model. Oil Saturation Scale is from 0.3 to 0.4. X:Y is 1:1.....	88
Figure 47 – 3D Oil Saturation Profile after 25 Hours for the Alkali Simulation Model. X:Y:Z is 1:1:3.....	89
Figure 48 - Sensitivity Study for the Alkali-Polymer Model Based on the Variables IFT, DPV, RRF, and Polymer Adsorption.	91
Figure 49 – Pearson Correlation Coefficient as the Function of Time for the Variables (IFT, RRF, Polymer Adsorption, DPV) Used in the Sensitivity Study for the Alkali Simulation Model.....	92

List of Tables

Table 1 – Parameters Investigated in Spontaneous Imbibition Laboratory Experiments	21
Table 2 – Average Proportions of the Core Plug.....	39
Table 3 – Proportions of the Total Model and the Core Part of the Model	40
Table 4 – Volume Preservation Parameters: Porosity and Initial Water Saturation for the Cores used in the Selected Laboratory Experiments and for the Corresponding Simulation Models	42
Table 5 – Properties of the Oil and the Test Water.....	43
Table 6 – Properties of the Chemicals Used as the Displacing Fluid.	44
Table 7 – Summarized Description of the Regions in the Simulation Models.....	47
Table 8 – Description of Variables Used in History Matching	51
Table 9 – Parameters of Relative Permeabilities and Capillary Pressure Curves used for the History Matching.....	56
Table 10 – A Sensitivity Study of the Capillary Pressure and k_v/k_h Influence on the Oil Production Based on the Test-Water Simulation Model.....	61
Table 11 – The Variables for the Probability Cases of the Test-Water Simulation Model.....	67
Table 12 – A Comparison Between the Regular Grid and the Big Grid Test-Water Model...	77
Table 13 – Additional Variables for Alkali Simulation Model. Initial Values.....	80
Table 14 - Values of the Variables for the History Match Simulation Cases of the Alkali Model.....	83
Table 15 – Sensitivity Study for the Alkali-Polymer Model Based on the Change of the Individual Variable for each Simulation Case (IFT, DPV, RRF, and Polymer Adsorption). .	90

Abbreviations

AFO	All-faces-open Boundary Conditions
AHM	Assisted History Match
AP	Alkali-Polymer
ASP	Alkaline-Surfactant-Polymer
CDC	Capillary Desaturation Curve
DPV	Dead-Pore Volume
EOR	Enhanced Oil Recovery
FIP	Fluid in Place
HPAM	Hydrolyzed Polyacrylamide
IFT	Interfacial Tension
LHA	Latin Hypercube Algorithm
OEO	One-end-open Boundary Conditions
PV	Pore Volume
RRF	Residual Resistance Factor
SI	Spontaneous Imbibition
TAN	Total Acid Number
TEC	Two-ends-closed Boundary Conditions

Chapter 1

Introduction

Imbibition is a dynamic process in which the saturation of the wetting phase in the rock increases. In the case of a water-wet reservoir, imbibition refers to a displacement of the oil by water from the reservoir (Dake, 1978). As oil and gas are immiscible fluids, the attraction of the molecules on the interface is unevenly distributed, which increases the free surface energy, or interfacial tension. The shape of the interface is curved, and the pressure from different sides of the interface differs: the fluid pressure on the concave side of the interface is higher than the pressure of the fluid on the convex side (Dake, 1978). This pressure difference of the fluids on the fluid-fluid interface is called capillary pressure.

Imbibition process can happen spontaneously driven by capillary pressure. In this case, the suction of the fluid into the rock is called spontaneous imbibition, or capillary imbibition. Capillary imbibition is an important mechanism for the production of oil from the fractured reservoirs (Schechter, et al., 1991). Injected water tends to flow in the fractures of the reservoir since they are the areas of least resistance. However, most of the oil in the fractured reservoir is originated in matrix blocks that are surrounded by fractures (Rangel-German & Kovsky, 2002). Hence, it is essential to understand the processes which are governing the flow between fractures and the matrix. One of the mechanisms of the interaction is spontaneous imbibition (SI), especially for the water-wet matrix.

As was mentioned earlier, the main driving force of spontaneous imbibition is capillary pressure. Additionally, due to the density difference of the fluids, gravity segregation contributes to oil production. The dominance of one of these forces is dictated by many factors as matrix blocks size, wettability, IFT between oil and water, and the value of oil-water capillary pressure (Babadagli, 2005). Hence, the mechanism of spontaneous imbibition differs with the type of fluid injected: brine, surfactant, alkali, polymer solution, etc.

A simple type of laboratory experiment to investigate the imbibition process is performed on the Amott cell, where the core saturated with oil is surrounded by imbibing fluid in all directions. The flow inside of the rock in this experiment is very complex. In the present work, the displacement front propagation in the core in the Amott cell experiment is visualized, and forces contributing to spontaneous imbibition are analyzed. Furthermore, a comparison of the experiments for different types of chemicals is implemented.

The data used for the simulation model is taken from the laboratory experiments conducted as part of the master's thesis (Arekhov, 2019) in the laboratory of OMV Upstream in Gänserndorf. Prior to the experiment, core preparation (cleaning, saturation with fluids, ageing), routine core analysis, fluid characterization, and evaluation of IFT between oil and imbibing fluids were performed. The main scope of the laboratory experiments was the evaluation of wettability alteration by alkali-polymer solution and its effect on the results of the spontaneous imbibition process.

The experiments were performed for two types of rock with different mineralogy: high permeable Nordhorn outcrop with low clay content and Keuper outcrop with high clay content. Two types of oil with high and low total acid number (TAN) were used to evaluate the effect of TAN on wettability alteration during alkali imbibition. The overview of the effect of clay and TAN on oil production by alkali will be given in 2.1.

In order to evaluate oil recovery depending on the type of imbibing fluid, five sets of spontaneous imbibition experiments were performed for both types of oil and rock. The imbibing solutions were brine, test-water, alkali, polymer and alkali-polymer. The test water is so-called simplified brine without the divalent ions.

Additionally, the experiments are conducted for the different primary wettability of the rock. Firstly, the water-wet state was achieved by saturating the cores with water before the injection of oil into the rock. Secondly, the restoration of the oil-wet state of the cores is performed by ageing under the reservoir temperature in the oven (Figure 1). Summarized table of the parameters investigated in the laboratory experiments is shown in Table 1.



Figure 1 – Aging of Cores under Reservoir Temperature in the Oven (Arekhov, 2019)

Table 1 – Parameters Investigated in Spontaneous Imbibition Laboratory Experiments

Type of Oil	high TAN 1.61 mg KOH/g oil		low TAN 0.17 mg KOH/g oil		
Mineralogy	Nordhorn Outcrop			Keuper Outcrop	
Imbibing Solution	Brine	Test-Water	Alkali	Polymer	Alkali-Polymer
Initial Rock Wettability	Non-aged			Aged	

None of the chemical interactions between fluids and fluid/rock is simulated in this work. Hence, only oil with high TAN, the rock with low clay content and test water were used for the simulation model. Three models were created: 1) for the test-water SI experiment, 2) for the alkali, and 3) for the alkali-polymer. The results from the experiments are shown in Figure 2. The shape of the curves differs depending on the type of fluid used. Test-water experiments show high oil displacement at the early stage, while alkali and alkali-polymer solutions are more efficient in the long term. Alkali reduces IFT between fluids, which results in decrease of the capillary pressure. As the capillary pressure decreases, the rate of spontaneous imbibition declines. However, the overall production of oil in alkali imbibition is higher due to reduction of the oil entrapment.

The thesis describes the construction of simulation models for these experiments and the results of history matching. In the simulation model of the alkali and alkali-polymer experiment, wettability alteration was not studied. Only the effect of the chemicals on the reduction of the interfacial tension (IFT) between oil and water was considered.

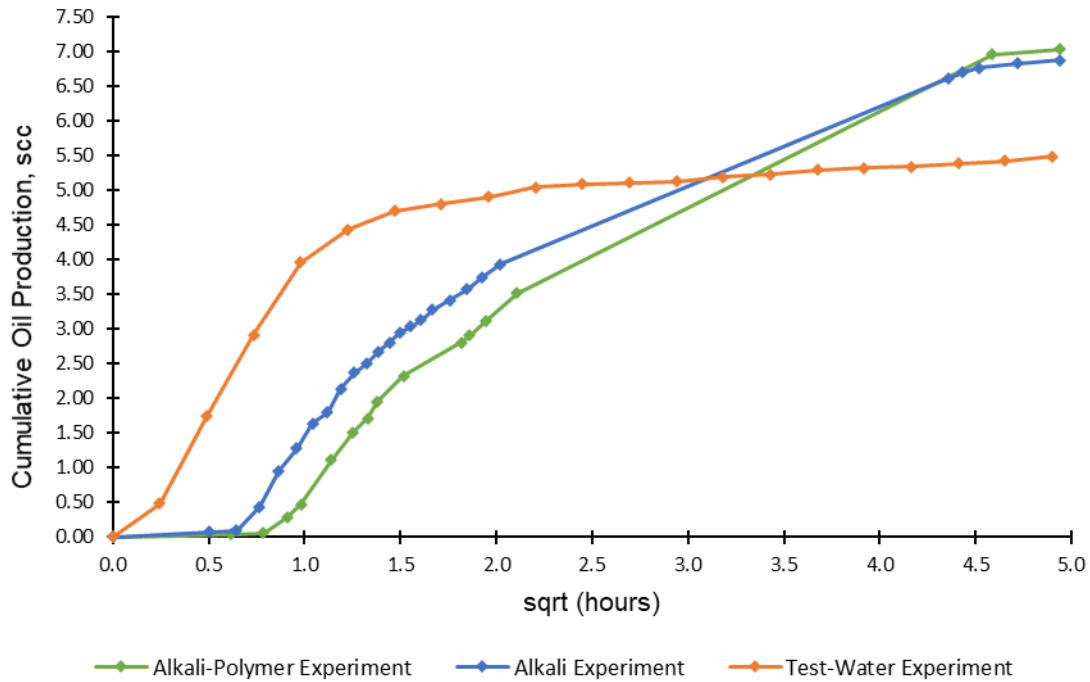


Figure 2 – Cumulative Oil Production for the Test-Water, Alkali and Alkali-Polymer Spontaneous Imbibition Experiment.

In the first chapter of the thesis, the literature review for the relevant topics is provided. The first subsection will give a short description of alkali EOR with displacement mechanisms and important parameters of rock and fluids that can affect alkali flooding performance. The second subsection covers polymer flooding and parameters that are essential for this type of the EOR process. And in the last subsection, an overview of spontaneous imbibition is presented.

The third chapter of the work covers the set-up of the geological models and simulation model initialization. It also includes a description of fluid characteristics and rock properties. Finally, the last chapter describes parameters for the history matching of the models with the experimental data as well as the results of the simulations.

Chapter 2

Literature Review

2.1 Alkaline EOR

The alkaline flooding or caustic flooding is the enhanced oil recovery method, performed by the injection of an alkali solution into a reservoir. The alkali creates a high pH environment and reacts with organic acids in the oil, forming in-situ anionic surfactant.

The most popular chemicals used are sodium carbonate and sodium hydroxide. Alternatively, potassium-based alkalis can be used; however, their price is higher than for the sodium-based alkalis (Sheng, 2011). The comparison of three alkalis (sodium hydroxide, sodium silicate and sodium carbonate) is performed by Fakher, et al. (2019). The paper shows that the lowest change of pH during injection is achieved by the sodium carbonate. It is explained by the dissociation of the chemical into sodium cation and carbonate anion. Each of the ions reacts with water, forming alkali (sodium hydroxide) and weak carbonic acid. The formation of sodium hydroxide is an exothermic reaction, which means a generation of heat that slightly increases the reservoir temperature. This heat release can have a positive effect on the heavy oils, as the temperature increase provides a small viscosity reduction.

Despite the lower pH, sodium carbonate is preferable for the alkali EOR, as an inexpensive alkali. Due to the presence of the carbonate ions, a dissolution of calcite and magnesite from the rock surface is resisted. Mineral dissolution increases with an increase of pH. As a weaker alkali, sodium carbonate reduces mineral dissolution and ion exchange (Sheng, 2011). A reduction of scaling in production facilities is another reason for the choice of alkali.

Alkali interaction with reservoir and fluids is highly complex. Different mechanisms and processes occur during alkaline flooding. The chemical solutions are characterized by reactivity and ion-exchange ability. Hence, consumption of the alkali should be considered for the design

of the alkaline EOR. The total alkali consumption is expressed by the following equation (Sheng, 2011):

$$C_i - C(t) = \Delta C_o + \Delta C_w + \Delta C_e + \Delta C_D, \quad (1)$$

where C_i and $C(t)$ are the initial and current concentrations; ΔC_o is the alkali consumption by the interaction of alkali with oil; ΔC_w is the alkali consumption by the interaction with water, ΔC_e defines ion-exchange of the alkali solution and the rock; ΔC_D is the consumption during the dissolution of the minerals.

2.1.1 Alkali Reaction with Oil

An injected alkali reacts with naphthenic acids of the reservoir oil. However, not all organic acids in the oil are reactive. Some of them become ionized by the presence of alkali; some stay neutral (Sheng, 2011). Ionized petroleum acids are hydrolyzed and create soluble anionic surfactant, generally are denoted as RCOO^- . A schematic representation of the surfactant creation in the reservoir is shown in Figure 3.

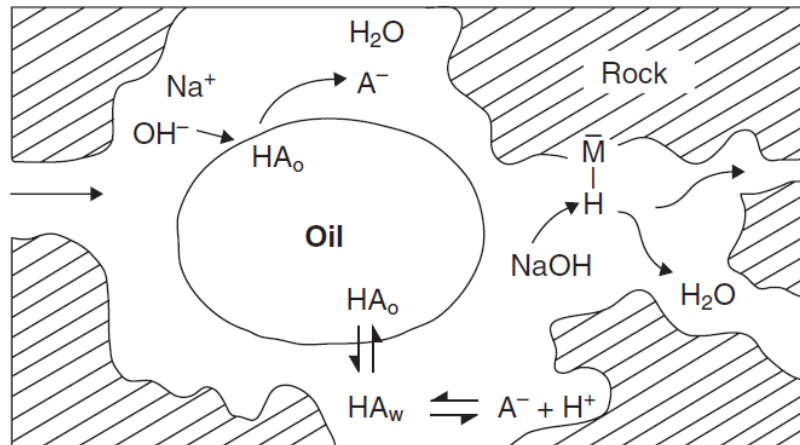


Figure 3 – Schematic of Anionic Surfactant Creation During Alkaline Flooding (deZabala, et al., 1982)

The potential of crude oil to react with alkali and create surfactant is highly dependent on the total acid number (TAN). The total acid number describes the reactive ability of oil with alkali solutions. It is calculated as a mass of potassium hydroxide, that is needed to neutralize one gram of oil with an unknown concentration of organic acids in it. Usually, the measurement of TAN is performed by non-aqueous titration (Fan & Buckley, 2007).

$$\text{TAN} = \frac{\text{mg (KOH)}}{\text{g (oil)}} \quad (2)$$

Created surfactant, which is adsorbed on the oil/water surface leads to a decrease of the IFT. The lower the interfacial tension is, the easier the emulsification process of the two phases occurs (Sheng, 2011). However, not all naphthenic acids create surfactant. It depends on the size of the acid – short ones may not behave like a surfactant. Additionally, asphaltenes and

resins, which also may have carboxylate functional group, are not dissolved in water. They have high adsorption activity on the oil/water interface, and create a thick film, increasing the stability of the emulsion (Sheng, 2011).

2.1.1 Alkaline Interaction with Water

Depending on pH value and a reservoir temperature, an ion exchange between the injected alkali and divalent ions, as magnesium and carbonate, in the brine happens. This results in calcium/magnesium hydroxide, carbonate or silicate precipitation. The process has both positive and negative effects on oil recovery. On one hand, precipitation of salts can occur in high permeable pores. In this case, an increase in sweep efficiency is expected, as the salts block high permeable areas and push the flooding process into uninvaded zones (Mayer, et al., 1983). On the other hand, alkali loss is expected, which decreases the effectiveness of the EOR method.

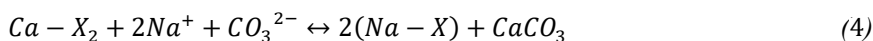
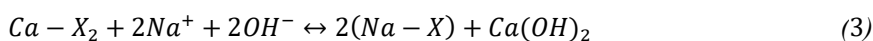
The reduction of the brine hardness also leads to more activity of the created surfactant; hence lower IFT values are achieved (Mayer, et al., 1983).

2.1.2 Alkali Interaction with Rock

There are many reactions occur between alkali and the rock surface. Initially, minerals are in the equilibrium with brine. When the alkali is injected, the pH of the environment is changed, and the ion exchange takes place. The reaction rate depends on the reservoir temperature, alkali concentration, type of alkali and rock surface area (Mayer, et al., 1983).

First of all, one of the most important parameters that need to be considered during alkaline flooding is the clay content of the reservoir rock. Clay includes hydrogen ions, that react with hydroxide ions, lowering the pH of the chemical solution (Sheng, 2011).

Secondly, calcium and magnesium ions, present in both carbonate rocks and clay, are released from the surface of the rock and interchange sodium cation from the alkali. This leads again to the lowering of pH of the solution. Additionally, salt precipitation and new mineral creation occur, according to the following equations (Sheng, 2011):



Precipitation may positively affect a recovery efficiency, as was described previously. Also, the ion exchange of sodium and divalent ions causes clay swelling, which reduces permeability and blocks pore channels (Mayer, et al., 1983).

Dissolution of the sandstone occurs during the alkali flooding too. However, the reaction rates are much slower than for the clay minerals, based on the overview of different studies, made

by Mayer, et al. (1983). According to Bunge & Radke (1982), silica dissolves in the presence of hydroxide ions as the following equation:



In comparison to sodium carbonate and sodium silicate, sodium carbonate shows lower sand and dolomite dissolution and ion exchange (Thomas, et al., 2016).

Among the minerals, the most important dissolution and ion exchange occur with clay minerals, as kaolinite and illite, and the lowest impact of alkali is on quartz (Shen & Chen, 1996). Similar results were obtained from the experiments performed by Mohnot and Bae (1989). The highest rate for the high concentration of alkali and high temperatures was observed for kaolinite. However, under moderate conditions, the dominated loss of alkali is for the montmorillonite (Mohnot, et al., 1987). Also, high loss during chemical reactions was observed for the illite and dissolution/precipitation of dolomite, low alkali loss by feldspar and quartz and the reaction of alkali with calcite considered to be insignificant.

2.1.3 Recovery Mechanisms

Johnson C.E (1976) summarized the mechanisms of the caustic flooding.

The first mechanism is related to the IFT reduction by the in-situ surfactant. The decrease of the interfacial tension leads to easier emulsification (Subkow, 1942). As an internal pressure in the droplets decreases, smaller forces are needed to break the droplets into smaller pieces (Sulaimon & Adeyemi, 2018). The intensity of the emulsification depends on the pH value, TAN of oil and salinity of brine (Sheng, 2011). Small oil droplets coagulate into bigger drops and are produced from the reservoir with the flow of the alkali/water solution.

The second mechanism is a rock wettability alteration from oil-wet to water-wet. It results in the effective permeability change of the phases. The relative permeabilities are shifted to the right and the water relative permeability decreases. Hence, water becomes less mobile, where oil is still flowing, which results in faster oil production.

The reversal of the wettability can happen another way around (from water-wet to oil-wet) under proper conditions (Cooke, et al., 1974). Discontinuous residual oil transforms into a continuous wetting film. At the same time, lowering of IFT induces an emulsion formation. The droplets of the emulsion block the flow and create high pressure gradient, that overcomes already lowered capillary forces and reduce oil saturation further.

The fourth process is related to a decrease of water mobility by the emulsion entrapment in the small pores (Jennings, et al., 1974). This reduces viscous fingering and improves volumetric sweep efficiency. However, the mechanism does not provide a significant reduction of the

residual oil saturation. In the distance from the injection well, where pressure gradients are not sufficient to overcome even low capillary forces, emulsified oil is entrapped and not produced (Johnson, 1976).

2.2 Polymer EOR

Polymer flooding is an enhanced oil recovery method, performed by addition of polymer to the water injected to the reservoir. It increases the viscosity of the injected fluid, preventing viscous fingering and early water breakthrough. Polymer flooding does not change the residual oil saturation of the reservoir; however, it reduces the remaining oil saturation. Theoretically, both regular waterflooding and polymer injection achieve the same residual oil saturation for a very long timescale. However, in the case of polymer flooding, this timeframe is beyond the development time of a typical oil and gas reservoir. The same amount of oil is produced faster by polymer flooding, than waterflooding, which means that the polymer brings the production profile forward in time (Sorbie, 2013).

The main principle of the polymer flooding is lowering of mobility ratio. The mobility ratio is defined as the ratio of the mobility of water to the mobility of oil.

$$M = \frac{\lambda_w}{\lambda_o} = \frac{k_{rw}/\mu_w}{k_{ro}/\mu_o}, \quad (6)$$

where λ_w is mobility of water, λ_o is mobility of oil, k_{rw} is relative permeability of water, k_{ro} is relative permeability of oil, μ_w is viscosity of water, μ_o is viscosity of oil.

When the mobility ratio is less than one, the displacement is close to a piston-like displacement; hence, there is no water viscous fingering and recovery of oil is more efficient. Increase in mobility ratio decreases volumetric sweep efficiency.

Polymer propagation through the porous media is controlled by irreversible adsorption, hydrodynamic retention, mechanical entrapment and inaccessible pore volume (Zaitoun & Kohler, 1987).

By decreasing the mobility ratio, polymer solution increases the fractional flow of oil. However, the effect is negligible for the low relative permeabilities of oil. Therefore, the effect of the fractional flow is more significant in the early stage of the waterflooding, when the oil saturations are high (Needham & Doe, 1987).

2.2.1 Types of Polymers

Several types of polymers are used for the EOR. Among natural polymers, the most common is xanthan gum. Hydrolyzed polyacrylamide (HPAM) is a widely used synthetic polymer. Polyacrylamides are partially hydrolyzed, which makes the polymer soluble in water. The

degree of hydrolysis is 30-35% of the acrylamide monomers (Lake, 1989). HPAM has carboxyl groups ($-\text{COO}^-$) that brings a negative charge to the molecules.

The ability of the polymer to increase the viscosity of water is related to the high molecular weight. Due to the repulsion forces between molecules, HPAM molecules are elongated and snagged on each other (Lake, 1989). The negative charges create a reticular structure of polymer molecules in the solution, which has good viscoelasticity (Zhang & Qin, 2011). The better the elongation is, the higher is the viscosity. However, the polymer is highly sensitive to the hardness and salinity of the water. High brine salinity causes ionic shielding of polymer molecules. Hence, the repulsion forces decrease, leading to clotting of the molecules and a reduction of the snagging (Lake, 1989). Hence, the hydraulic radius of the polymer molecules decreases, resulting in the drop of the polymer viscosity (Mishra, et al., 2014).

Polysaccharides (xanthan gum) are relatively nonionic, therefore are not sensitive to the shielding effect. However, in comparison to synthetic polymers, they are vulnerable to the bacterial attack. The natural polymers increase the viscosity of water by the snagging effect and the rigid structure of the molecules (Lake, 1989). Also, the polysaccharides are relatively expensive.

2.2.2 Polymer Retention

Retention is one of the processes in the polymer flooding, characterized by the polymer adsorption on the rock surface, mechanical entrapment of the small pore throats and hydrodynamic retention. All three mechanisms are shown in Figure 4. The rate of the retention depends on the type of the polymer, size of the pores, salinity of water, flow rate and temperature (Lake, 1989). The retention causes a decrease in the polymer concentration in the solution.

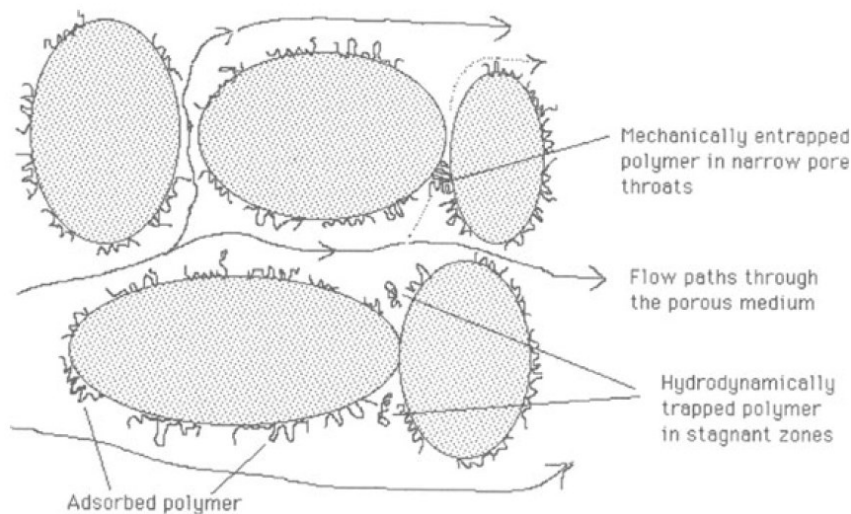


Figure 4 – Schematic Representation of the Polymer Retention Mechanisms (Sorbie, 2013).

The adsorption is related to the interaction of the polymer with the rock surface. Slight anionic nature of the polymer makes it affinitive to the positively charged surface of the rock. The clay content of sandstone plays an important role in the total adsorption of polymer: with an increase of the clay content, the adsorption increases. At low pH, acidic nature of the solution makes the sand surface more positively charged, which increases the affinity of polymer to the rock surface (Mishra, et al., 2014). Some scientists refer to polymer adsorption as a physical mechanism rather than a chemical reaction, stating that polymer/rock interaction happens by the van der Waal's and hydrogen bonding (Sorbie, 2013).

Adsorbed polymer layers increase water wettability and irreducible water saturation. Hence, effective water permeability decreases (Lu, 2005).

Mechanical entrapment occurs due to the large size of the polymer molecules, that cannot flow through the narrow pore channels, and cause trapping (Willhite & Dominguez, 1977).

The mechanisms of hydrodynamic retention are less understood. Some polymer molecules are temporally trapped in a stagnant flow region by the hydrodynamic drag forces (Sorbie, 2013). In these regions, the polymer concentration is higher. The hydrodynamic retention depends on the flow rate.

2.2.3 Inaccessible Pore Volume

Inaccessible pore volume (IPV) is the fraction of the pore space that cannot be entered by the polymer. The size of the polymer makes it difficult to enter small pores. Hence, not all pores can be invaded by the polymer solution, and the oil from these regions stayed unproduced. The second, less common explanation of the IPV is the aggregation of the polymer molecules at the centre of the pores (Lake, 1989). The area close to the pore walls has lower viscosity of the solution leading to the slippage of the water. In some distance from the wellbore, hydrodynamic forces become too weak to push polymer through the pore space, especially in low permeable reservoirs (Zaitoun & Kohler, 1987).

IPV depends on the polymer molecular size and weight, the permeability of the reservoir, porosity, and pore size distribution.

2.2.4 Permeability Reduction

Additional to the viscosity increase, the mobility of water is decreased since adding polymer to water reduces its relative permeability. Permeability reduction is caused by irreversible polymer retention. The presence of the adsorbed polymer layer reduces the cross-flow section of the pore throats (Zaitoun & Kohler, 1987). The change of mobility of water before and after polymer flooding is described by the residual resistance factor:

$$RRF = \frac{\lambda_w}{\lambda_{wa}}, \quad (7)$$

where λ_w is mobility of water before polymer flooding and λ_{wa} is mobility of water after.

RRF indicates the permanence of the permeability reduction effect by the polymer solution (Lake, 1989). Permeability reduction and entrapment of pore throats lead to a diversion of the water flow into zones, that were not flooded. Hence, more oil is displaced.

2.2.5 Polymer Degradation

Polymers are characterized by chemical, mechanical and biological degradation. Chemical degradation happens due to thermal oxidation, free radical substitution, hydrolysis, and biological degradation (Lake, 1989). The reaction rate depends on the pH, salinity of water and temperature and increases with the change of the pH from the neutral values and with a rise of the temperature. Mechanical degradation occurs under high flow rates and also in the subsurface and surface equipment (perforations, screens, pumps, tubing, valves etc.).

2.3 Alkali-Polymer EOR

Simultaneous injection of alkali and polymer improves the performance of both alkaline and polymer EOR.

Addition of the alkali to the polymer influences the viscosity of the solution by an increase of the pH and ionic strength of the solution (Sheng, 2017). As was discussed earlier, HPAM molecules have a slight negative charge. Positive sodium ions create a charge shielding layer on the polymer solution. Thus, there is a decrease of the repulsion forces between HPAM molecules, which changes the stretching degree of the polymer and leads to curl up of the molecule chains. Hence, an increased ionic strength decreases the hydraulic radius of the polymer. As the radius decreases, the viscosity of the polymer solution declines. On the other hand, alkali reacts with polymer, hydrolyzing the amide group – CONH₂ of the polymer into – COO⁻. This process causes an increase in the viscosity of the solution because of an increase in negative electric charges (Zhang & Qin, 2011).

The change of the viscosity of the polymer solution highly dependent on the alkali concentration. With a small amount of alkali added the effect of hydrolysis is dominant, and the viscosity increases. When the alkali concentration exceeds the critical value, the shielding of the polymer molecules occurs and the viscosity decreases (Zhang & Qin, 2011). It is indicated with the experiments, that if the polymer solution is prepared using distilled water, the shielding effect is dominated at the beginning of the injection, which leads to a decrease of the viscosity. Further, hydrolysis by alkali causes the rise of the viscosity of the solution till the

stabilization proceeds gradually. If salty water was used, the processes would occur in the opposite order (Sheng, 2011). However, if the salinity of brine, especially the concentration of the divalent ions, is very high, the effect of alkali on the polymer viscosity is not significant (Sheng, et al., 1994). It is generally considered that the impact of the charge shielding is more pronounced. Therefore polymer solution viscosity decreases with alkali concentration (Kang, 2001). The reaction of alkali and polymer induces an alkali consumption. Hence, the alkali concentration and the pH decline with time (Sheng, 2011).

According to the observations by Sheng, et al. (1993), the IFT between chemical solution and oil decreases with the polymer hydrolysis. The authors assume that it can be related to the small negative charges of polymer molecules, that differentiate hydrophilic and hydrophobic parts of the polymer chain, similar to the nature of surfactants. Also, many polymers contain a small amount of surfactant, which provides additional IFT reduction (Krumrine & Falcone Jr, 1983). The effect on the IFT differs for the various alkali and polymer (Potts & Kuehne, 1998). Generally, a polymer is believed to have a minor influence on IFT but increases the time to reach an equilibrium IFT, because of the slowdown of the rate of the surfactant transfer to the interface caused by high viscosity of the chemical solution (Sheng, 2011).

The high pH environment created by the alkali alters the charge of the rock surface, which results in the reduction of the polymer adsorption. At the same time, as some polymer still adsorbs on the rock surface, it decreases alkali consumption as well (Sheng, 2017). Due to high viscosity, the polymer decelerates diffusion and mass transfer of the alkali, reducing the consumption and the adsorption of the alkali (Krumrine & Falcone Jr, 1983). The decrease of the polymer adsorption means a lesser reduction of the water permeability in comparison to the effect of the polymer alone. As a result, the residual resistance factor is expected to be smaller for the alkali-polymer flooding than for the polymer flooding (Kazempour, et al., 2011).

Also, the polymer can divert the flow from the high permeable areas into unswept pore channels. It allows alkali to enter these zones, react with the oil and make easier displacement of oil by lowering the IFT. While the polymer improves mobility ratio and enhances current oil production, the alkali increases the capillary number, which leads to an increase in the total oil volume that can be extracted. Combining these mechanisms, the alkali-polymer EOR improves both the sweep efficiency and displacement efficiency.

2.4 Spontaneous Imbibition

Spontaneous imbibition is the process in which the wetting phase imbibes into the rock spontaneously, displacing the non-wetting fluid. The driving force in spontaneous imbibition is the capillary force (Sheng, 2019). The process is important during water flooding in fractured

reservoirs, as the oil is displaced from the matrix by spontaneous imbibition of water from the fractures if the system is water-wet (Tavassoli, et al., 2005). The injected brine flows primarily to the fractures, as a high permeable area of the reservoir, and surrounds matrix blocks. When the rock is water-wet, the water is drawn from the fractures to the matrix. The oil droplets are driven out into the main flow in the fracture to preserve the local volume balance (Rangel-German & Kavscek, 2002).

In oil-wet rock, water must be forced to flow into the sample to displace oil. The process is no longer spontaneous. However, during spontaneous imbibition experiments on oil-wet rock, the water still partially displaces the oil, but further increase in the water saturation of the sample is possible only by a change of the capillary pressure sign by the alteration of rock-wettability or by an additional driving force (Morrow & Mason, 2001). The spontaneous and forced parts of the capillary pressure curve are shown in Figure 5.

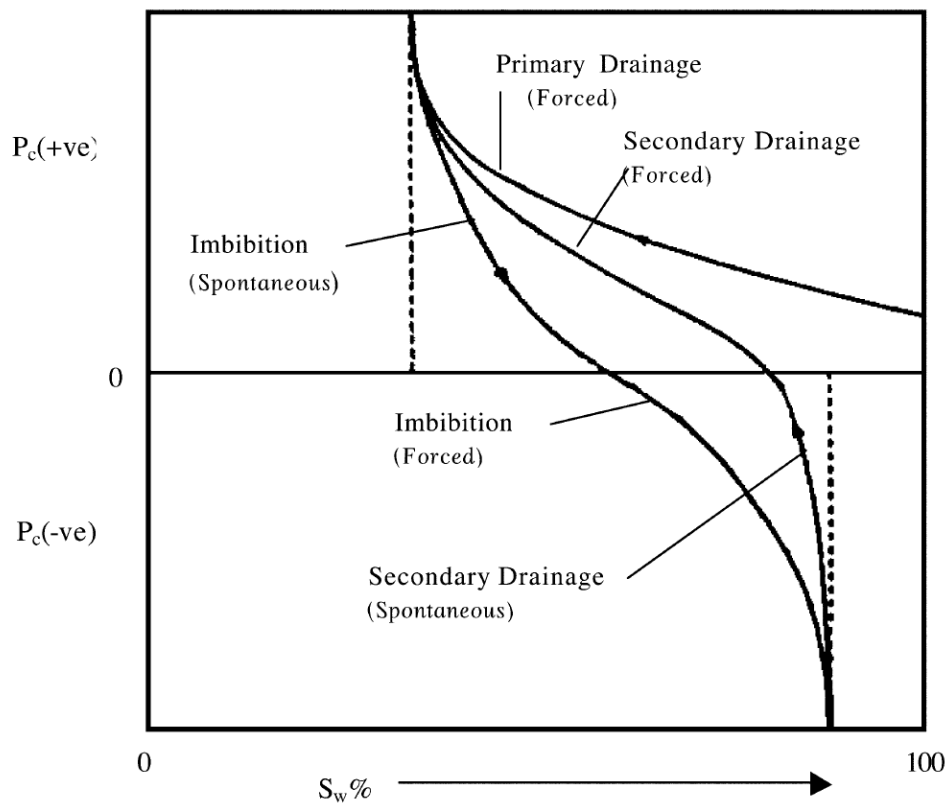


Figure 5 – Illustration of Forced and Spontaneous Imbibition and Drainage Capillary Pressure Curve (Morrow & Mason, 2001).

In the laboratory, the process can be modelled using core plugs with different boundary conditions: one end open (OEO), two ends closed (TEC), all faces open (AFO) (Fischer & Morrow, 2005). The simplest way is AFO boundary conditions, using the Amott cell. The experiment is easy to perform, as there is no need to seal any surface of the core. However, the flow in such an experiment is very complex even for homogeneous rock. Hence, it is very

difficult to simulate the process by analytical models (Meng, et al., 2017). Only AFO type of the boundary conditions on the water-wet cores will be discussed in this work. Hence, the oil and water will be referred to as non-wetting and wetting phases, respectively.

2.4.1 Driving Forces

As was mentioned earlier, the main driving force in spontaneous imbibition is the capillary pressure. It is opposed by viscous drag and the capillary back-pressure at the surfaces of the rock (Mason & Morrow, 2013). In the spontaneous imbibition experiments on the core, the displaced non-wetting phase is produced as droplets that initially adhere to the surface of the core. These droplets create a layer on the rock and oppose further production. The opposing pressure that is generated by the droplets is called capillary back-pressure (Unsal, et al., 2009). The production of oil is restored when the oil droplets on the surface snap off as their shape becomes unstable with respect to the capillary forces (Unsal, et al., 2009).

In an oil reservoir, where the matrix size is large enough, the additional driving mechanism is gravity effect, which may also enhance production. In laboratory experiments, due to the small size of the core plugs, gravity forces do not play a significant role in production performance (Li, et al., 2006). However, this is the case for the low permeable rock samples (Kalaei, et al., 2010).

Simulation models demonstrated the importance of both capillary and gravity forces (Kalaei, et al., 2010). Several experiments showed that at the different stage of the imbibition process, different forces are acting (Sheng, 2019). Imbibition curve (recovery vs time) can be divided into three stages: 1) capillary dominated, 2) capillary and gravity dominated, 3) gravity dominated (Hou, et al., 2015). In this context, the dominance of gravity does not imply the absence of capillary forces. The suction of water into the core is still due to decreased capillary force. However, the direction of the flow and location of water entrance (from all faces, top or down of the core) are defined by the gravity force.

Addition of the IFT-reducing chemicals into the imbibing solution makes the gravity segregation the dominant displacing process, which decreases imbibition rate (Kalaei, et al., 2010). However, the ultimate oil production increases in comparison to the system with higher IFT, because of suppression of the entrapment of oil.

2.4.2 Flow Regimes of Spontaneous Imbibition

Two types of flow of the wetting phase can occur during spontaneous imbibition: counter-current and co-current flow. Counter-current imbibition is characterized by the flow of oil and water in opposite directions. Capillary imbibition occurs in a counter-current manner in the vertically placed cylindrical cores (Babadagli, 2005).

In co-current SI, both oil and water flow in the same direction. This flow regime may happen in the upper part of the core and depends on the strength of the capillary force. In the vertically placed core, the presence of the co-current flow is controlled by the height of the core.

Graphic representation of two flow regimes is shown in Figure 6.

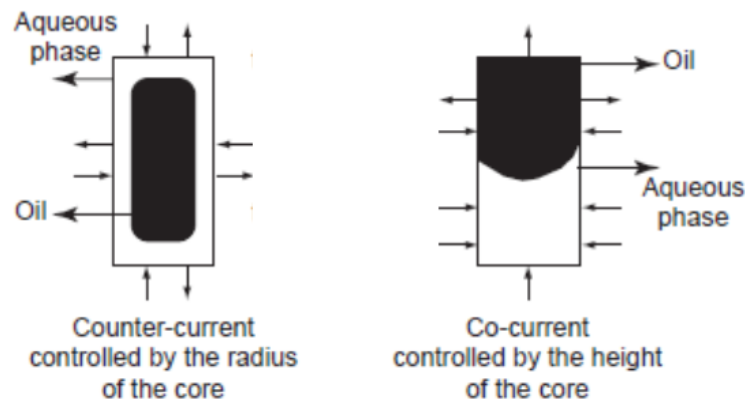


Figure 6 – Schematic of Counter-Current and Co-Current Flow Regimes in Vertically Situated Cylindrical Core (Babadagli, 2005).

2.4.2.1 Counter-Current Imbibition

This type of flow is typically achieved for the strongly water-wet cores in the Amott cell or other experiments performed with all-faces-open boundary condition (Mason, et al., 2008). Water imbibes from all sides of the plug, and consequently, oil is produced from all faces of the sample. Hence, the counter flow occurs. The pressure gradients of the two phases are in opposite directions (Li, et al., 2006). The mass balance is preserved during perfect counter-current SI, which means that the absolute values of the net volumetric flows of the two phases are equal (Mason, et al., 2008).

The experiments performed by Li et al. (2006) for the linear imbibition (OEO boundary condition) showed that the rate of oil recovery has a linear relationship with a square root of time until imbibition front reaches the end of the core. The same results were obtained by (Tavassoli, et al., 2005).

The flow pattern is very complex for the AFO cores. However, the assumption of the leaky piston-like displacement provided good results for the number of modelled experiments (Mason & Morrow, 2013). The frontal imbibition into a cylindrical core is described by Mason et al. (2008). The authors suggest that the flow can be described as a piston-like displacement front for both flat ends and lateral surface of the plug. This means that the flow pattern is separated into two types. The first one is linear imbibition, forming cones. It occurs in the bottom and the top of the core. Depending on the length of the core, the cones can be full and truncated. The

second one is radial imbibition, forming a toroid ring displacement front. Respectively to each other, the shapes have a no-flow boundary in the intersection between two flow regimes. If the half-length of the core is less than the core radius, the conical imbibition reaches the centre of the core early, and as a result, the truncated cones are formed. This means that the imbibition front from the cylindrical surface of the core does not reach the axis of the core. Two situations of imbibition profile for the long and the short plugs are shown in Figure 7.

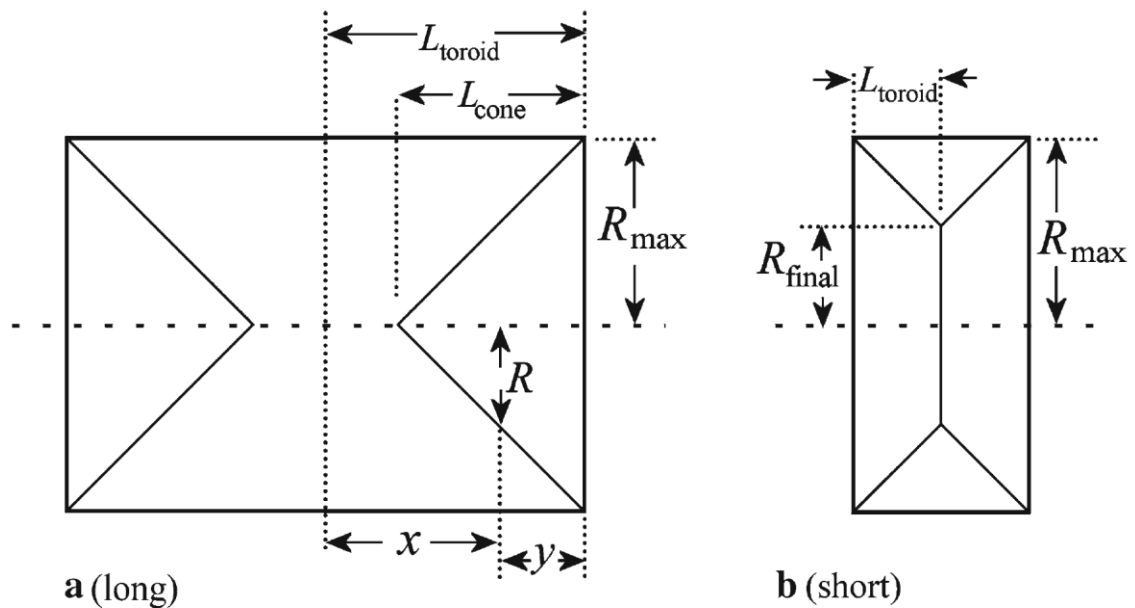


Figure 7 – Spontaneous Imbibition in a Long (a) and a Short (b) Core with All Faces Open.

2.4.2.2 Co-Current Imbibition

When the IFT is reduced by the addition of chemicals, the capillary pressure is decreased, and the gravity force may influence the flow behaviour. Water will imbibe from the bottom of the core, pushing oil upwards. Hence, both fluids flow out of the top face of the core. The flow is in the same vertical direction. Such imbibition is called as co-current (Sheng, 2019).

Chapter 3

Model Set-Up of the Amott-Cell Experiment

3.1 The Amott Cell for the Laboratory Experiment

The experiment of spontaneous imbibition process was performed using the Amott cell. The structure of it is simple and shown in Figure 8. The core saturated with oil until irreducible water is placed in the centre of the cell's bottom. The cell is filled with displacing fluid (further will be mentioned as cell fluid) and stored under reservoir temperature in the oven.

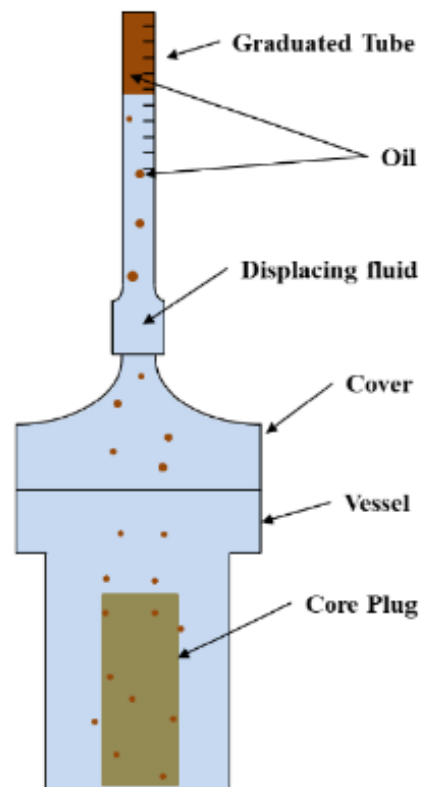


Figure 8 – Scheme of the Amott Cell (Arekhov, 2019)

Displaced oil is transported to the upper part of the Amott cell (cover) by buoyancy force. This oil is then accumulated in the graduated tube, where the volume of the produced phase is measured visually.

3.2 Geological Model

A simulation model for the experiment is built in tNavigator [version 19.4] package, using the geology designer module. The whole set-up was simplified and presented as a rectangle in order to decrease the time for the simulation run. The volume of the entire cell with core inside is 300 ml.

Proportions of the Amott cell in a laboratory experiment are shown in Figure 9. The most important parameter is the height of the model, as it is one of the components defining gravitational forces acting on the saturated plug.

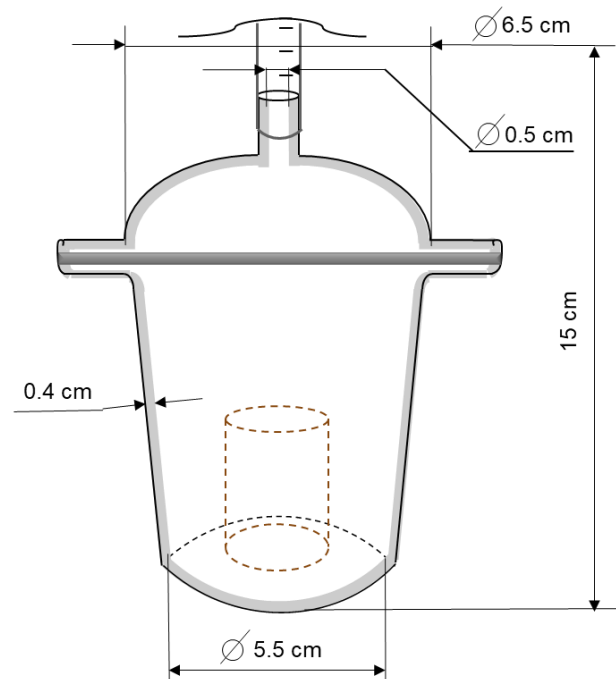


Figure 9 – Proportions of the Amott Cell.

The best solution for the simulation flow would be radial flow; however, it is not supported by the selected simulation software. Therefore, a rectangular grid was used. The size of the grid blocks is different through the whole model: the blocks are small at the centre of the model and increase to the sides. In order to still preserve the cylindrical shape of the core plug, the top and bottom area of the sample is made as close as possible to a circular shape. The polygon used to differentiate the plug inside the Amott cell model is shown in Figure 10.

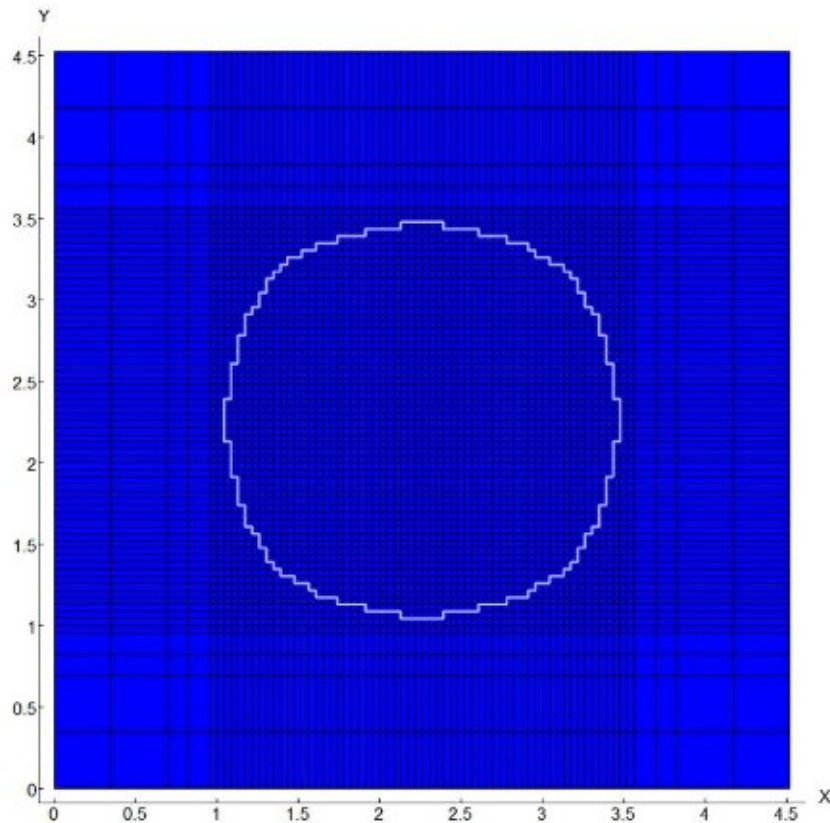


Figure 10 – Polygon for the Plug Region inside of the Amott Cell (white contour). Model Cross-Section (view from the top).

The higher the area of contact between rock and displacing fluid, the higher production is expected. As stated previously, the height of the plug region should be equal to the real height of the sample. Average proportions of used core samples are as follows (Table 2):

Table 2 – Average Proportions of the Core Plug.

Parameter	Value
Total volume, cm ³	54.42
Height, cm	8.01
Diameter, cm	2.96
Area of the Bottom, cm ²	6.812
Lateral Surface Area, cm ²	73.98

Due to the box-like shape of the grid blocks, it is impossible to preserve both areas of the top and the side of the plug cylinder. During several runs, it was concluded that major displacement is taking place from the side of the plug. This indicates that the lateral surface area is more important for consideration. The area of the top and the bottom of the core, therefore, is reduced.

Taking these statements into consideration, a simulation model was built (Table 3). A small grid size (0.0435cm x 0.0435 cm x 0.0625 cm) was chosen to maximize the volume of the core region and make it as close as possible to the real value.

Table 3 – Proportions of the Total Model and the Core Part of the Model.

Parameter	Total Model	Core Region
Grid	68x68x144	2500x128
Total Volume, cm ³	301.35	37.845
Height, cm	14.75	8.0
Area of the Bottom, cm ²	20.43	4.73
Lateral Surface Area, cm ²	–	77.952

Differentiation between core zone and Amott cell itself filled with water or chemicals is done through two fluid in place regions and two saturation regions. Figure 11 and Figure 12 demonstrate created areas of the model.

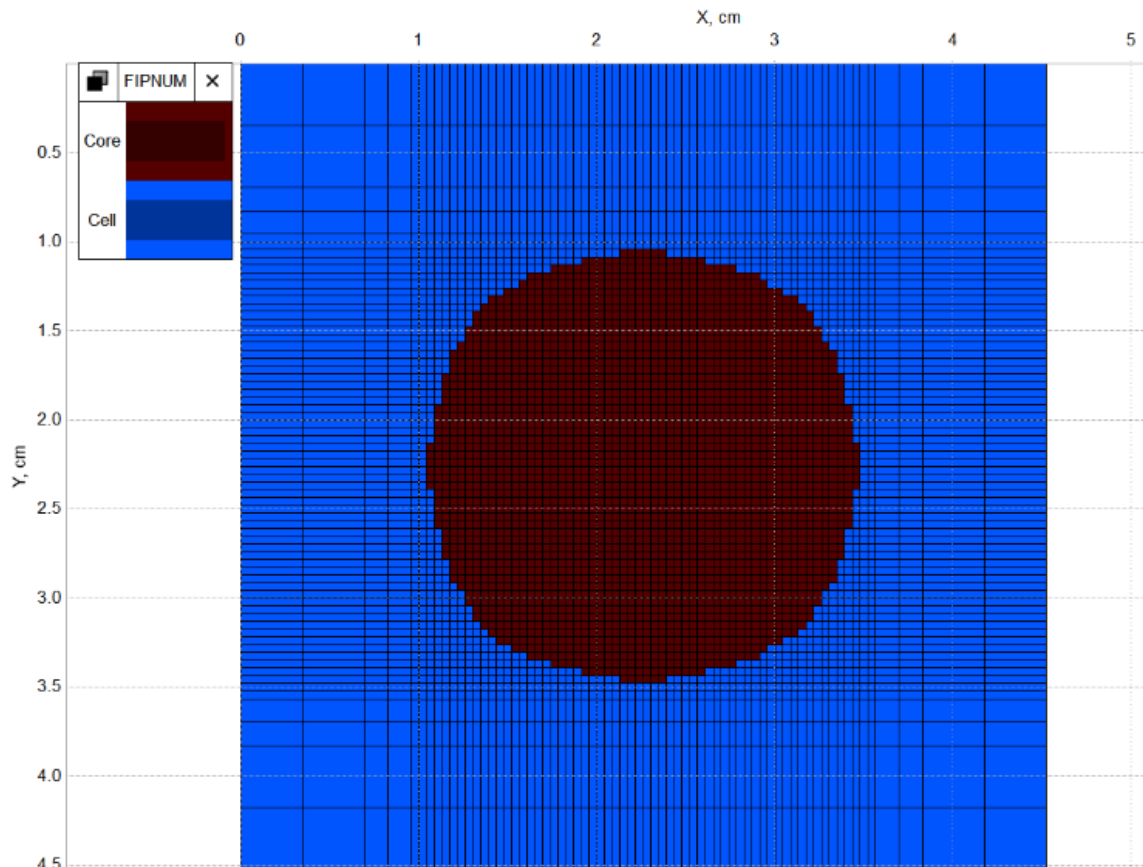


Figure 11 – Fluid in Place Regions in the Model. Region of the Displacing is Blue, and the Plug Region is Brown. The Cross-Section is in Z-Direction.

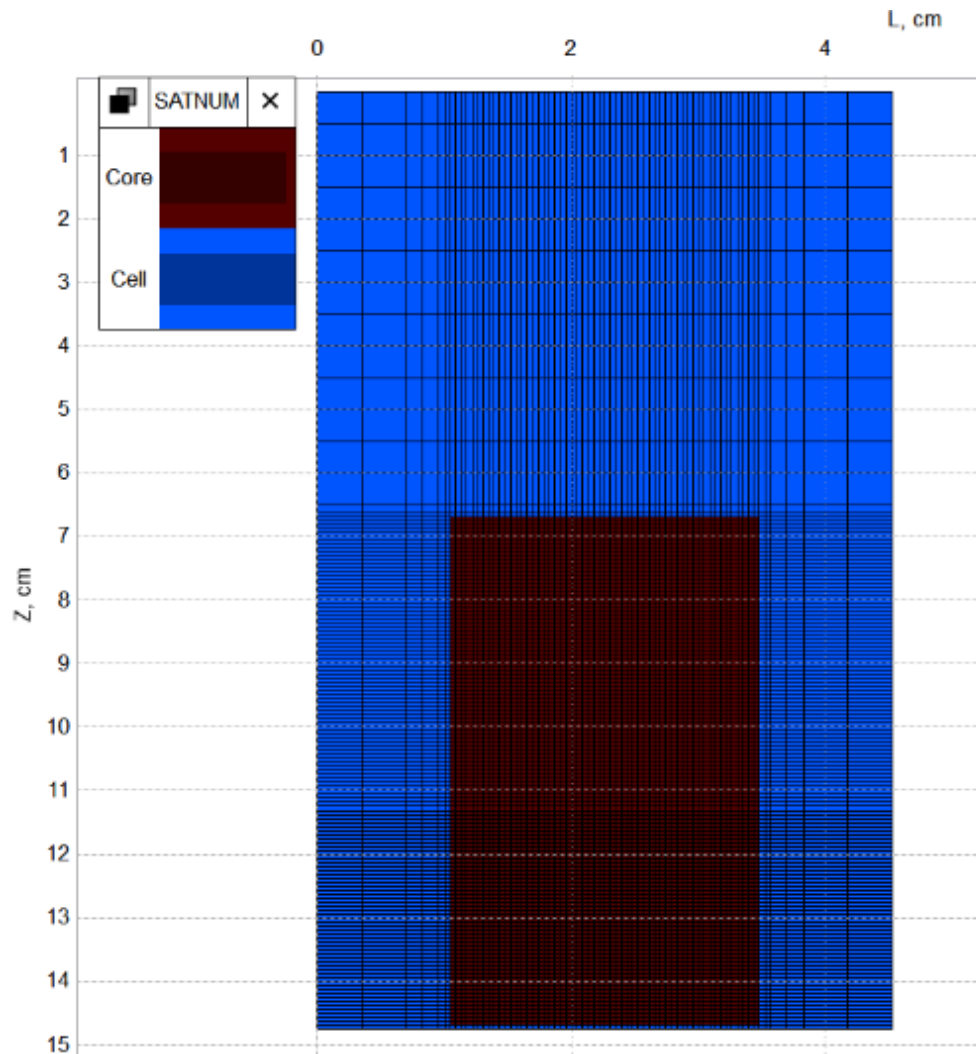


Figure 12 – Saturation Regions in the Model. Region of the Displacing is Blue, and the Plug Region is Brown. The Cross-Section in X-Direction (the Scale is 1:2 in Z)

Initial water saturation is set at 100 % in the displacing fluid region and as initial water saturation in the plug region from the experiment. The porosity of the Amott cell region is also set to 100 %.

In microscale, the sample has a rough surface, which means that there could be a small space between the rock and glass. One layer of water was added in the model below the plug region with the thickness of one grid cell to account for this space.

To preserve the real volume of fluid in place in the model, the porosity of the plug region in the simulation model is much higher than actual laboratory measurements. Such alteration is explained by the difference in the total volume of core in reality and in the computer model. Recalculation of porosity was made, through the known pore volume.

The values of initial water saturation and porosity for the cores used in the experiment with different chemicals are shown in Table 4.

Table 4 – Volume Preservation Parameters: Porosity and Initial Water Saturation for the Cores used in the Selected Laboratory Experiments and for the Corresponding Simulation Models

Parameter	Displacing Fluid		
	Test Water	Alkali	Alkali-Polymer
Porosity in Lab., %	23.67	24.26	23.15
Porosity in the Model, %	34.03	34.88	33.29
Initial Water Saturation, %	20.60	28.94	21.20

3.3 Simulation Model Initialization

3.3.1 Grid Coarsening

The open part of the Amott cell in the simulation model (FIP region two) does not have any barriers for fluid to flow. Continuity of fluid gives an ability to coarsen the grid in this region. Coarsening was implemented as part of model initialization using “Coarsen” keyword. The difference between the static model and the dynamic model is shown in Figure 13.

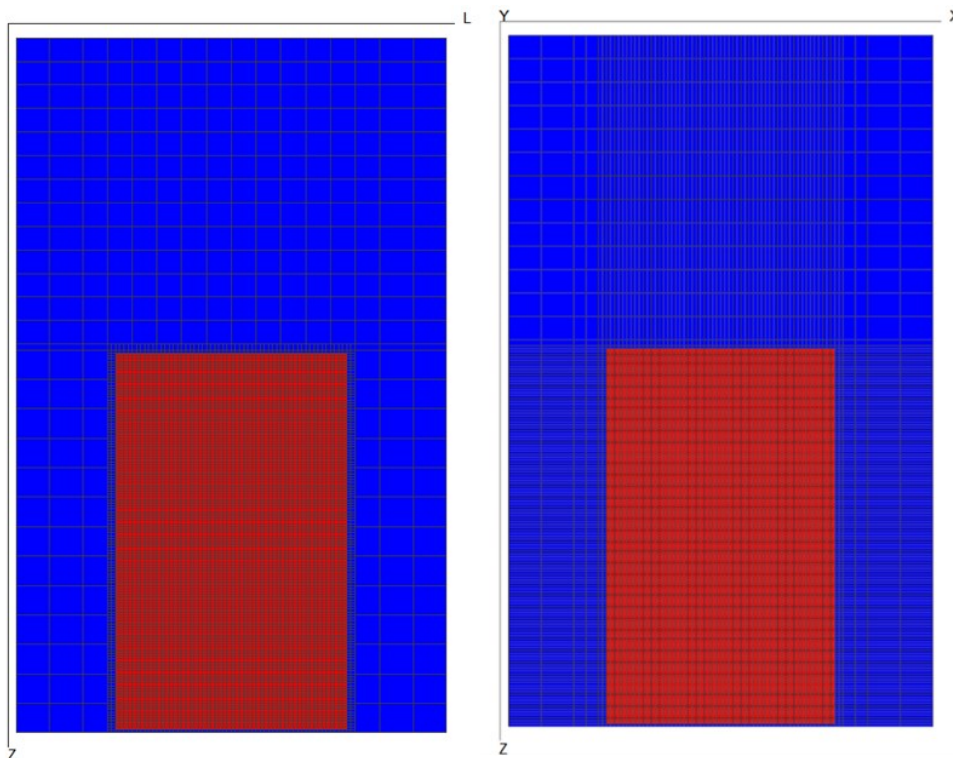


Figure 13 – Comparison of the Dynamic Model Grid (Left) and the Static Model Grid (Right). A Side View. Aspect Ratio is 2:5.

The grid was changed from original 665,856 to 477112 grid cell, which helps to reduce simulation time significantly.

3.3.2 Fluid Characterization

In the laboratory experiments, two different types of oil that mainly differ in the total acid number (TAN) were investigated. Only one of them was used for the simulation as the determination of the influence of TAN requires a software that can simulate chemical reaction kinetics, which cannot be done in tNavigator.

The higher TAN oil was used for the simulation because a higher amount of the surfactant can be created by the reaction of the alkali with acidic components of the oil. In the model, the alkali was simulated as a surfactant with the same concentration (further notes are in 3.3.5). The substitution of alkali by a surfactant is possible only in case if all alkali reacts with oil. Because the amount of the surfactant created during the laboratory experiment was not tracked, it is safer to assume that the oil with the higher TAN creates the amount of surfactant that is closer to the initial alkali concentration in the solution, compared to the amount of surfactant created by the lower TAN oil-alkali reaction. Therefore, the parameters of the higher TAN oil were used as an input for the model.

In this project, a black oil model was chosen because no third phase is observed in the previously conducted phase experiments at the used concentrations (Schumi, et al., 2019).

Dead oil is used for the experiments; therefore, solution gas-oil ratio is zero. All Amott cells were put in the oven to achieve a reservoir temperature of 60°C. Viscosity and density of all phases are set for this temperature in the model. The properties of the oil and test water used in the experiment are shown in Table 5.

Table 5 – Properties of the Oil and the Test Water.

Parameter	Oil	Test-Water
Density@60°C, kg/m ³	884.3	997.10
Viscosity@60°C, cP	11.90	0.571

The experiments are performed under atmospheric pressure. Hence, minor viscosity change with pressure change is put in PVT tables. Both oil and water are considered as incompressible.

In spontaneous imbibition experiments with different chemicals, the properties of water in the core plug and the outer part of the cell are different. In favour of representation of these

difference in fluids, two PVT regions were created, which are the same as the earlier described saturation regions.

The properties of chemical solutions prepared in the laboratory are presented in Table 6.

Table 6 – Properties of the Chemicals Used as the Displacing Fluid.

Parameter	Alkali	Polymer	Alkali-Polymer
Density@60°C, kg/m ³	1005.20	998.50	1004.2
Viscosity@60°C, cP	0.559	19.536	18.054

3.3.3 Pressure Distribution

Due to the difference of densities between the fluids inside and outside of the core, the system is not in equilibrium. In the beginning, the displacing fluid starts to imbibe into the plug sample due to the pressure difference in the rock and the Amott cell, bringing the whole system to equilibrium.

Two initialization methods were considered. The first one is to define the rock and the Amott cell as two equilibrium regions. In order to do so, the software requires the values for the depth of the water-oil-contact (WOC), where the capillary pressure is assumed to be zero. For the Amott cell, the WOC can be assigned at the top of the cell. However, for the plug region, it is hard to assume a specific value for the WOC. It can be calculated backwards from the capillary pressure between oil and water at the initial water saturation. However, firstly, the value of the capillary pressure is unknown. And secondly, the calculation approach bounds the value of the capillary pressure, which should be varied later in the history matching of the model. Therefore, the approach of the equilibrium regions was not used. Instead, it was decided to initialize the non-equilibrium state in the model by the creation of pressure distribution. The initial pressure in the model was input manually as hydrostatic pressure distribution, calculated by the following equation:

$$P_i = 1 + \frac{S_{wi} \rho_w + (1 - S_{wi}) \rho_o}{101325} \cdot g \cdot h, \quad (8)$$

where P_i – initial pressure [atm], S_{wi} – initial water saturation, ρ_w – water density [kg/m³], ρ_o – oil density [kg/m³], g – gravity acceleration [m/s²], h – depth [m]. For the pressures in the Amott cell, the depth is calculated from the top of the cell, while for the pressures in the plug region, zero-depth is assigned for the top of the plug.

For the core region, the water column above the core was not accounted in pressure calculations. The core plug saturated with water and oil was in atmospheric conditions before was put into

the empty Amott cell. Further, the water (or other chemical solution) was poured into the Amott cell. Hence, it can be assumed that some droplets of oil may start to be displaced from the core at the moment when water column becomes higher than core in the cell. To account for this assumption, the pressure at the top of the core region in the model is assigned to atmospheric pressure.

3.3.4 Rock Characterization

A laboratory investigation of spontaneous imbibition process was performed on two different types of rock. The main disparity between them is clay content which affects absolute permeabilities, and the wettability state of the rock. One of the cores used in the laboratory experiment is a Bentheimer sandstone outcrop (Arekhov, 2019) with low clay content. The core was chosen for the simulation model due to simple mineralogy of the rock and near homogeneous structure that allows a simplification of the model permeability distributions.

The core plugs were not aged so that they preserved water-wet wettability state. Measured permeability of the Nordhorn core plugs is 2313 mD (Arekhov, 2019). This value is used as absolute permeability in x, y, z directions in the plug region of the simulation model. For the Amott cell region, the permeability was chosen as a very high value of 100 D.

Bulk rock compressibility value ($C_{bc}=0.13$ 1/GPa) was taken from (Pimienta, et al., 2017) for the Bentheimer sandstone rock sample at 1 MPa as a reference pressure.

3.3.5 Insertion of Chemical Solutions in Simulation Model

Spontaneous imbibition was investigated using polymer alone, alkali and alkali-polymer solution. In the simulation model, alkali was introduced via surfactant keywords, not alkali keywords. This is in order to be able to set interfacial tension values as a function of concentration, to work with wettability alteration through the variation of relative permeability curves, and to input capillary number values. These options are not entirely possible by using only alkali keywords in tNavigator.

High TAN of oil indicates high reactivity of the oil with alkali due to a high concentration of organic acids in the oil. The sodium carbonate reacts with the acid components of the oil, creating soaps (surfactants). With the presence of alkali surfactant adsorption is decreased, as the hydroxide ions attach to divalent cations of the rock surface (e.g. clay), preventing surfactant from adsorbing on the rock. Due to this fact, it was decided to neglect the adsorption of alkali on the walls of the pores.

In the laboratory experiment, sodium carbonate (NaCO_3) at a concentration of 7000 ppm and 2000 ppm of FLOPAAM 3630S (HPAM Polymer) was used (Schumi, et al., 2019; Arekhov, 2019)

Set-up of the alkali and the polymer as the displacement fluids were made by insertion of surfactant and polymer regions, where the core region indicated zero concentration of chemicals, and the Amott cell was set as the region with values of concentrations specified above.

The surfactant created by the reaction of acidic oil components and alkali decreases the IFT between oil and water, hence the entrapment of oil by capillary pressure, which results in lowering of the residual oil saturation. Due to these mechanisms, the change of the relative permeability curves of the oil and water is taking place. Reduction of the IFT till ultra-low makes the fluids as near-miscible, which results in the straightening of the relative permeability curves (Leverett, 1939; Bo, et al., 2003). Surfactant miscible regions were created using keyword “SURFNUM” to adjust permeability curves in the simulation model in the presence of alkali. The software treats SURFNUM regions as additional saturation regions. The earlier described saturation regions (3.2) simulates relative permeability and capillary pressure curves for the immiscible fluids in the model (water and oil). In contrast, surfactant regions set new relative permeability and capillary pressure curves for the near-miscible fluids (alkali solution and oil). The description of all regions in the simulation model is shown in Table 7.

Table 7 – Summarized Description of the Regions in the Simulation Models.

Keyword	Description of the keyword	The numbering of the regions	
		Core plug	Amott cell
FIPNUM	Fluid-in-place region	FIPNUM 1	FIPNUM 2
SATNUM	Saturation function region Used to specify relative permeability and capillary pressure curves	SATNUM 1	SATNUM 2
SURFNUM	Surfactant miscible region Used to assign saturation regions with the presence of surfactant and to specify relative permeability and capillary pressure curves	SURFNUM 1 (corresponding to SATNUM 3)	SURFNUM 4 (corresponding to SATNUM 4)
PVTNUM	PVT region Used to assign different fluid properties for the regions. In this work used in alkali and alkali-polymer models	PVTNUM 1	PVTNUM 2

Chapter 4

Simulation Models

A total time of 25 hours per experiment was chosen for the simulation as, during this time, most of the oil production is observed in the experiment. In order to depict early production, the first time-step is set to 15 minutes, and then it is gradually increased to one hour. The small size of the grid blocks in the sample region often lead to convergence problems. To solve the issue, the minimum time step was reduced to 10^{-4} - 10^{-9} s, depending on the model.

None of the experiments fully represent the slope of the production in the first hours. Simulation results suggest high production from the first minutes of spontaneous imbibition. Before the primary oil production (at the initialization), the system comes to an equilibrium, balancing pressure distribution along with the whole model. This leads to the recalculation of oil saturation in the grid blocks of the core region, as for the new higher pressures a larger amount of water should be kept by each grid cell. As a result, a dramatical increase in oil production has already been observed for the first time-step. The example is shown in Figure 14.

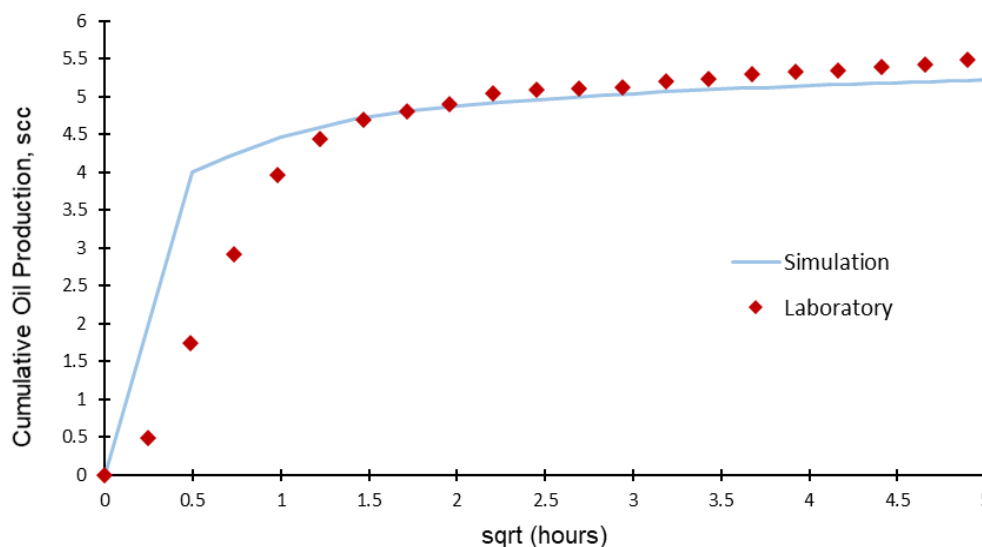


Figure 14 – Example of Cumulative Oil Production for the Laboratory Experiment and Simulation Model

The second possibility of the discrepancy between simulation and laboratory results can be related to the presence of the rock particles with oil-wet properties. Such a situation allows an attachment of oil droplets to the outer surface of the plug until the volume of droplets is big enough to flow upwards to the graduated tube. This can cause difference between oil volume measurements from the graduated tube and the actual volumes of oil extracted.

A delay of production or a very slow imbibition rate at the beginning of production is mentioned in many articles about spontaneous imbibition and referred to as an induction time by Mason and Morrow (2013). Such phenomena can happen even in the strongly water-wet system and can be related to the development of the curvature at the interface between two immiscible phases prior to the imbibition process (Morrow & McCaffery, 1978; Mason & Morrow, 2013). Possible induction time creating phenomena are summarised by (Føyen, 2016). Other reasons for the delay could be low effective permeabilities of the wetting phase for the low water saturation (Behbahani & Blunt, 2005) and local heterogeneities (Mason, et al., 2012).

In the experiments performed by Andersen et al. (2019) on fully oil-saturated core plugs, the delay of the spontaneous imbibition was observed as well, which is explained by the authors as the presence of the oil film on the surface of the rock. The film should be torn in order to get capillary contact and the start of spontaneous imbibition.

It should be mentioned that the term “production” is not fully applicable to the simulation of spontaneous imbibition. No fluid injection is taking place; no wells are needed for the model. If a production well was inserted, the oil flow from the well would not be the same as the actual amount of the phase flowing out of the core plug. Hence, a huge delay in production would be seen in the simulation charts. Another issue with the insertion of wells is the pressure drop from the bottom hole to the wellhead, which gives an additional drive of the fluid. These artificial pressure effects would make it hard to understand the real driving mechanisms of the oil displacement from the simulation model.

The oil production in the simulator is, therefore, investigated as the change of the fluid-in-place in the Amott cell region. To avoid misunderstanding, the oil change in this region still will be referred to as cumulative oil production. Considering the issue with early oil movement explained above, the focus of the model was put in the achieved final cumulative oil.

4.1 Description of the History Matching

History matching was performed using the Assisted History Match tool in tNavigator package. However, due to the fact that the observed production is a change in fluids in place, the analysis of the results and the influence of each parameter was done manually in Excel. This is again the consequence of avoiding using wells in the model. Hence, no history production

information can be inserted in the software to allow the use of automatic history matching algorithms.

In tNavigator, there are several options for experimental algorithms in assisted history matching (AHM). These algorithms define which values for the variables from the assigned ranges will be implemented into the simulation model. In this work, the Latin hypercube sampling (LHS) algorithm was used. In LHS, the cumulative distribution function for each variable is divided into the number of running cases, creating hyperplanes. In each hyperplane, only one value for the variable is randomly selected (Goda & Sato, 2014). A uniform distribution was chosen for all parameters.

Three simulation models were set up for the three spontaneous imbibition laboratory experiments using the following imbibing fluids: test-water (the base case), alkali, alkali-polymer.

The reason for the creation of three different models (Table 4) is the slight difference in porosities and initial water saturations of the used cores. To preserve the original volume of oil in place, it is essential to take into account this variance.

The uncertainty parameters considered more relevant were included in the history matching process Table 8.

In all simulation cases, parameters from capillary pressure and relative permeability curves were implemented with different ranges in the history match. Vertical to horizontal permeability ratio (k_v/k_h) was varied only in the test-water case. The k_v/k_h value taken from the test water model history match then was used in the alkali and alkali-polymer simulation models. The main reason for this is to reduce the number of uncertain parameters as the complexity of the models grew.

In the cases with chemical imbibing solutions, the interfacial tension was considered as an uncertain parameter even though several laboratory measurements were conducted. As discussed in 3.3.4, miscible saturation regions (SURFNUM) were introduced in the model. Regular saturation regions (SATNUM) area set with relative permeability and capillary pressure curves for the high-IFT immiscible fluids – water and oil, while SURFNUM regions represent a set with relative permeability and capillary pressure curves for low-IFT near-miscible fluids, applied for alkali SI. The connection between alkali concentration and relative permeabilities in tNavigator is explained further.

Table 8 – Description of Variables Used in History Matching

Parameter	Description of the Parameter	Type of Model
k_v/k_h	Vertical to horizontal permeability ratio	Test-Water
k_{rowr_S1}	Relative permeability of oil at the irreducible water saturation (SATNUM 1)	Test-Water, Alkali, Alkali-Polymer
k_{rwr_S1}	Relative permeability of water at the residual oil saturation (SATNUM 1)	Test-Water, Alkali, Alkali-Polymer
n_{ow_S1}	Oil Corey exponent (SATNUM 1)	Test-Water, Alkali, Alkali-Polymer
n_w_S1	Water Corey exponent (SATNUM 1)	Test-Water, Alkali, Alkali-Polymer
S_{owcr_S1}	Residual oil saturation (SATNUM 1)	Test-Water, Alkali, Alkali-Polymer
S_{owcr_S3}	Residual oil saturation (SATNUM 3)	Alkali, Alkali-Polymer
S_{wcr_S3}	Irreducible water saturation (SATNUM 3)	Alkali, Alkali-Polymer
P_{cow_S1}	Capillary pressure at the irreducible water saturation (SATNUM 1)	Test-Water, Alkali, Alkali-Polymer
n_{pow_S1}	Curvature degree of capillary pressure (SATNUM 1)	Test-Water, Alkali, Alkali-Polymer
IFT (0)	IFT for zero alkali concentration	Alkali, Alkali-Polymer
IFT (Alk)	IFT for the maximum alkali concentration	Alkali, Alkali-Polymer
SURFCAPD1	Capillary number for zero alkali concentration	Alkali, Alkali-Polymer
Delta	Capillary number difference for zero and maximum alkali concentration	Alkali, Alkali-Polymer
PLYADS	Polymer adsorption table	Alkali, Alkali-Polymer
DPV	Dead pore volume	Alkali, Alkali-Polymer
RRF	Residual resistance factor	Alkali, Alkali-Polymer

SATNUM relative permeabilities and SURFNUM relative permeabilities are treated by the software as extremum cases for the fluids flow behaviour in case of zero alkali concentration in the grid cell and maximum alkali concentration (7000 ppm) in the grid cell, respectively. As the alkali displacing fluid propagates into the core, the distribution of alkali concentration varies in space and time. Depending on the concentration of the alkali, the IFT between oil and water varies. Only two values of the IFT are defined in the model manually (IFT(0) and IFT(Alk)), therefore, for the concentrations of alkali higher than zero and less than 7000 ppm, the software

calculates IFT by linear interpolation between these two values. Then, this IFT value is used to calculate the capillary number, by the following equation:

$$N_{vc} = v\mu/\sigma, \quad (9)$$

where N_{vc} – capillary number, v – velocity of water [m/s], μ – viscosity of water [Pa·s], σ – IFT between oil and water [N/m].

Capillary desaturation curve (CDC) is input in the model as a table of logarithmic values of capillary number and corresponding values of a miscibility factor. Miscibility factor is a special weighting parameter used by tNavigator to recalculate relative permeability curves, creating the curves that are between the relative permeability curves that are set in SATNUM and SURFNUM regions. The miscibility factor is a function of the capillary number. Hence, it is defined from the CDC by the capillary number calculated with (9). More detailed information about miscibility factor and the equation used for calculation of relative permeability curves is in 4.1.5.

Those relationships between parameters, starting from alkali concentration and ending by relative permeability curves indicate that at any moment in time, some grid blocks in the core plug zone in the model can use relative permeability curves, defined by immiscible saturation region or by miscible surfactant region, or even curves that are created using the miscibility factor.

In the alkali-polymer simulation model in addition to mentioned parameters and functions, polymer adsorption, inaccessible pore volume and permeability reduction (residual resistance factor) were implemented into the history match and will be discussed in 4.1.6-4.1.7.

The AHM module of the simulation software has several options for incorporating parameters for history match. Predefined options allow the easy inclusion of parameters like capillary pressure curve, relative permeability, critical saturations and k_v/k_h . For more specific studies, it is possible to write user defined variables for the history match using the keyword “defines”.

The primary ranges of values for each parameter will be described further in this chapter. All prior parameters were considered to have uniform distributions.

4.1.1 Capillary Pressure Curve

The capillary curve is one of the important properties to be considered when dealing with spontaneous imbibition. The most important feature of the capillary curve is the maximum capillary pressure at the irreducible water saturation.

In this work, the hysteresis phenomenon was not included and was not analyzed, but it could be a good option for future work. Entry capillary pressure is not implemented in the simulation

software for the selected curvature option. The Li and Horne model for the imbibition capillary pressure curve (Li & Horne, 2001) was used:

$$P_{cow} = P_{cow}(S_{wc}) \cdot \left(\frac{1-S_w-S_{owcr}}{1-S_{wcr}-S_{owcr}} \right)^{n_{pow}}, \quad (10)$$

where P_{cow} – capillary pressure between oil and water [atm], $P_{cow}(S_{wc})$ – capillary pressure at irreducible water saturation [atm], S_{owcr} – residual water saturation, S_{wcr} – irreducible water saturation, n_{pow} – fitting coefficient, or capillary degree as referred to in the software.

So, the curve is regulated by the capillary degree, the maximum pressure at the irreducible water saturation, the value the irreducible water saturation and the residual oil saturation. Particularly, in this work, the negative part of the capillary pressure is out of interest, as water imbibes spontaneously into the rock. All parameters except irreducible water saturation were used for the history matching, as it is fixed as initial water saturation to preserve the experimental volumes.

In the previous laboratory project (Arekhov, 2019) the parameter dP_c/dS_w was calculated with an estimated value of capillary diffusion coefficient. This derivative of the capillary pressure was used as an approximate estimation for the ranges of the maximum capillary pressure at the irreducible water saturation used in history matching. The range was chosen as 0.1-1 atm. With runs, the range was decreased to 0.16-0.8 atm, as the lower capillary pressures did not give sufficient oil recovery and the higher values from 0.8 to 1 atm did not show increase in the oil production. The capillary degree was varied from 5 to 15. The homogeneous structure of the rock leads to a narrower range of the pore-throats. This means that the range of possible capillary pressures in the rock is narrow as well (Ahmed, 2019). Hence, the capillary degree is expected to be quite high.

4.1.2 Relative Permeability Curves

There are high uncertainties regarding the relative permeability curves. Initial water saturation in the cores was achieved by injection of oil into water saturated core till the point when no more water can be extracted. Hence, the value of initial water saturation may be used as irreducible water saturation. To reduce the number of parameters with uncertainties, the irreducible water saturation was considered as known and was not used in the history match.

There is a high uncertainty on the non-altered residual oil saturation. For all experiments, it was modified, and the value was ranging from 0.1 to 0.3 in SATNUM 1. Simulation time is not accounting for the production of oil until the residual oil saturation is achieved in the core. Hence, the knowledge of the residual oil saturation was not used for prediction of the total volume of oil, which can possibly be displaced from the core. The main function of this

saturation point on the graph is rather the control of the oil relative permeability and, as a result, the oil velocity in the grid blocks with high water saturations. Such a situation occurs in the lower part of the core plug, filled mostly by water at some time step of the imbibition, due to gravity segregation of oil and water in the sample. The value of the residual oil saturation did not affect capillary pressures for the simulation models in this work, as the high curvature of the capillary pressure curve make dP_c/dS_w extremely low closer to the residual oil saturation. The modified Brooks-Corey model (Brooks & Corey, 1964; Alpak, et al., 1999) is used for relative permeabilities:

$$k_{rw} = k_{rw}(S_{owcr}) \cdot \left(\frac{S_w - S_{wcr}}{1 - S_{wcr} - S_{owcr}} \right)^{n_w}, \quad (11)$$

$$k_{ro} = k_{ro}(S_{wcr}) \cdot \left(\frac{1 - S_w - S_{owcr}}{1 - S_{wcr} - S_{owcr}} \right)^{n_{ow}}, \quad (12)$$

where k_{rw} and k_{ro} – relative permeabilities for water and oil, respectively, $k_{rw}(S_{owcr})$ – relative permeability of water at residual water saturation, $k_{ro}(S_{wcr})$ – relative permeability of oil at irreducible water saturation, S_{owcr} – residual water saturation, S_{wcr} – irreducible water saturation, n_w and n_{ow} – Corey exponents for water and oil, respectively.

The wettability of the sample gives an idea of the shape of the relative permeability curves. Because the oil is the non-wetting phase, the movement of the non-wetting fluid should be faster and with more freedom than that for the aqueous phase. Accounting for this, the oil relative permeability at the irreducible water saturation ($k_{ro@Swcr}$) was varied from 0.5 to 1, and the range for water relative permeability at residual oil saturation ($k_{rw@Sor}$) was 0.1-0.7 in the history match. In the history match, only simulation cases with $k_{ro@Swcr}$ higher than $k_{rw@Sor}$ were considered. Corey exponents for each phase were chosen according to the wettability: n_{ow} is 2.0-4.0 and n_w is 5.0-8.0.

So far, the relative permeability curves for the core region in test water experiments were described. For the alkali and alkali-polymer cases, there were four relative permeability and capillary pressure curves, the first two represent the core and the Amott cell under “immiscible”, or non-altered IFT conditions, and the second two under “miscible”, or reduced IFT conditions. The terms non-miscible and miscible that used here are taken from the simulation software terminology to describe the IFT change. These parameters were entered in the model, using the keyword „Coreywo”. Example of the script is shown in Figure 15, where S_{WL} is maximal water saturation; S_{WU} – maximal water saturation; S_{WCR} – critical water saturation; S_{OWCR} – residual oil saturation in the water-oil system; k_{FOLW} – oil relative permeability at S_{WL} ; k_{FORW} – oil relative permeability at S_{WCR} ; k_{FWR} – water relative permeability at $(1 - S_{OWCR})$; k_{FWU} – water relative permeability at S_{WU} ; P_{cow} – oil-water capillary pressure at

S_{WCR} ; n_{OW} – Corey exponent for oil; n_W – Corey exponent for water; n_P – exponent of capillary pressure curve; S_{pCO} – point, where capillary pressure becomes zero in the water-oil system.

The corresponding plot of relative permeability curves taken from (tNavigator 19.4, 2020) is shown in Figure 16.

COREYWO													
-SWL	SWU	SWCR	SOWCR	KROLW	KRORW	KRWR	KRWU	PCOW	NOW	NW	NP	SPCO	
0.212	0.856175	0.212	0.143825	0.76	0.76	0.635833	0.635833	0.339867	3.49777	5.22651	11.0791	0.856175	/-- initial rock
0	1	0	0	1	1	1	1	0	1	1	4	0	/-- water
0	1	0	0.05	1	1	1	1	0.34	1	1	4	0	/-- altered rock
0	1	0	0	1	1	1	1	0	1	1	4	0	/-- water

Figure 15 – An Example of "Coreywo" Keyword, used in the Simulation Model for the Relative Permeability and the Capillary Pressure Curves. A Description for Each Saturation Region.

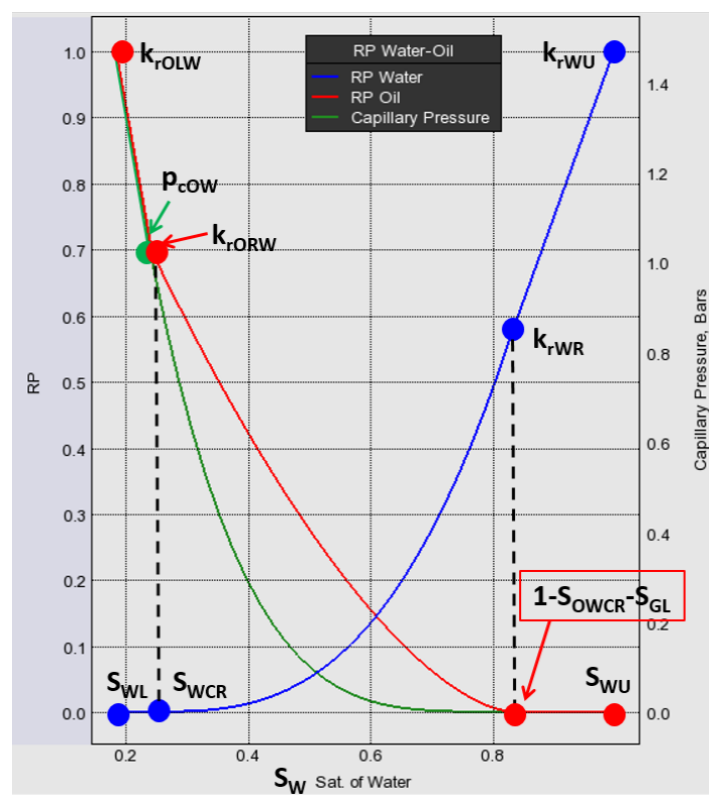


Figure 16 – Schematic of the Relative Permeabilities for a Water-Oil System (tNavigator 19.4, 2020).

The second and the fourth lines of the script correspond to Amott cell region, they were left untouched. The third saturation region represents the influence of alkali on interfacial tension. As the new IFT between water and oil is low, extremums of relative permeabilities for oil and water for SURFNUM 1 are chosen as 1.0, and Corey exponents for oil and water are 1.0, too.

In the preparatory part of the laboratory experiment, the oil was injected to the cores till irreducible water saturation. That is why irreducible water saturation for SATNUN 1 was not altered. However, alkali influences the wettability alteration of the rock; hence, irreducible water saturation may change. Therefore, the irreducible water saturation for SURFNUM 3 was

varied in the history matching. The residual oil saturation for this region was used in the history match as well.

All parameters of the capillary pressure curve and relative permeability curves used in history match are shown in Table 9 with the corresponding ranges.

Table 9 – Parameters of Relative Permeabilities and Capillary Pressure Curves used for the History Matching of three Models.

Parameter	Description	Region	Range	Type of Model
k_{rowr}	Oil relative permeability @ S_{wcr}	SATNUM 1	0.5-1.0	Test-Water, Alkali, Alkali-Polymer
k_{rwr}	Water relative permeability @ S_{OWCR}	SATNUM 1	0.1-0.7	Test-Water, Alkali, Alkali-Polymer
n_{ow}	Oil Corey exponent	SATNUM 1	2.0-4.0	Test-Water, Alkali, Alkali-Polymer
n_w	Water Corey exponent	SATNUM 1	5.0-8.0	Test-Water, Alkali, Alkali-Polymer
S_{ower_S1}	Residual oil saturation	SATNUM 1	0.1-0.3	Test-Water, Alkali, Alkali-Polymer
S_{ower_S3}	Residual oil saturation	SURFNUM 1 = SATNUM 3	0.0-0.1	Alkali, Alkali-Polymer
S_{wcr_S3}	Irreducible water saturation	SURFNUM 1 = SATNUM 3	0.0-0.4	Alkali, Alkali-Polymer
P_{cow}	Capillary pressure @ S_{wcr} [atm]	SATNUM 1	0.16-0.8	Test-Water, Alkali, Alkali-Polymer
n_{pow}	Capillary degree	SATNUM 1	5.0-15.0	Test-Water, Alkali, Alkali-Polymer

4.1.3 Vertical to Horizontal Permeability Ratio

It is essential to understand the impact of viscous, capillary, and gravitational forces on the oil flow. In the reservoir by application of different injection and production rates and controlling pressures in the well, the change of Darcy velocity of the fluid in pores is achieved. In the case of spontaneous imbibition, the pressure gradient is low. Hence, the viscous force does not play a major role in oil displacement. This means that the influence of gravity and capillary forces should be studied more extensively. Gravity segregation is related to the density difference between oil and water. As the density of water is higher, gravity forces make it to accumulate at the bottom of the core, pushing oil to flow upwards.

A reduction of vertical permeability of the core region was proposed in order to decrease the influence of gravity force. This can be achieved by the change of vertical to horizontal permeability ratio (k_v/k_h). Due to a reduction of the vertical permeability, the velocity of oil flow decreases, which reduces the impact of gravity forces. Moreover, the parameter k_v/k_h accounts for the uncertainties related to the absolute permeability of the core. A standard deviation in the distribution of permeability measurements allows playing with absolute permeability of the plug. k_v/k_h was chosen as a history match parameter and was ranged from 0.1 to 1.

4.1.4 Interfacial Tension Between Oil and Water

IFT reduction as a function of alkali concentration is implemented as “Surfst” keyword. At least two data points have to be set in the keyword:

- 1) IFT for zero surfactant/alkali concentration.
- 2) IFT for the maximum concentration of the surfactant

Linear interpolation between these two points gives interfacial tensions for the intermediate surfactant concentration in the model.

Several laboratory measurements of IFT were done previously. Results of these experiments are shown in Figure 17. The values of the test water experiments give an idea of the ranges used for zero alkali concentration, where measurements of IFT for the alkali and the alkali-polymer experiments provide information for the second point of “Surfst” keyword. Both IFT values were chosen for the history match.

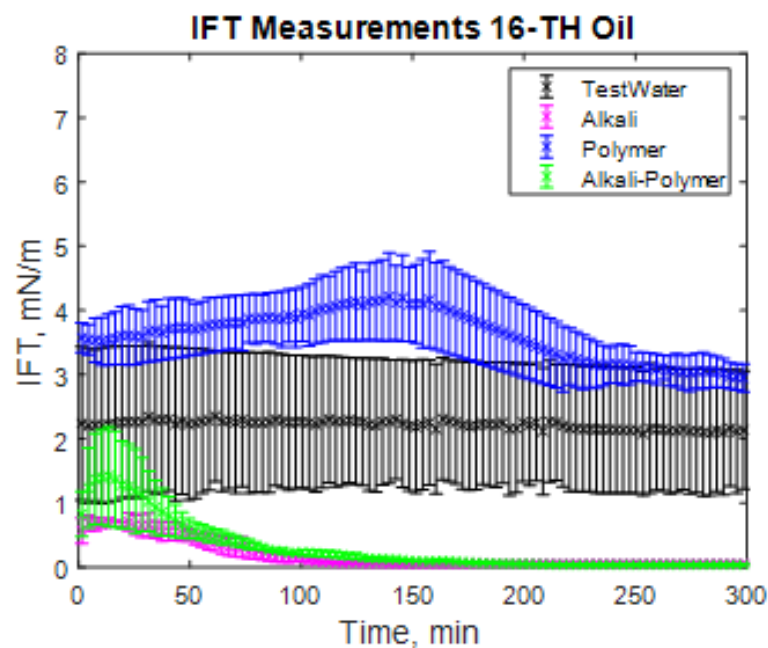


Figure 17 – IFT Measurements for the Test-Water, Polymer, Alkali and Alkali-polymer Experiments (Arekhov, 2019).

Interfacial tensions are used by the simulation software for recalculation of the capillary pressure for SURFNUM 3 according to the following equation:

$$P_{cW}^{EOR} = P_{cW} \frac{\sigma_{surf}(C_{surf})}{\sigma_{surf}(0)}, \quad (13)$$

where P_{cW}^{EOR} – capillary pressure after chemical imbibition [atm], P_{cW} – capillary pressure before chemical imbibition [atm], $\sigma_{surf}(0)$ – IFT between oil and water for zero surfactant concentration [mN/m], $\sigma_{surf}(C_{surf})$ – IFT between oil and water for the particular surfactant concentration [mN/m].

The interfacial tension for zero concentration of alkali (surfactant in the model) was ranged from 1.5 to 8 mN/m. The range was chosen bigger than the one shown by the laboratory experiment in order to check the influence of the higher IFTs. The range of interfacial tension for 7000 ppm of alkali in the model is 0.01-0.6 mN/m. The range is also slightly bigger than in the laboratory measurements again to check the influence of the lower IFTs. The values are in agreement with the results from (Castor, et al., 1981), where the observed IFT in the alkaline flooding is about 0.1 mN/m.

4.1.5 Capillary Number

In the simulation model, the capillary desaturation curve (CDC) is controlled by the surfactant-bonded keyword “Surfcapd”. However, the keyword does not define the CDC in the way that we typically see in the literature: a plot of the residual nonwetting phase as a function of capillary number (Fulcher, et al., 1985). “Surfcapd” includes miscibility factor depending on the capillary number. This factor is 0 for the immiscible situation and 1 for miscible. The desaturation curve looks like Figure 18. Points A is a critical capillary number, and point B is the maximum capillary number that can be achieved. As both parameters are important, they were chosen as variables for the history match.

Besides the value of the critical capillary number, the slope between these points on the graph also plays an important role, which was shown by the runs. A new variable “delta” was introduced to the model to represent the slope of the curve. “Delta” represents a difference of logarithms of the capillary number in the points A and B. It was varied from 1 to 3 in the history match. The logarithm of the capillary pressure in point A (immiscible case) was in the range of [-6, -3]. Point B was entered as the sum of the value in point A and “delta” with the limit of -2. In the experiments performed by Castor et al. (1981), the capillary number of 10^{-4} - 10^{-3} was achieved for the dynamic conditions in the alkaline flooding.

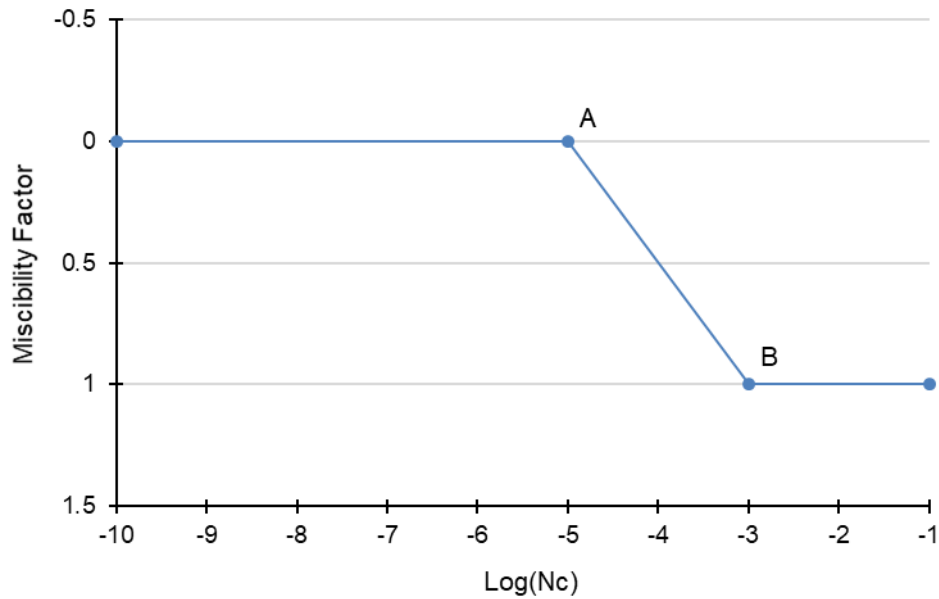


Figure 18 – An Example of the Capillary Desaturation Curve for the Keyword "Surfcapd" in tNavigator.

According to the calculated capillary number in each grid cell, a particular miscibility factor is assigned. This miscibility number is then used by the software to determine relative permeability curves of the fluids and to define effective permeability of the phases in the grid block based on the water saturation. The calculated relative permeability curve is between two plots of relative permeabilities assigned by “Coreywo” for the first and the third saturation regions. The following equations are used:

$$k'_{rW}(S_w) = F_{capd}(N_{cv})k'_{rW}{}^{mis}(S_w) + (1 - F_{capd}(N_{cv}))k'_{rW}{}^{imm}(S_w) \quad (14)$$

$$k'_{rOW}(S_w) = F_{capd}(N_{cv})k'_{rOW}{}^{mis}(S_w) + (1 - F_{capd}(N_{cv}))k'_{rOW}{}^{imm}(S_w) \quad (15)$$

where $k'_{rW}(S_w)$ and $k'_{rOW}(S_w)$ – calculated phase relative permeability (water and oil respectively); $k'_{rW}{}^{imm}(S_w)$ and $k'_{rOW}{}^{imm}(S_w)$ – phase relative permeabilities for immiscible case (SATNUM 1); $k'_{rW}{}^{mis}(S_w)$ and $k'_{rOW}{}^{mis}(S_w)$ – phase relative permeabilities for miscible case (SURFNUM 1); $F_{capd}(N_{cv})$ – miscibility factor from the keyword “Surfcapd” as the function of the capillary number.

4.1.6 Polymer Adsorption

Polymer adsorption is reduced by the influence of alkaline. However, because no alkali flooding keywords were used, this reduction is not modelled. Initial adsorption rates are unknown as no experiments were conducted. In the script, the parameter is defined as a table representing dependency between polymer adsorption and concentration of polymer.

Ten polymer adsorption tables were created using the Langmuir approach (Langmuir, 1918; Dada, et al., 2012):

$$Ad = (C_{surf} \cdot a)/(1 + b \cdot C_{surf}), \quad (16)$$

where a and b are Langmuir isothermal constants. The parameter a was ranged from 0.01 to 0.02, and b was varied from 0.4 to 10. In total, ten different tables covering the uncertainty spectrum for a and b were used in the simulation. The tables are presented in Appendix A.

4.1.7 Polymer Retention and Inaccessible Pore Volume

Retention of the polymer due to the adsorption of polymer molecules on the rock surface and/or mechanical entrapment was varied from 1 to 10 in the history match. In the simulation model, it was presented as a residual resistance factor (RRF), which defines the degree of decrease of effective water permeability. Adsorption of the polymer is considered to be irreversible in the model. Dead pore volume (DPV), also called inaccessible pore volume, was ranged from 0 to 0.3 of pore volume (PV). Both parameters were chosen as variables for the history match and were controlled via the “Plyrock” keyword. The keyword is used for alkaline-surfactant-polymer (ASP) EOR. It defines RRF and DPV at the maximum concentration of the polymer.

4.2 History Match Results

4.2.1 Simulation Model for the Test Water Experiment

The imbibing fluid is the test water in the first experiment. The properties of the aqueous phase in the core are the same as for the test water. Hence, only one PVT region was used for the whole simulation model. Eight parameters were used as the variables for the history match, described in 4.1.1-4.1.3. Among them are the parameters of capillary pressure curve and relative permeability curves (Table 9) and k_v/k_h .

4.2.1.1 Sensitivity Study for Capillary Pressure and Permeability Relationship

Before the history match, the effect of gravitational forces was investigated, as mentioned in 4.1.3. The influence of two variables on the production was studied: the vertical and horizontal permeabilities relationship and the capillary pressure at the irreducible water saturation for the core region. Six cases were built using AHM tool in tNavigator, which are presented in Table 10.

Table 10 – A Sensitivity Study of the Capillary Pressure and k_v/k_h Influence on the Oil Production Based on the Test-Water Simulation Model.

# Case	1	2	3	4	5	6
k_v/k_h	0	0	1	1	0.1	0.1
P_c [atm]	0	0.3	0	0.3	0	0.3

With zero capillary pressure and zero vertical permeability, the cumulative oil production is close to zero. With the increase of the capillary pressure at the irreducible water saturation to 0.3 atm, the volume of oil displaced from the plug raised to 3.5 scc (Figure 19), as the driving force was introduced to the system. No extra oil is removed from the plug in the further time steps. These two cases with zero vertical permeability represent TEC boundary conditions.

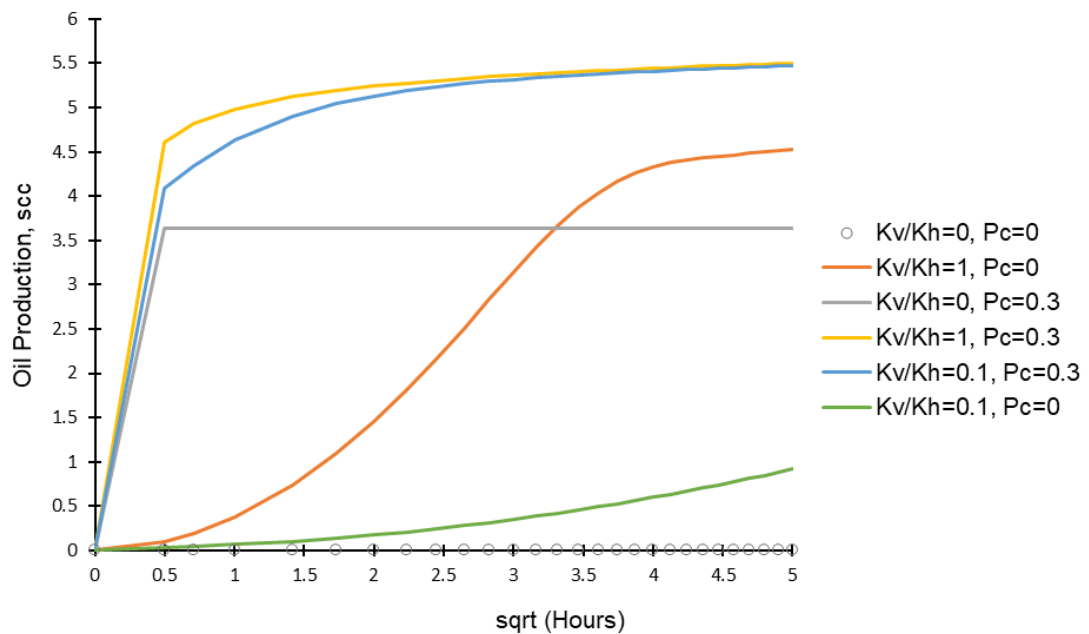


Figure 19 – Cumulative Oil Production for the Sensitivity Study of the Influence of k_v/k_h and P_c on the Test-Water Simulation Model.

In comparison to the second case from Table 10, the oil production is happening gradually in each time step for the cases with an absence of the capillary forces and non-zero vertical permeability (the orange and green lines in Figure 19). The cumulative oil production after 25 hours depends on the value of k_v/k_h : for the $k_v/k_h = 0.1$ the cumulative oil production is around 1 scc only, where when $k_v = k_h$, 4.5 scc of oil is displaced from the core plug. As a result, the slope of the cumulative production increases with the increase of k_v/k_h value. Both cases are characterized by the smoothness of the cumulative oil production function.

When the capillary pressure is introduced to the core sample in addition to the gravitational forces, the high volume of oil (more than 4 scc) is displaced at the first time-step as in the case 2 from Table 10. However, in contrast to zero vertical permeability, the further time-steps in cases 4 and 6 (the blue and yellow lines) show some production of oil, decreasing with time. For the same capillary pressure but different k_v/k_h , the cumulative oil production after 25 hours is around 5.5 scc. The lower k_v/k_h is, the slower is the slope of the production in the first 15 minutes of the experiment.

Described observations lead to the following conclusions:

- With an absence of both gravitational and capillary forces in the plug, no displacement of the oil is observed.
- Cumulative oil production is mostly affected by the value of the capillary pressure at the irreducible water saturation in the core.
- With the presence of the capillary forces, high production of oil is expected from the first time-step.
- k_v/k_h affects the smoothness of the cumulative production function and the slope of the line. Decrease of the vertical permeability slows down the production.
- Strongly gravity dominated SI is effective in the long term and gives higher production than a strongly capillary dominated case.

Based on the chosen simulation runs the plot of Pearson's correlation coefficient between variables (k_v/k_h and P_c) and cumulative oil production is shown as a function of time in Figure 20. The closer the value is to zero, the less correlation between variable and oil production is observed. The plot shows that the capillary pressure plays a more important role than k_v/k_h during all time of the oil displacement. The values correlate with the statement of the high influence of capillary pressure on the total volume of oil produced. The plot also shows that the correlation coefficient for k_v/k_h is low at the first time-steps and increases with time still not showing a high correlation with the production (maximum value is 0.5). Figure 20 concludes the importance of the capillary forces on the cumulative oil production from the first minutes of the imbibition process and the long-term influence of gravitational forces on the total volume displaced.

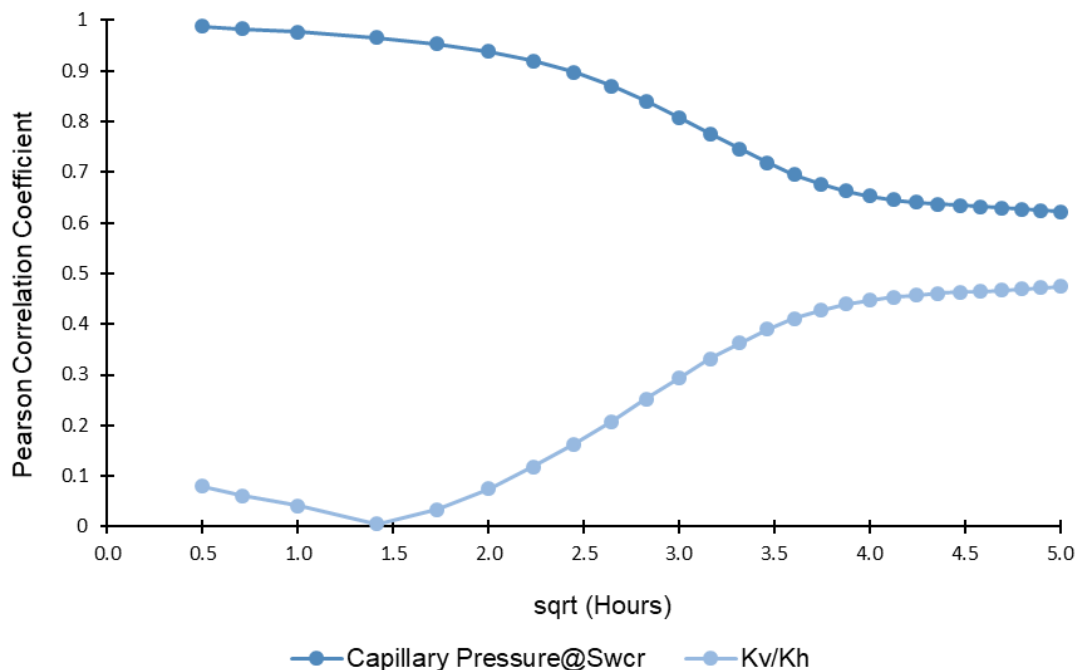


Figure 20 – Pearson Correlation Coefficients Between the Variables (Capillary Pressure @ Irreducible Water Saturation and k_v/k_h) and the Cumulative Oil Production as the Functions of Time.

4.2.1.2 History Matched Simulation Runs

For the history matching 120 runs were created using a Latin Hypercube algorithm for sampling. The models were created based on the change of the uncertainty parameters: k_v/k_h , the residual oil saturation (S_{owcr}), the relative permeability of water at the residual oil saturation (k_{rwr}), the relative permeability of oil at the irreducible water saturation (k_{rorw}), the Corey exponent for water (n_w), the Corey exponent for oil (n_{ow}), the capillary pressure at the irreducible water saturation (P_{cow}), the degree of curvature of the capillary pressure curve (n_{pc}). Several models gave calculation error.

The cumulative oil production after 25 hours of the spontaneous imbibition is 5.49 scc in the laboratory experiment. Most of the created runs showed the cumulative production to be less than 5.49 scc, making the range of the lines in the plot denser at the lower values of the production in comparison to the number of models that showed the cumulative oil production to be more than 5.5 scc. The objective was to define such range of the cumulative production, where P50 case will be the model which is the closest to the real results. As it is not possible to put the history (laboratory) data into the model, the exclusion of the models that gives much higher or much lower production was done manually until P50 case corresponded to the best-matched simulation model. The analysis of simulation runs was done on MS Excel, using the cross-plots of the variables with the cumulative production, the plots of the cumulative oil production and the cumulative distribution function of all simulation results.

After the elimination procedure, only 45 simulation model remained. Figure 21 shows the range of the cumulative oil production achieved by these 45 models after the history match. As was mentioned at the beginning of Chapter 4, it was impossible to preserve the slope of the cumulative production at the first hour of the imbibition process due to the numerical pressure equilibration error. Cumulative production of oil is in the range of 5.15-6.66 scc.

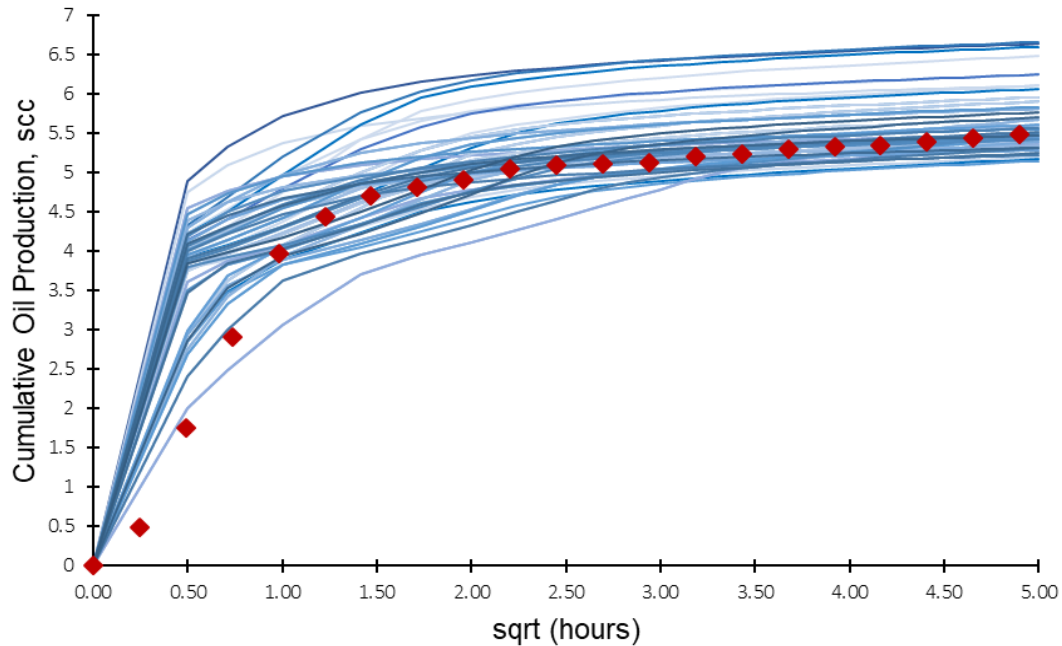


Figure 21 – The Range of the Cumulative Production of Oil for the Test Water Experiment. Blue lines Indicate Created during History Match Models, and Red Dots Represent Laboratory Data.

The number of simulation results below and above of the experimental results (red dots) is equal. However, the distribution of cumulative oil production among 45 simulation cases is not uniform (Figure 22). Most of the models have shown 5.15-5.60 scc of oil produced.

Figure 23 shows the probability cases in comparison to the achieved laboratory results. As it can be seen, the shape of the function is perfectly matched after 2 hours of production by P50 simulation cases. The cumulative oil volume displaced after 25 hours is 5.49 scc. as in the laboratory experiment. P90 case corresponds to 5.22 scc of oil produced, and P10 is 6.24 scc.

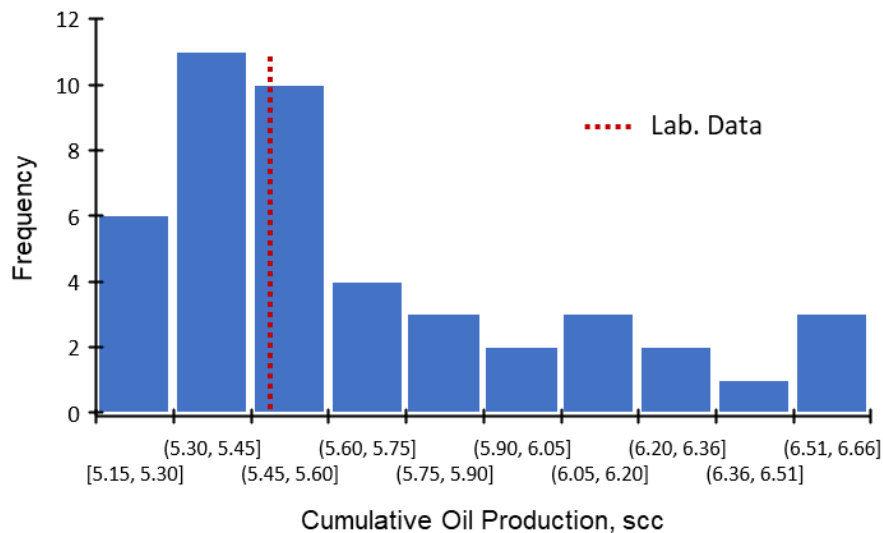


Figure 22 – Distribution of Cumulative Oil Production after 25 hours for History Matching Simulation Models for the Test-Water Experiment.

As can be seen from the graph (Figure 23) the mismatch between P50 case and the laboratory results of production is around 2 scc. Hence the saturation profiles in the model do not represent reality at least at the early production. Further in the thesis, the discussion of the saturation profile and the relative permeability and capillary pressure curves will be strictly based on the model results. They are not considered as a perfect representation of the processes that happen in reality.

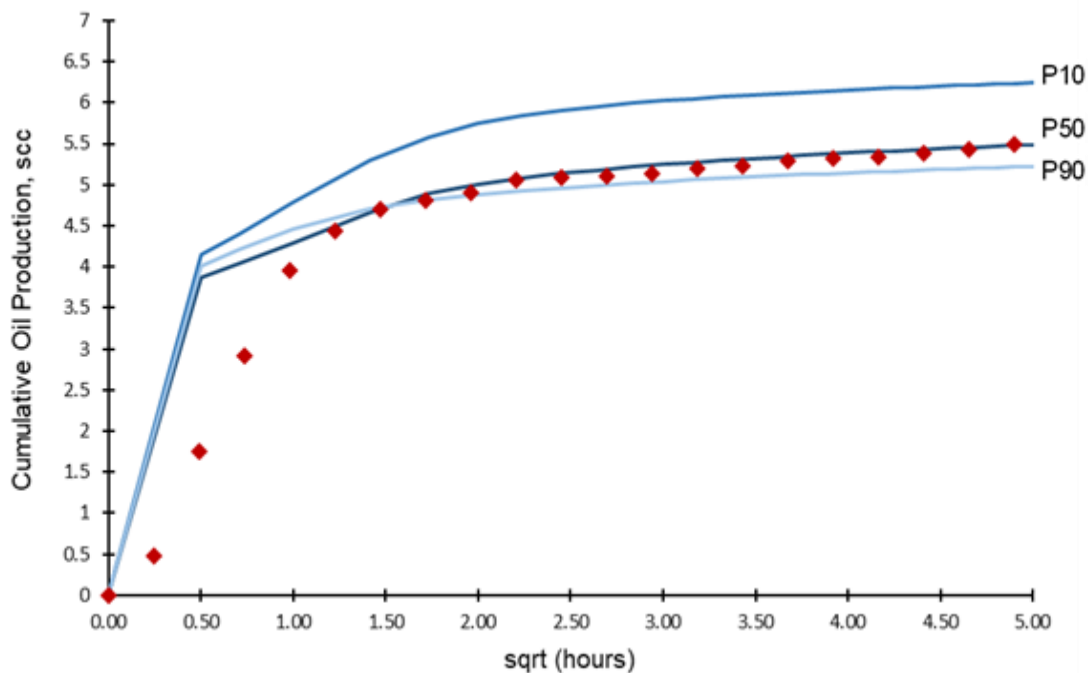


Figure 23 – Cumulative Oil Production as a Function of Time for the Laboratory Experiment and Three Simulation Cases (P90, P50, P10). The Red Dotted Line represents Laboratory Data.

Figure 24 illustrates the cumulative distribution function for the oil recovery based on 45 simulation cases for the history match. The values are calculated for the 25 hours of the production. In the laboratory experiment, the oil recovery is around 53.7%, which corresponds to P50 simulation case on the graph. The oil recovery ranges from 50.35% to 65.10%. It also can be seen from the plot, that P50 oil recovery is much closer to P90 case of 51.06%.

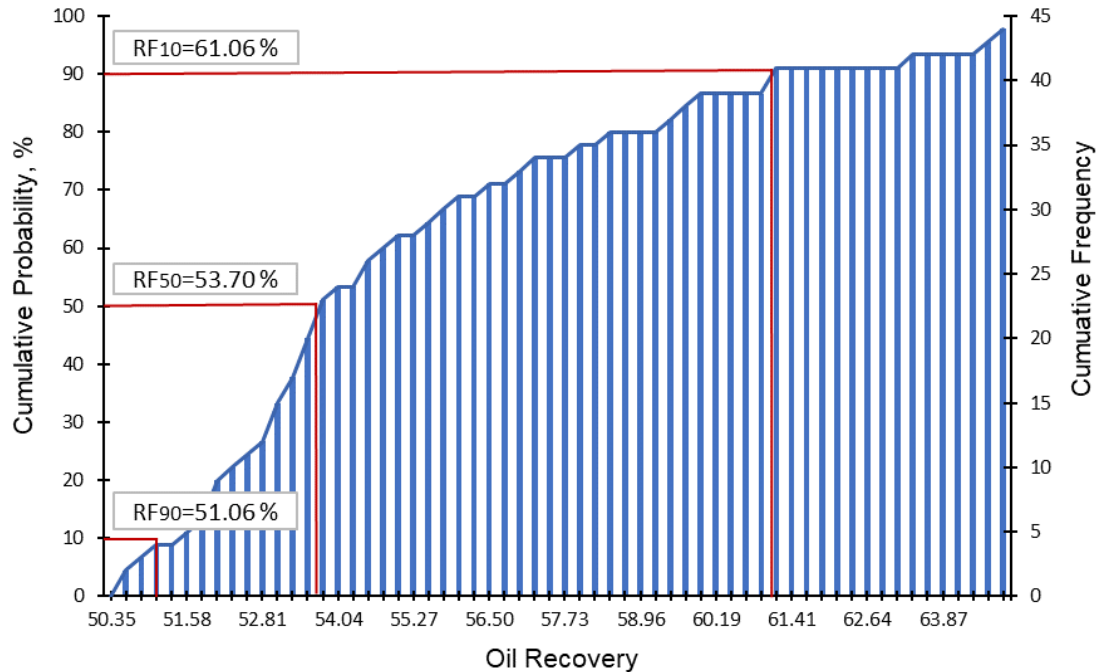


Figure 24 – Cumulative Distribution Function for the Oil Recovery According to the 45 Chosen Cases from the History Match on the Left Axis and Cumulative Frequency for the Bar Charts on the Right Axis.

4.2.1.3 Distribution of the Variables for the Simulation Cases

The variables distributions for the chosen 45 simulation cases are shown in Figure 26. Before the elimination of the cases, the values were uniformly distributed for each variable; however, after the exclusion of the runs, all distributions have an irregular shape. The Corey exponents still have close to the uniform distribution, which gives an idea of the small impact of these parameters on the production. The relative permeability of oil at the irreducible water saturation has an interesting close to the bimodal shape of the histogram with picks on 0.76 and 0.92. The same shape is observed for k_v/k_h , where most simulation cases had a value of either 0.42 or 0.7. However, according to the sensitivity analysis described in 4.2.1.1, the relationship between the vertical and the horizontal permeability does not impact the cumulative oil displacement a lot with the presence of the capillary forces. A vast range of the water relative permeability at the residual oil saturation is covered by the simulation cases (0.12-0.7). The relatively big range is also observed for the shape of the capillary curve. The degree of curvature

of the capillary curve is significant and similar for all P90, P50 and P10 probability cases. Residual oil saturation for most cases is lower than the irreducible water saturation 0.206.

The values of the variables of the probability cases are presented in Table 11. The capillary pressure at the irreducible water saturation is close to the value, calculated from the dP_c/dS_w taken from the experimental data. The calculated capillary pressure at the irreducible water saturation is 0.3. As can be seen, the value of P50 case is pretty close. All three cases show a weakening of the gravitational forces by the values of k_v/k_h less than one.

Table 11 – The Variables for the Probability Cases of the Test-Water Simulation Model.

	k_v/k_h	k_{rORW}	k_{rWR}	n_{ow}	n_{pw}	n_w	P_{cow}	S_{owcr}
P10	0.42	0.92	0.39	3.22	8.22	7.00	0.89	0.17
P50	0.63	0.76	0.64	3.50	11.08	5.23	0.34	0.14
P90	0.68	0.92	0.70	3.63	8.93	5.56	0.62	0.24

The relative permeability curves and the capillary pressure for the matched simulation model (P50 case) are shown in Figure 25. From the difference of the extremum relative permeabilities for the two phases, it can be confirmed that the rock is indeed water-wet. The shift of the intersection of the permeability functions to the right side from the central position ($S_w=0.5$) also illustrates an affinity of the aqueous phase towards the rock. The total mobility of fluids in the plug is deficient at the intersection point, which is approximately 0.6 of the water saturation.

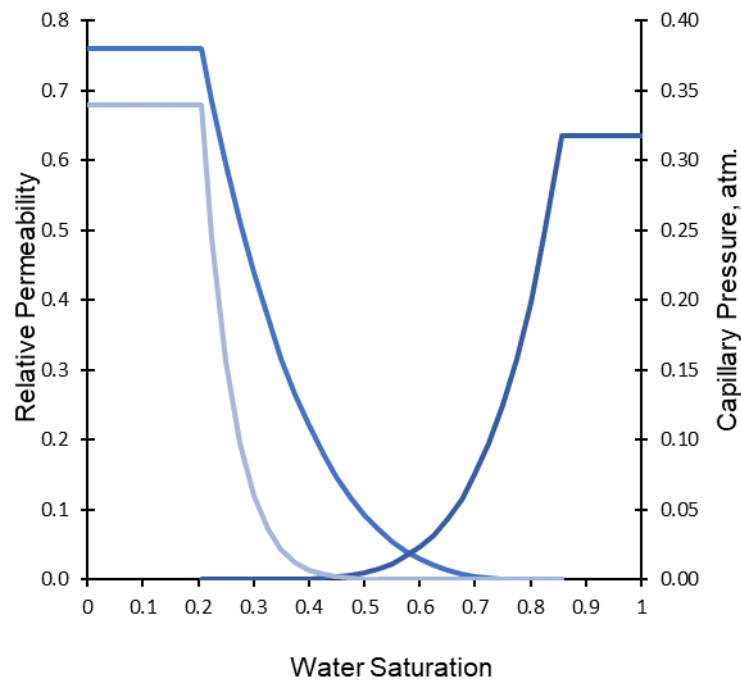


Figure 25 – Relative Permeabilities and Capillary Pressure Curve for P50 Simulation Case.

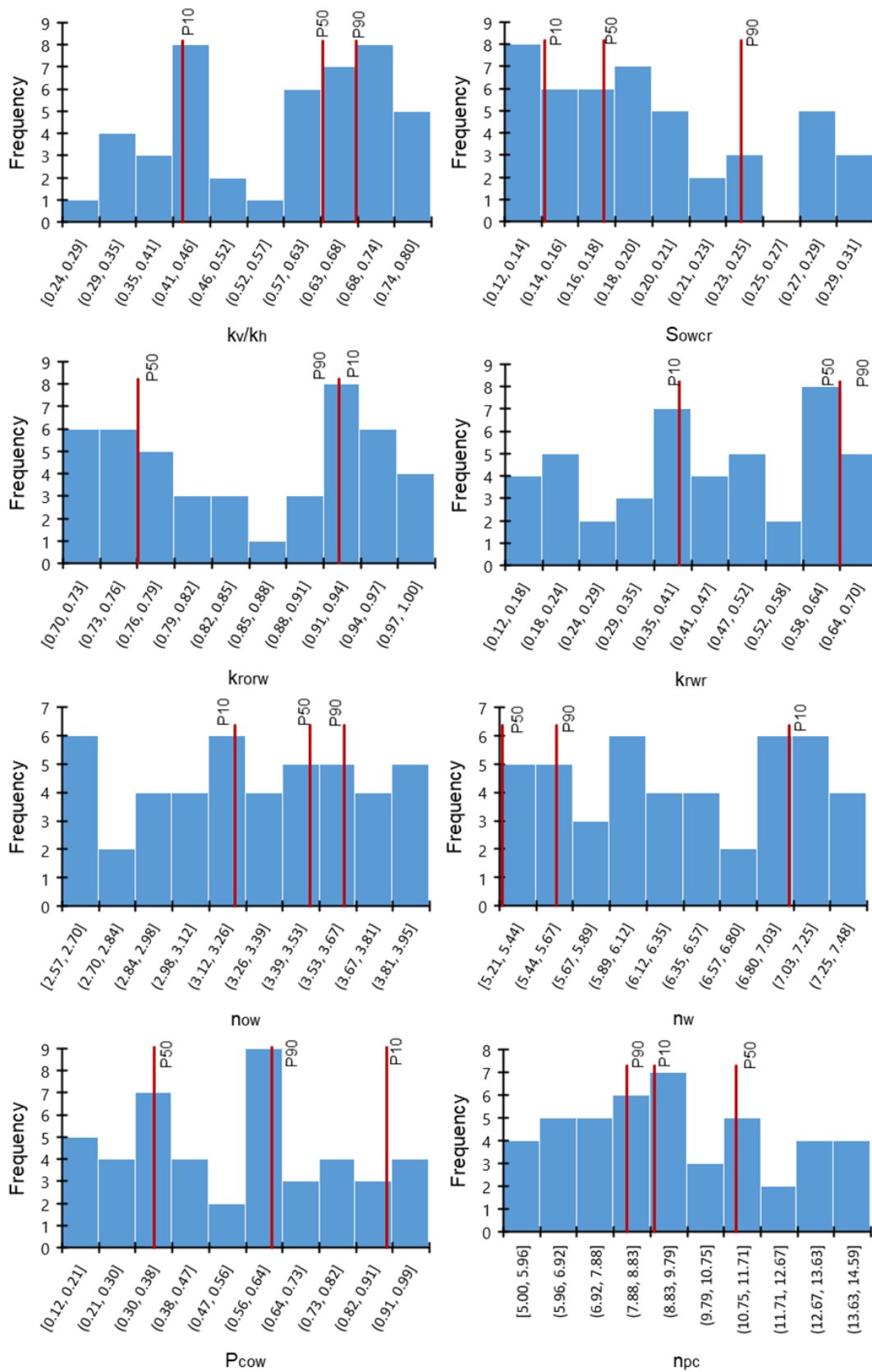


Figure 26 – Distributions of the Variables Used in History Match for 45 Chosen Simulation Models, where the Red Lines Correspond to P90, P50 and P90 Cases of the Cumulative Oil Production.

The oil saturation profiles in the cross-sections of the model for the different times-steps (Appendix B, Fig. 1) show a decrease of the oil production from the sample and a decline of the production rate at 0.39 of the mean oil saturation in the model. The maximum oil saturation is concentrated in the centre of the plug and decreases to the sides of the sample, as shown in the horizontal cross-section (Figure 27).

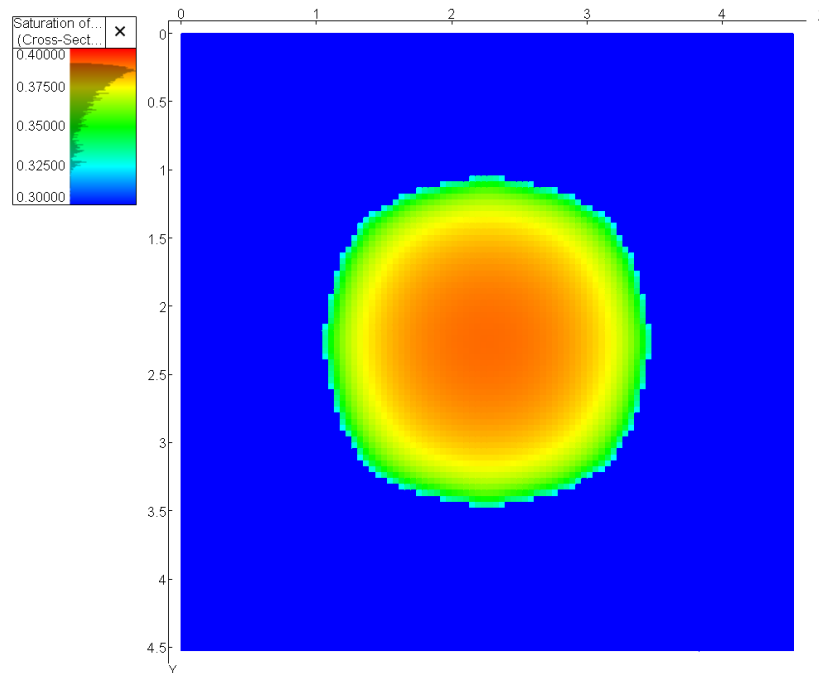


Figure 27 – The Oil Saturation Profile after 25 Hours (Z Cross-Section) for the Test Water Simulation Model. Oil Saturation Scale is from 0.3 to 0.4. X:Y is 1:1.

Two types of fluid flow are taking place in the experiment: co-current and counter-current imbibition. Counter-current imbibition is characterized by the capillary forces. During this type of flow, the oil and the water move in opposite directions. Co-current flow corresponds to the gravity driven flow, and the movement of oil and water is in the same direction. During this type of imbibition, the water imbibes from the lateral surface, and the bottom of the core and the oil is produced from the top of the core plug.

As all surfaces of the plug are surrounded by water and IFT between oil and water is relatively high, both co-current and counter-current flows are observed at the beginning of production. The oil is displaced in all directions from the plug. Hence, the high production rates are in the early stages of spontaneous imbibition. Due to the presence of the water layer between the core and the bottom of the Amott cell, the oil displacement is happening even downwards against buoyancy forces. Most oil is displaced from the sides of the core plug region. A small oil

saturation change is observed in the grid cells above the plug region. It is better visible on the first time-steps of the production (Appendix B, Fig. 1).

At the later time, approximately 2 hours of the production, the oil is produced mostly from the upper surface, which means co-current flow regime. As the capillary pressure decreases with the increase of the water saturation, in this stage, the flow is gravity dominated: the suction phenomena is still due to capillary pressure, however, the fluid flow direction is defined by gravity forces. The most volume of oil is produced within the first 5 hours of the simulation — the increment of the oil displaced drops afterwards.

The oil saturation profile after 25 hours is shown in Figure 28. An upward increase of the oil saturation in the center part of the plug is due to gravitational segregation of oil and water. The accumulation of oil at the bottom of the core is related to the change of the fluid flow behavior from the counter-current to co-current imbibition. The earlier produced oil at the bottom of the Amott cell starts to enter the plug, when the flow becomes co-current. Hence, the rise of oil saturation is also visible towards the bottom of the cell in the lower part of the core plug (Figure 28). The observation from the simulation corresponds to the schematic view of the co-current and counter-current imbibition (Figure 29).

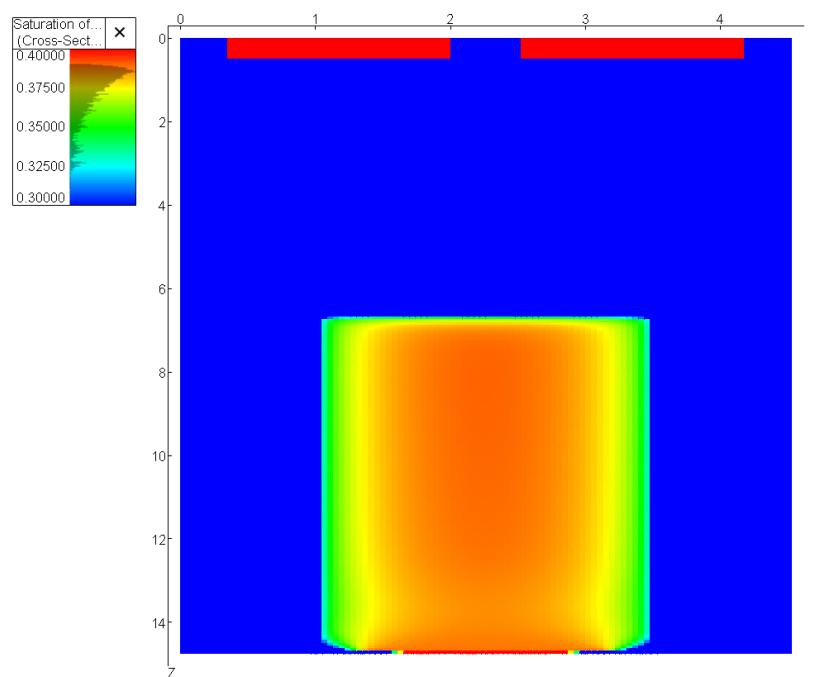


Figure 28 – The Oil Saturation Profile after 25 Hours (X Cross-Section) for the Test Water Simulation Model. Color range is from 0.3 to 0.4. $L:Z$ is 1:3.

Hamad (2019) performed laboratory experiments on the Amott cell for the high and low salinity water imbibition. Visual results of his experiments confirm the same change of the imbibition type with time. At the early time, the oil was produced from the full height of the plug and

showed a high oil volume produced. Hence, the flow is counter-current dominated. At the later time, the oil droplets are visible only on the upper surface of the plug and the lower parts of the rock became clean for the low salinity water or the density of the oil droplets stayed the same for the high salinity water.

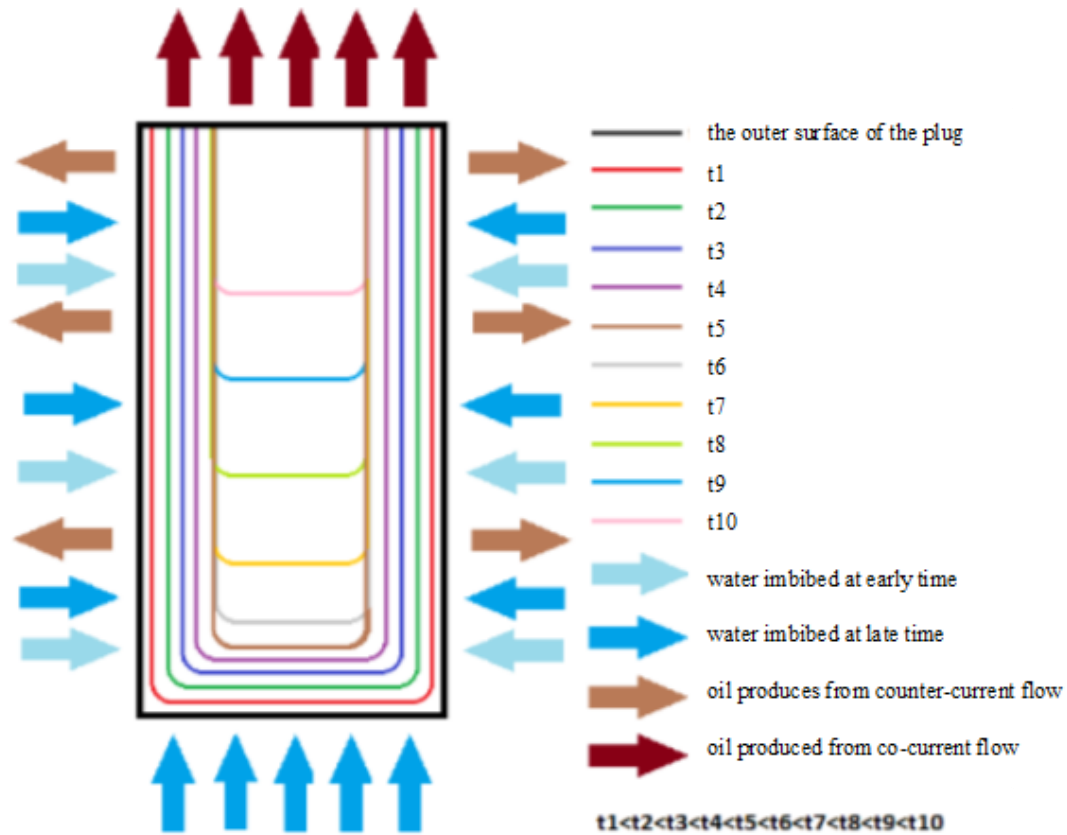


Figure 29 – Schematic of the Water Profile during Spontaneous Imbibition (Hamad, 2019).

The studies of spontaneous imbibition on two-ends-open boundary conditions also show an asymmetric production of the spontaneous imbibition. In such experiments, performed by Fernø, et al. (2013) the imbibed water formed a hemispheric front at the early stages of the spontaneous imbibition. Later, when the front reached the lateral surface of the plug, the flow showed piston-like displacement. Mason et al. (2010) and Meng et al. (2016) suggest the reason for the imbalanced production the presence of the bubble pressure, or as Fernø, et al. (2013) refers it, the capillary back pressure. The droplets of the non-wetting phase drained into the water. Hence, the second capillary pressure (the bubble pressure) on the interface of two fluids is created during spontaneous imbibition experiments with different types of boundary conditions. When this pressure becomes zero, the imbibition is co-current (Haugen, et al., 2014). In the plugs with all faces open, the increase of the oil droplets density on the upper surface leads to a decrease of the bubble pressure, which promotes co-current imbibition upwards.

Figure 30 shows oil accumulation on the upper part of the model after 25 hours of production. The oil is spread as a circular shape in the upper layer of grid cells of the model, with less oil saturation in the centre of the circle. This again indicates the slow production of the oil due to lower vertical permeability, thus lowered the influence of gravitational forces. Most oil is produced from the sides of the core plug, where the water imbibition forced by capillary forces is taking place.

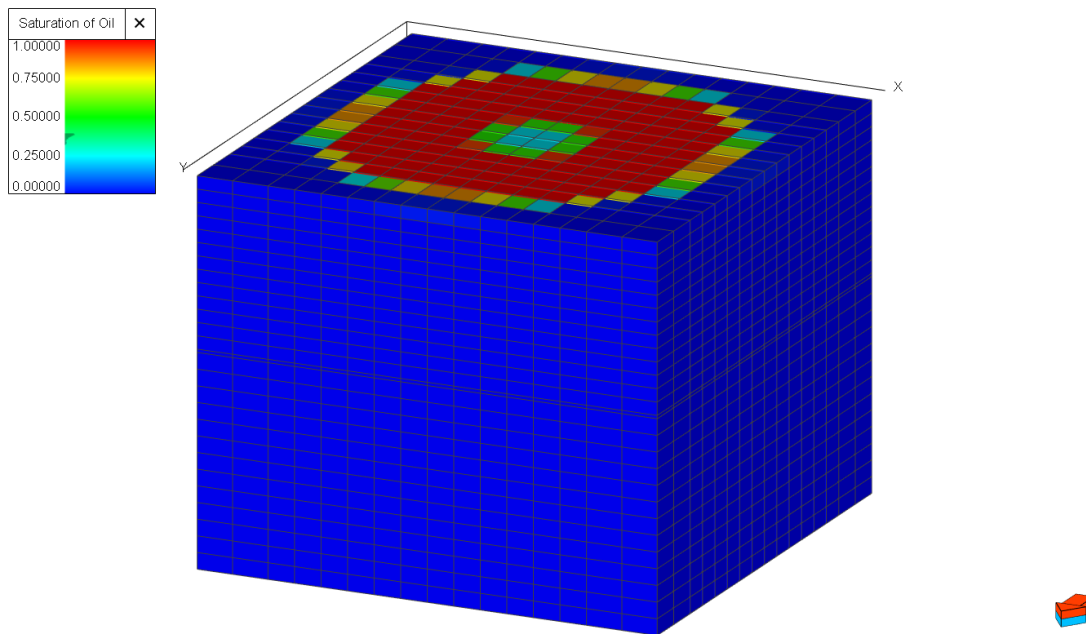


Figure 30 – 3D Oil Saturation Profile after 25 Hours for the History-Matched Test-Water Simulation Model. X:Y:Z is 1:1:3.

The slowdown of the oil production is predicted from the capillary pressure curve as well (Figure 25). The high curvature of the plot indicates the homogeneous structure of the plug. From the water saturation of 0.45 to the residual oil saturation, the capillary pressure is close to zero.

At the beginning of the production, the core plug region is characterized by the maximum capillary pressure of 0.34 atm at the initial water saturation. The most oil production in the simulation model happens within the first time-step of the simulation run. Hence, there is a dramatic drop of the maximum capillary pressure in the model from 0.34 to 0.0007 atm after 15 minutes of production (1st time-step) due to the decrease of the oil saturation in the grid cells Figure 31. More detailed views are in Appendix B, Fig. 2. The negative sign of the pressure is due to the opposite direction of the capillary pressure relative to the pressure drop (in this case, the difference in hydrostatic pressure). The further changes of the capillary pressure on the vertical cross-section of the model mimic the oil saturation profiles. After 25 hours of

production, the maximum capillary pressure in the model is 0.00001 atm, corresponding to the grid cells with the lowest water saturation in the core region.

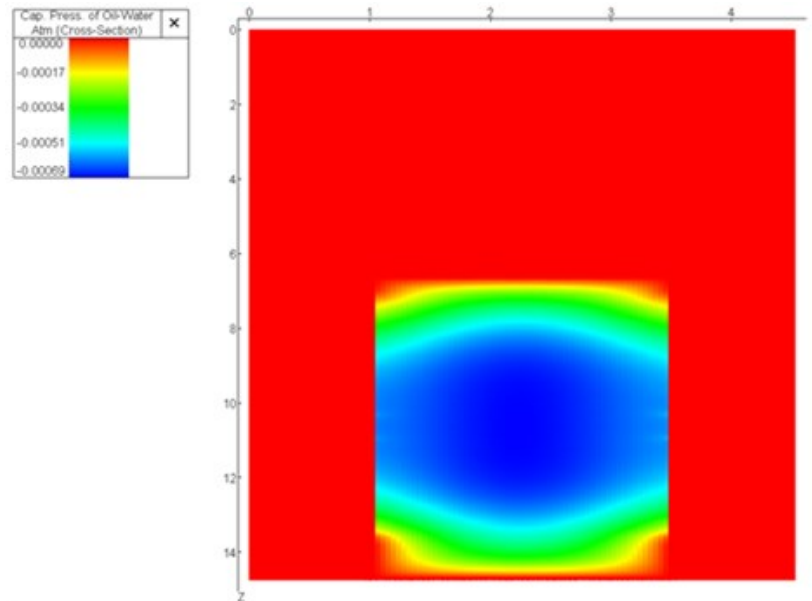


Figure 31 – Capillary Pressure Distribution for the Central X Cross-Section for the History-Matched Test-Water Simulation Model after 15 minutes. Picture Scale 2:3.

The cross-plots of the variables and the cumulative oil production at 25 hours for 45 simulation cases are shown in Figure 32. No relationship between parameters is observed. Very chaotic spreading is characterized by most of the variables, which indicates that more simulation runs should be created to see any relationship between parameters and oil production.

The only plot that shows exponential behaviour is oil production as the function of the residual oil saturation. However, it is hard to indicate any dependency of the oil production from the variables as no sensitivity runs were made to point out the influence of the change of one variable. In the created study, it is challenging to observe any relationship as the impact of the variables on each other should be taken into account. A global sensitivity analysis (GSA) would have to be performed to see not only the primary relationship of each variable on the oil displacement but also the relationship between variables. Special tools as another AHM software or special scripts are needed to perform such a study, which was not done in the framework of the thesis.

Pearson correlation coefficient helps to understand the influence of the variables on the cumulative oil production. As explained in the previous chapter, the coefficient varies from 0 to 1, where one corresponds to a perfect linear relationship between parameters. Figure 33 and Figure 34 show correlation coefficients for the variables used in the history match as the functions of time, based on the 45 simulation models.

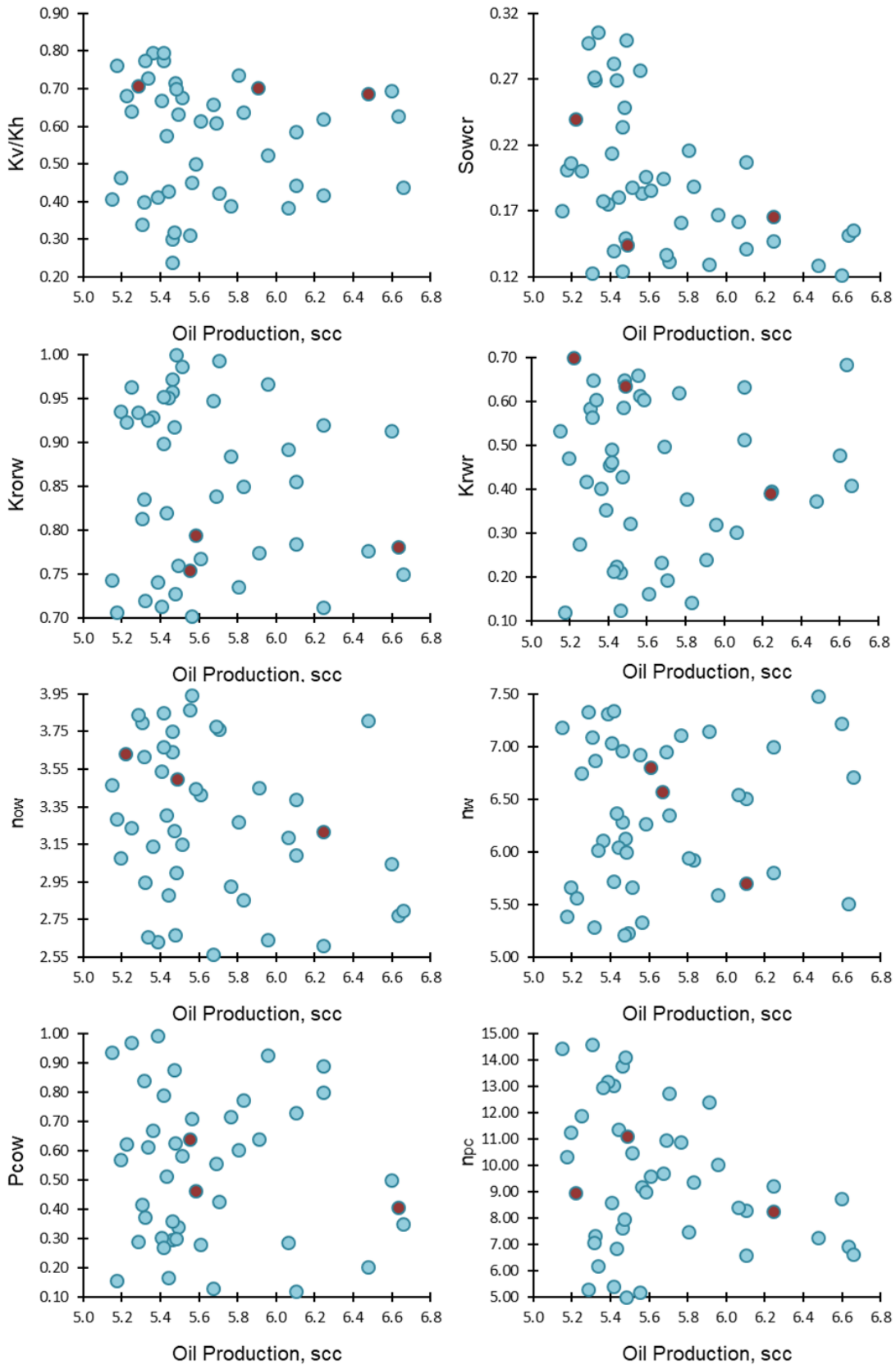


Figure 32 – Cross-Plots for the Variables Used in the History Match for the Test-Water Model and Cumulative Oil Production at 25 Hours. Red dots represent P90, P50, P10 Simulation Cases.

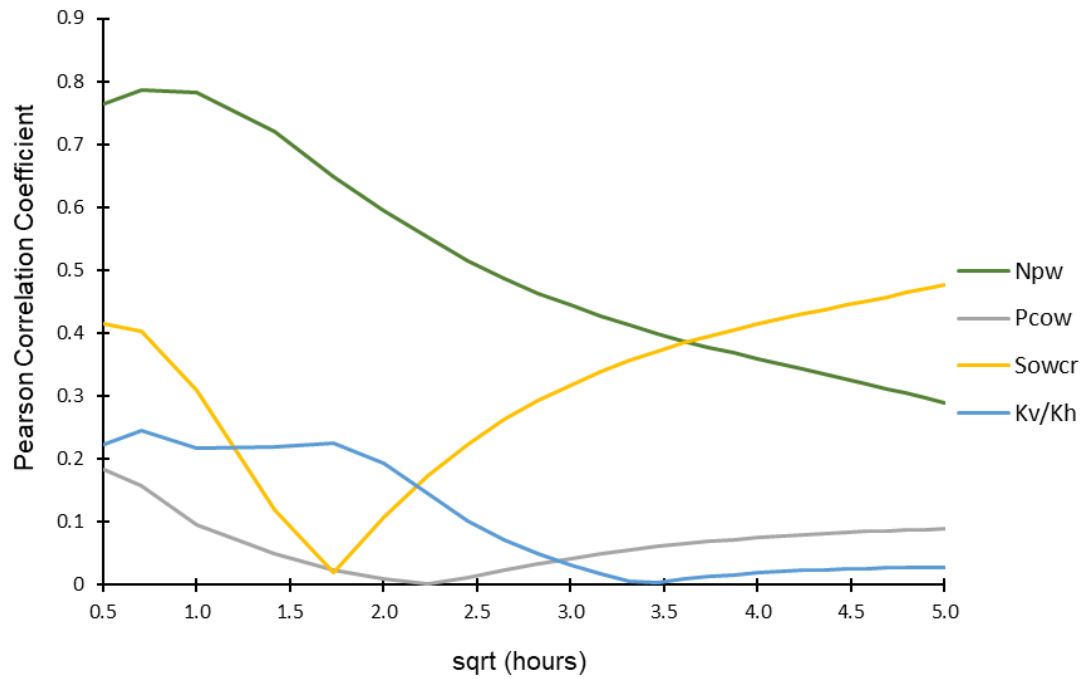


Figure 33 – Pearson Correlation Coefficient as the Function of Time for the Variables (n_{pw} , P_{cow} , S_{owcr} , k_v/k_h) Used in the History Match for the Test-Water Simulation Model.

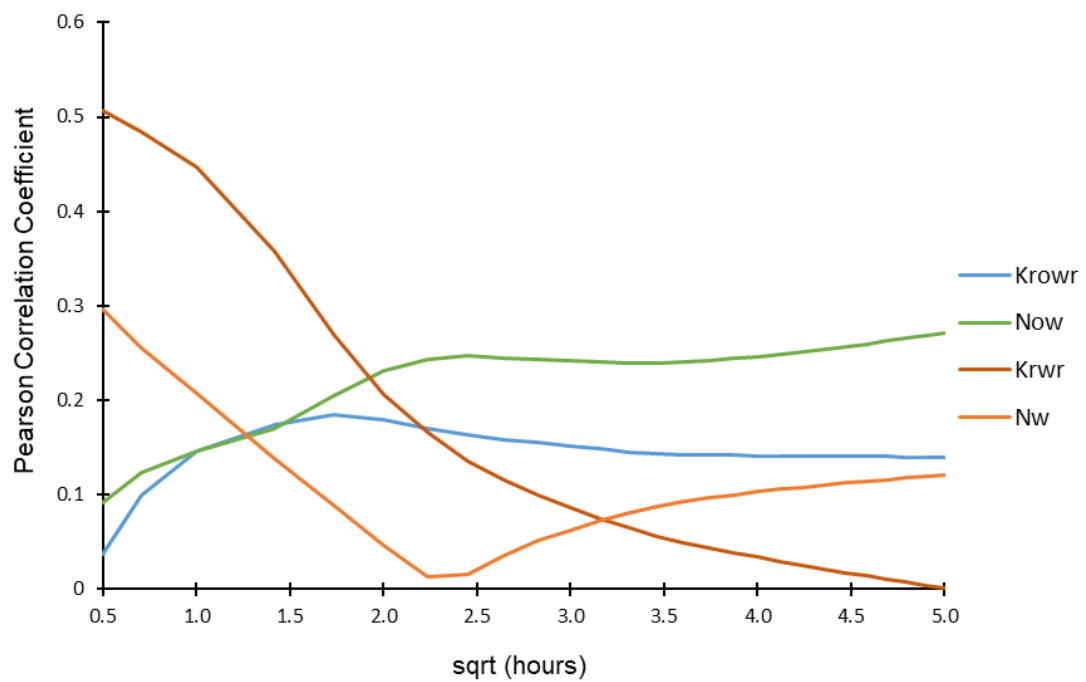


Figure 34 – Pearson Correlation Coefficient as the Function of Time for the Variables (k_{rowr} , k_{rwr} , n_{ow} , n_w) Used in the History Match for the Test-Water Simulation Model.

At the beginning of the production, the curvature of the capillary pressure has the most significant influence, which is presented by the correlation coefficient of 0.8 in Figure 33. The impact of the variable decreases with time. A similar behaviour, but with lower starting value is observed for the extremum of water relative permeability. This indicates that oil production is affected by the velocity of the aqueous phase in the core plug and not so much by the velocity of oil itself, as an average Pearson correlation coefficient is equal to 0.2 for the maximum oil relative permeability. The influence of water relative permeability decreases because the most amount of water imbibes into the plug by the capillary forces at the beginning of the simulation. The impact of the residual oil saturation on oil production increases with time, as the closer to this value the oil saturation in the grid cells gets, the slower is an oil movement. It is interesting to note that neither capillary pressure nor k_v/k_h have a good regression with the cumulative oil production relative to other variables. The correlation coefficients are less than 0.3 at the first time-steps and less than 0.1 at the end of the simulation.

4.2.1.4 Grid Size Sensitivity Analysis

A sensitivity study for the grid size of the core plug region of the model was done. A new geological model with tartan grid was created. The runs were performed with the values of the variables taken from the probability cases (P90, P50, P10). The comparison of the grid design and size on the X cross-sections of the upscaled regular grid simulation model and the model with big grid size is shown in Figure 35.

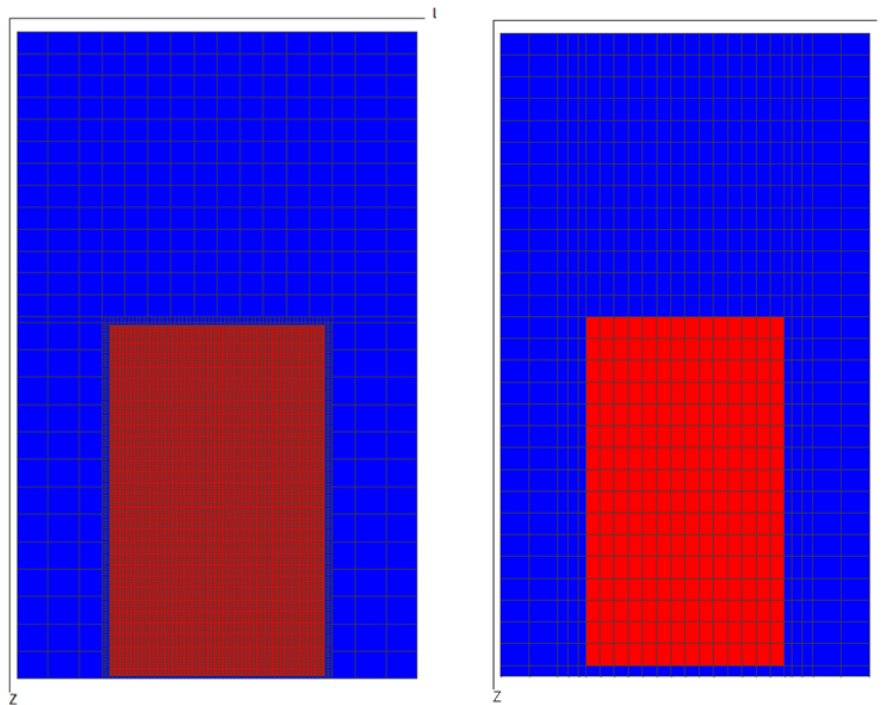


Figure 35 – The Cross-Section in X-Direction for the Test-Water Model: a Coarsened Regular GRID (Left) and a Tartan GRID (Right). Scale 2:5.

In the tartan grid, the cell size on the plug zone of the static model was modified, which led to the change of the size of the cells above the sample zone and the height of the layer below the core. No coarsening keyword was used in the tartan grid in contrast to the orthogonal grid used in the history matched model.

As a result of the grid alteration, the polygon used to identify the plug fluid-in-place region was changed. Z cross-section of the new model is shown in Figure 36. The cross-section of the plug region has a more angular shape and a smaller bottom area.

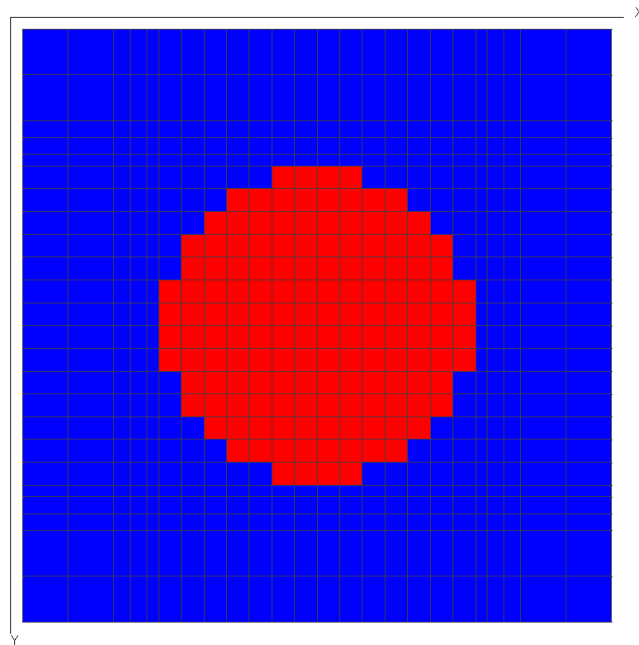


Figure 36 – The Cross-Section in Z-Direction for the Tartan GRID of the Test-Water Model. Scale 1:1.

The new region for the sample has reduced total volume, which means that the porosity is higher than in the regular grid size model. The difference in proportions and the number of cells is shown in Table 12.

Table 12 – A Comparison Between the Regular Grid and the Big Grid Test-Water Model.

Parameter		Regular GRID	Big GRID
Grid	Total Model	68x68x144	24x24x30
	Plug Region	2500x128	148x16
Area of the Bottom, cm ²		4.73	4.48
Porosity, %		34.03	35.93

Overall, the shape of the oil saturation profile is similar to the regular grid model (Figure 37): the values decrease from the centre of the core to the sides. There is also an increase of the oil

saturation towards the bottom of the core plug. However, the distribution of oil saturation in the vertical direction is different in the centre part of the plug.

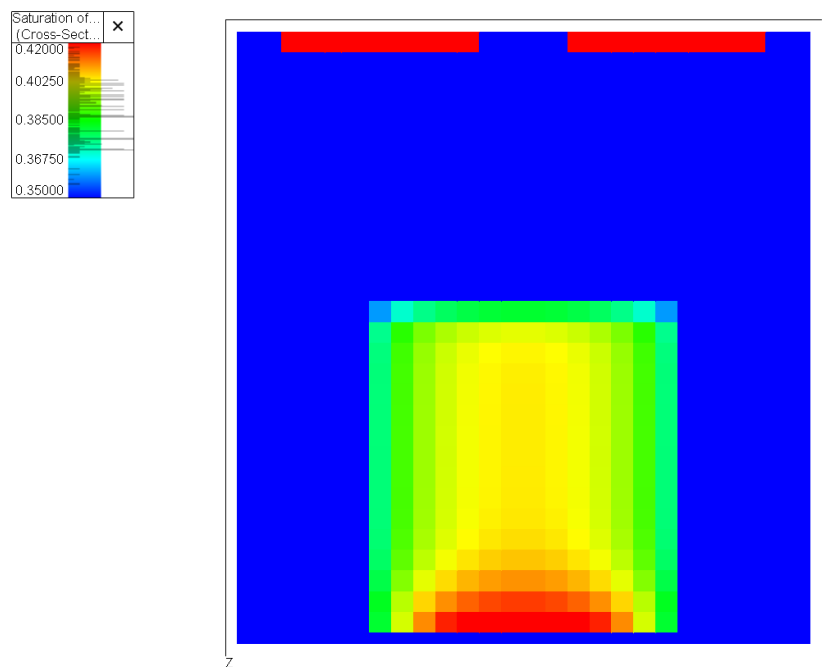


Figure 37 – Oil Saturation Profile after 25 Hours (*X* Cross-Section) for the Tartan GRID of the Test Water Simulation Model. Oil Saturation Scale is 0.35-0.42. Scale 2:3.

The comparison of the cumulative oil production in two different grid sizes is shown in Figure 38 for the history match probability cases. The cumulative oil displaced after 25 hours is almost the same for both models. However, the values at the first time-step differ.

After pressure equilibration, more oil is displaced from the plug region for the new tartan grid model. As the grid is coarser, the higher is a pressure drop between cells and, as a result, faster is an oil displacement. When the effect of spontaneous imbibition decreases the plots of production for the two grids overlap each other. The difference between plots increases with an increase in cumulative oil production (from P90 to P10 case).

According to (Alzayer, et al., 2017) in the core-scale, the use of a finer grid allows to mitigate numerical dispersions; hence, the water-breakthrough is slower. In a coarser grid, the pressure drop is sometimes high, which dominates the effect of capillary pressure on fluid-flow behaviour. The study described in the paper is related to the oil production driven by injection or an aquifer, which is different than the spontaneous imbibition process. Still, it can be assumed, that in work on the core scales of spontaneous imbibition processes it is better to have a small enough grid to ease numerical pressure distribution errors and, as a result, avoid a fast oil displacement at the beginning of production.

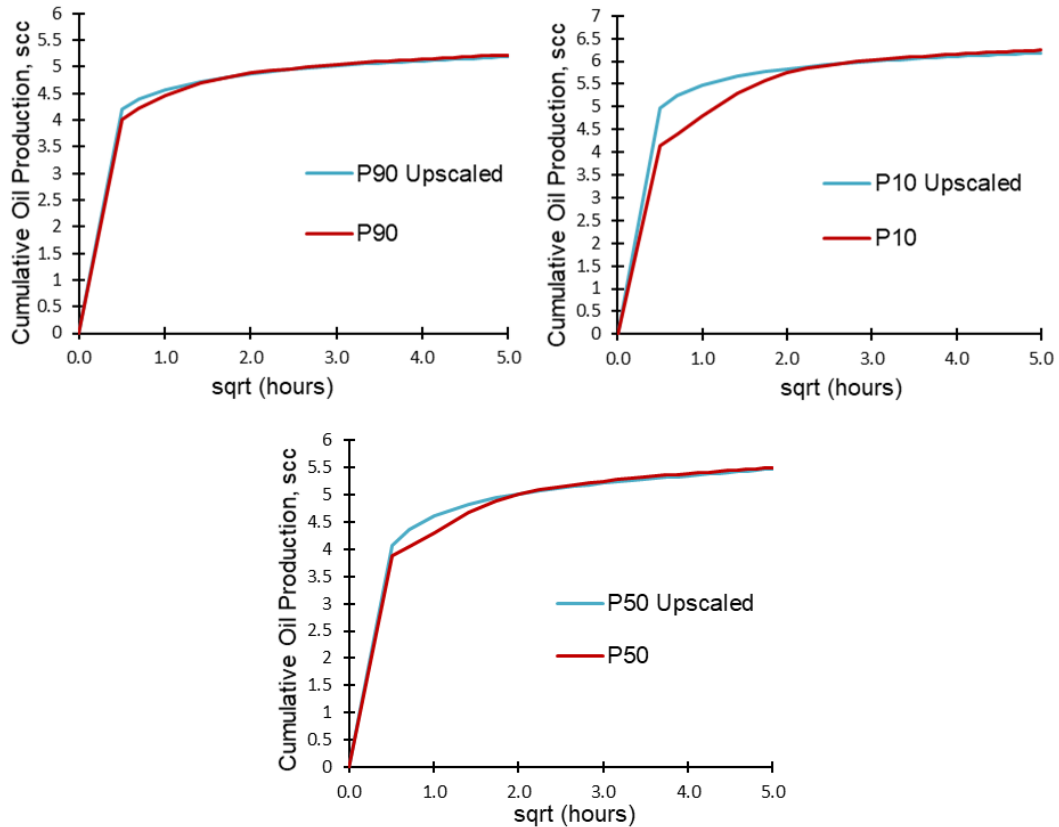


Figure 38 – The Cumulative Oil Production for the History Match Probability Cases for the Regular (in red) and the Tartan GRID (in blue) of the Test-Water Model.

4.2.2 Simulation Model for the Alkali Experiment

In the alkali simulation model, the fluid properties of the core region stay the same as for the test-water simulation model. In the fully water-saturated zone, the properties of the fluids are assigned as described in 3.3.2 for the alkali solution.

The main focus was put on the parameters regarding the alkali properties: the ability to decrease IFT between oil and water and, as a result, an increase of the capillary number. The values of the variables of the history matched simulation case for the test-water model (P50 case) were used to check the influence of the surfactant specific keywords on the oil production results. Additionally to the variables used in the history match for the test-water simulation model, the parameters for the surfactant option were set to the values shown in Table 13. Initial values for interfacial tension are described in 4.1.4.

Table 13 – Additional Variables for Alkali Simulation Model. Initial Values.

Parameter	Value
IFT @ zero surfactant concentration	2.5 mN/m
IFT @ maximum surfactant concentration	0.334 mN/m
Capillary Number for Immiscible case	10e-6
Capillary Number for Miscible Case	10e-5

The simulation of the alkali model shows an increase in cumulative production in comparison to the test-water model due to the decrease of the interfacial tension between oil and water. The results of the two models are shown in Figure 39, where the test-water model corresponds to the history-matched case (P50). In addition to the increased production at the first time-step, the slope of the alkali model is higher than for the cumulative production in the test-water model. However, the volume of the oil produced after 25 hours in the first alkali simulation model is more (7.4 scc.) than the volume got from the laboratory experiment.

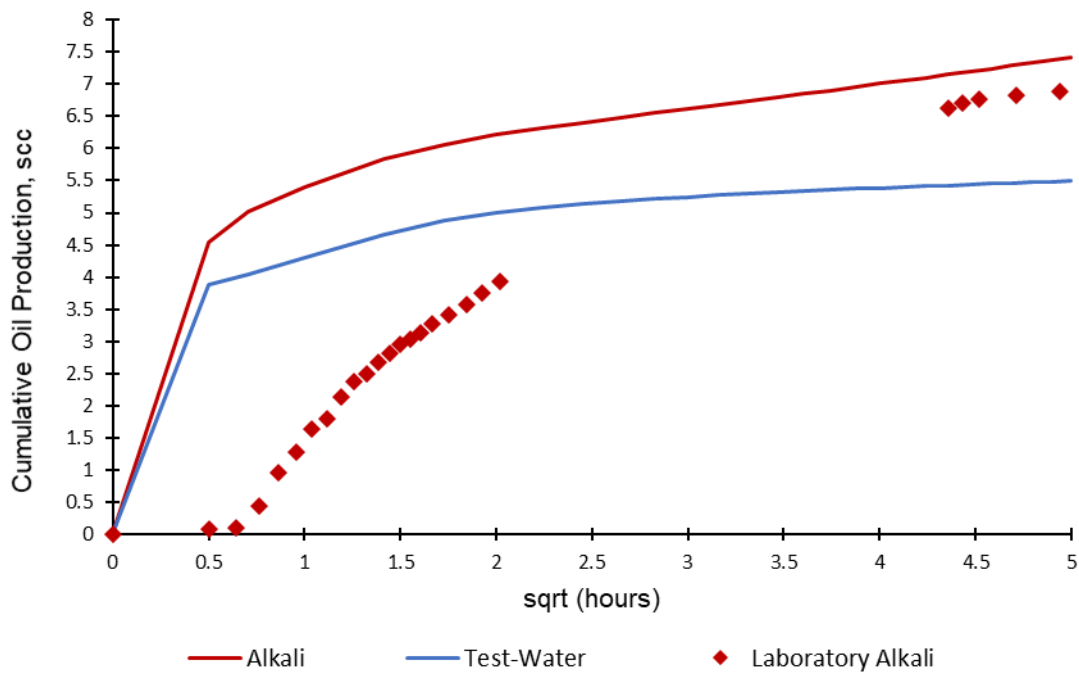


Figure 39 – The Cumulative Oil Production for the History Matched Test-Water Model and the Alkali Model with the same Values for Variables and Initial Values for the Surfactant Keywords.

Figure 40 shows the simulation cases for the history match. The red dots in the graph represent the laboratory experiment results. The volumes were not read in the time-frame from 4 to 18 hours in the laboratory.

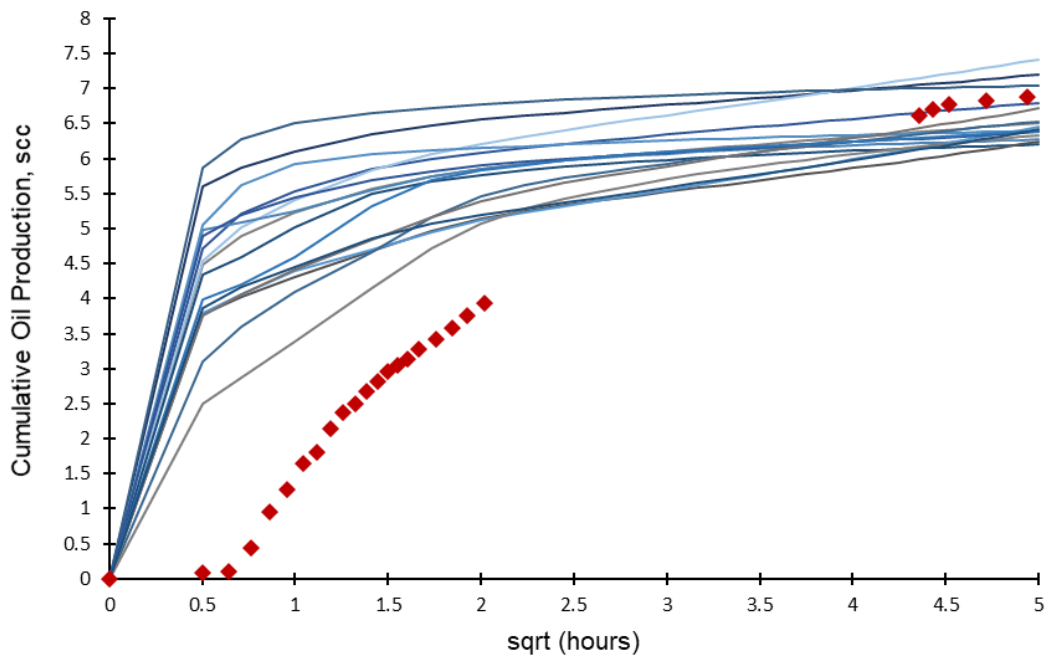


Figure 40 – The Cumulative Oil Production for the History Match of the Alkali Simulation Model. k_v/k_h is Fixed and Equal to 0.63. Blue lines Indicate Created during History Match Models, and Red Dots Correspond to the Laboratory Data.

The cumulative oil production after 25 hours is 6.88 scc. in the laboratory experiment. The simulation cases were chosen in the range of 6.2-7.5 scc of the total oil produced.

The induction time of 40 minutes of the oil displacement is observed in the laboratory experiment. A reduction of the IFT by the alkali leads to a decrease in the capillary pressure and therefore, a decrease of the imbibition rate. The slope of the plot of the laboratory results in the alkali solution is smaller than for the water experiment. At the same time, due to an increase in the capillary number, more oil can be extracted from the rock. Hence, the total production in the alkali experiment is higher in comparison to the amount of oil produced by test-water imbibition.

As can be seen from the graphs, again none of the simulation cases gives the same production results as the real laboratory data within the first hours of the experiment. If the induction time is not accounted for, the slope of the production curve from the laboratory can be matched by the decrease of the IFT for the maximum alkali (surfactant) concentration down-to ultra-low values close to zero. Some of the models show such slope in Figure 40. However, these models do not provide the same cumulative produced volume after 25 hours. Therefore, only the production points at the time steps from 18 to 25 hours are taken into account for the history match. Two simulation cases give the best match for the latest production. These cases are

shown in Figure 41. The first models give 6.72 scc of cumulative oil production, and in the second model, 6.8 scc. of oil is displaced.

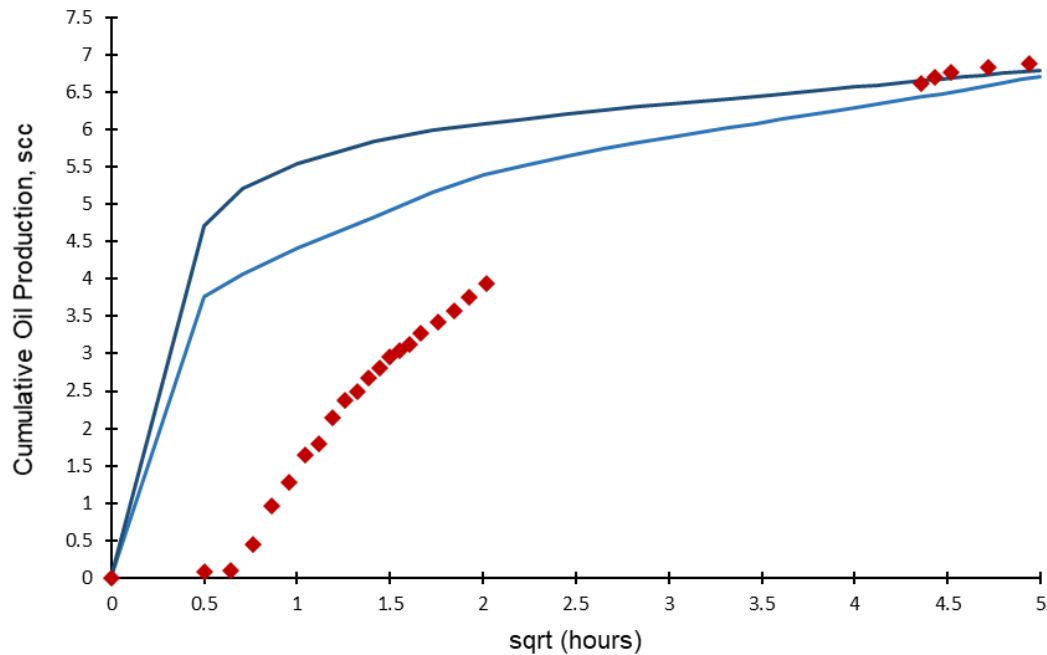


Figure 41 – The Cumulative Oil Production for the Best Achieved Simulation Cases of the History Match for the Alkali Simulation Model. Red Dots Correspond to the Laboratory Data.

The values of the variables for the two cases shown in Table 14. As was mentioned in the discussion of the test-water results, the values of parameters presented in the table and the results of the saturation profiles are not counted as representative for the real laboratory experiment. The mismatch of the early production indicates that some mechanisms are missing in the simulation model and should be investigated in the future work Residual oil saturation decreases by the influence of alkali. As the interfacial tension declines, less oil is trapped by capillary forces in the rock. Relative permeability curves for the immiscible case (before alkali injection) still characterize the system as water-wet. The shape of the capillary pressure curve and the values of the maximum capillary pressure are close to the ones that were received from the test-water experiment. The values of the capillary number before alkali imbibition are similar in both models and close to $10e^{-6}$.

Table 14 - Values of the Variables for the History Match Simulation Cases of the Alkali Model.

Case #	Cum.Oil Prod.	k_{rorw}	k_{rwr}	n_{ow}	n_w	$S_{owcr}(0)$	$S_{owcr}(Al.)$
1	6.72 scc.	0.95	0.46	3.67	4.33	0.11	0.03
2	6.80 scc.	0.78	0.36	3.25	7.31	0.23	0.08

Case #	P_{cow}	n_{pw}	IFT(0)	IFT(Al.)	$\log(Nc(0))$	$\log(Nc(Al.))$	$S_{wcr}(Al.)$
1	0.43	11.11	3.27	0.18	-5.88	-3.29	0.41
2	0.73	10.92	6.37	0.27	-5.95	-4.57	0.39

The most important parameters that are taken from the history match are the capillary number and the residual oil saturation before and after the alkali imbibition. The relationship between variables is described by the capillary desaturation curve. CDC indicates the sizes and arrangement of pores in the rock and distribution of wetting and non-wetting phase in the pores (Guo, et al., 2017). The effect of chemical flooding is usually related either to an increase of the sweep efficiency or an increase of the capillary number. Traditionally it is considered that the CDC describes the change of the displacement efficiency; the sweep efficiency is neglected on the curve.

Increase of the microscopic displacement efficiency is related to a decrease of residual oil saturation. The larger the capillary number is, the lower is the residual oil saturation. When the capillary number exceeds a certain number, the so-called critical capillary number, the oil droplets break up into smaller droplets, leading to partial mobilization of oil (Guo, et al., 2017)

The critical capillary pressure is one of the variables used for the history match. The laboratory studies showed that for the water-wet sandstone, the critical capillary number is around 10^{-5} (Humphry, et al., 2013). However, higher permeabilities of the rock lead to a reduction of the capillary number (Garnes, et al., 1990). The values observed for the two history matched models are consistent with the studies and close to 10^{-6} .

During the simulation, it was discovered that not only the critical capillary value and the change in residual oil saturation affect oil production. The slope of the curve after the critical value also plays an important role in combination with other variables. The tangent of the angle, shown in Figure 42, varies from 0.02 to 0.1 for the range of the history matched simulation cases.

As was described in 4.1.5, the CDC in the simulator is described through the miscibility factor, where the miscibility factor of zero corresponds to the immiscible region – test-water and oil in the core. When alkali (surfactant) imbibes into the rock due to the decrease of the interfacial tension between two phases, the displacement of oil close is close to miscible, which corresponds to the miscibility factor of zero. As the IFT drops, the capillary forces decrease, the capillary number rises. The dependency of the miscibility factor on the capillary number of the two history matched simulation cases is shown in Figure 42.

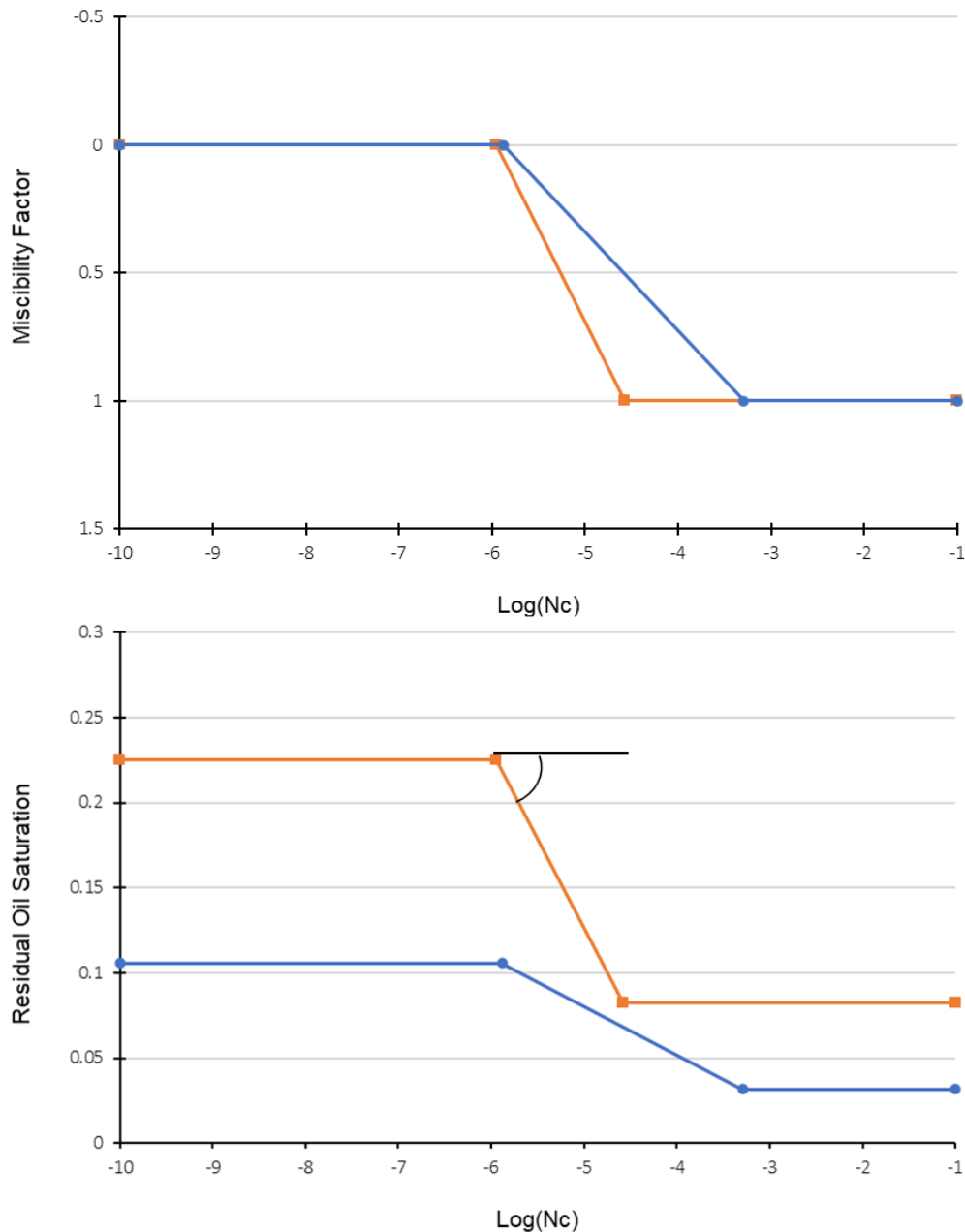


Figure 42 – The Capillary Desaturation Curve as a Function of Miscibility Factor (Top) and Residual Oil Saturation (Bottom). The Orange Line is for the Case 1, and the Blue Line is for the Case 2 of the History Match.

The CDC from the simulator (Miscibility factor vs N_c) is converted into the typical classical CDC (S_{or} vs N_c) using the relationship of the miscibility regions with corresponding residual oil saturation. Both graphs are shown in Figure 42.

The cumulative oil production after 25 hours is closer to the historical data for the second case (Table 14). Therefore, the results of this simulation model will be described further in work. Saturation profiles for the vertical cross-section of the model are shown in Fig. 3, Appendix C. A scale of the oil saturation ranges from 0 to 0.5 for a convenient comparison of the figures with the test-water simulation model results. The water imbibes from all sides of the plug region. On the first time-steps, the cross-section of the plug region can be divided into three zones: 1) the cells close to the edges of the core region; 2) the central zone of the core; 3) the cells between zone 1 and 2 (Figure 43).

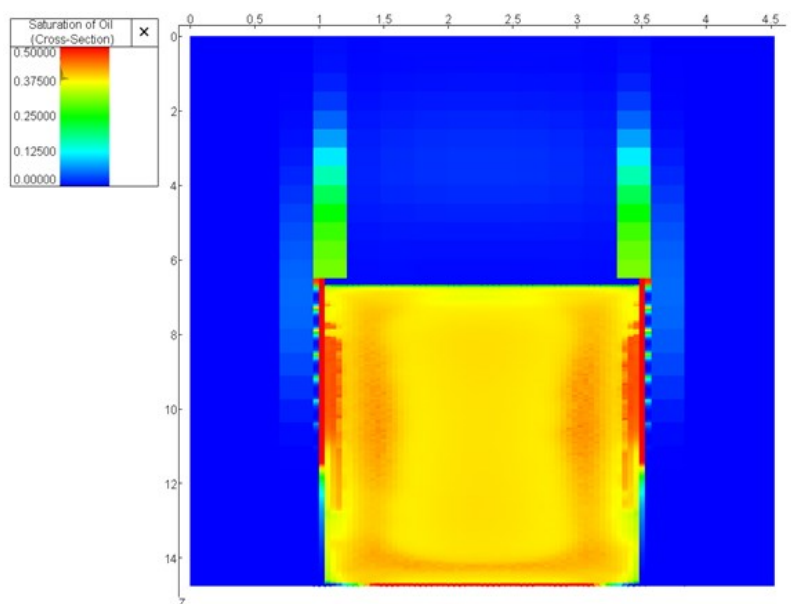


Figure 43 – Oil Saturation Profile for the Central X Cross-Section for the History-Matched Alkali Simulation Model after 1 Hour. Oil Saturation Scale is 0.0-0.5. Picture Scale 2:3.

The highest oil saturation is in the third zone, the lowest is observed at the bottom and the top layers of the core region. The central part of the core (zone 1) has an intensive drop of the oil saturation as well, which did not happen in the test-water model. This phenomenon is related to the difference in the water compositions used as an imbibing fluid. In the test-water experiment, the water at the irreducible water saturation in the core plug and the water used as the imbibing fluid has the same physical and chemical properties. In the second experiment, the imbibing fluid is the alkali solution, so there are three different phases (oil, test-water, and alkali solution) involved in oil production. When the alkali imbibes the core plug, it pushes both the oil and the core water, creating an oil bank. An approximate illustration of the oil bank creation

is shown in Figure 44. Due to capillary pressure diffusion, the smearing out of the sharp front is taking place, but for simplicity, this effect is not included in the figure.

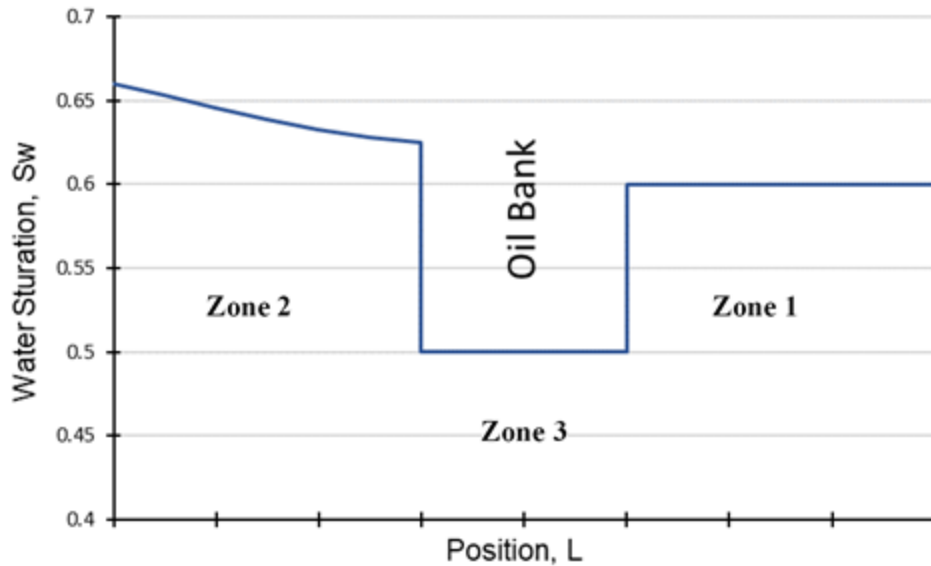


Figure 44 – A Simplified Example of The Water Saturation Profile for the Case of an Oil Bank Creation. No Smearing Effects Influenced by Capillary Pressure Diffusion are Included.

The alkali solution is displacing both the oil and the water from the pores. The core water flows faster than the oil in the core, as it is more mobile, and pushes the oil from the plug to be produced. Hence, in the central zone of the cross-section of the core region, there is a decrease in the oil saturation observed. The slower phase (the oil) displaced by the alkali solution and overpassed by the core water; it creates an oil bank such as zone 3 in the cross-section. At the same time, the diffusion of alkali is happening, as the concentration of the alkali in the water is different outside and inside of the core.

Overall, the oil saturation in the core plug region of the alkali model is lower than in the test-water model after 15 minutes of the production. This contradicts to the laboratory experiments, where the rate of the oil production is much lower at the first hours for the alkali experiment than for the test-water.

The oil flows out of all the surfaces of the plug region similarly to the test-water experiment. This means that again flow behaviour is more counter-current dominated at the early stage of the production. The decrease of the IFT leads to a fast reduction of the bubble pressure, hence the effect of the co-current flow behaviour is seen earlier than for the test-water experiment. The production from the lateral surface of the plug stops after an hour, further in time oil is displaced only upwards. In the test-water experiment, the shift of the flow behavior happens after two hours.

However, in the experimental production curve is more in agreement with the gravity dominated case from the sensitivity study showed in **Error! Reference source not found.** Small oil displacement at the beginning, slow spontaneous imbibition process and high recovery further are clear indicators of the gravity dominated co-current SI. It could be that achieved IFT values, in reality, are even lower than the ones collected from the history match.

As the capillary pressure decreases with an increase of the water saturation, the effect of the spontaneous imbibition declines and the oil is driven mostly by gravity segregation. Hence, the oil saturation at the bottom of the core is lower – 0.125 in average (light blue in Fig. 3, Appendix C). The amount of the oil displaced downwards, to the layer between the plug region and the bottom of the model (the Amott cell), decreases with time. The oil accumulated in this layer starts to enter the core plug. This process is indicated as the presence of the reddish layer on the lower part of the core region in the figures for 2-10 hours (Fig. 3, Appendix C).

After 25 hours of the production, there are two peaks on the oil saturation scale: the average oil saturation is 0.35 in the upper part of the plug region, and the oil saturation is 0.13 for the lower part of the plug region (Figure 45). The oil is mostly displaced from the bottom of the core plug and in the middle part of the plug from the side.

As all faces of the plug are open, the created imbibition front has an extremely complex nature. The flow cannot be described as a linear or radial flow. The saturation profile has a toroidal shape. It is better visible for the alkali model than for the test-water model. Mason et al. (2008) suggest that the flow can be described as a combination of toroid ring and cones, as described in 2.4.2.1. However, in the alkali model formation of the cones has not happened. The toroidal ring is clearly visible from the beginning of the run until 25 hours as in both saturation profile figures and alkali concentration profiles (Fig. 5, Appendix C). One explanation for this could be that the simulation time is not long enough for the cone formation, and the radial flow is dominated. Another possible reason is the existence of the co-current flow behaviour from the beginning of the production, which does not allow the cones to develop.

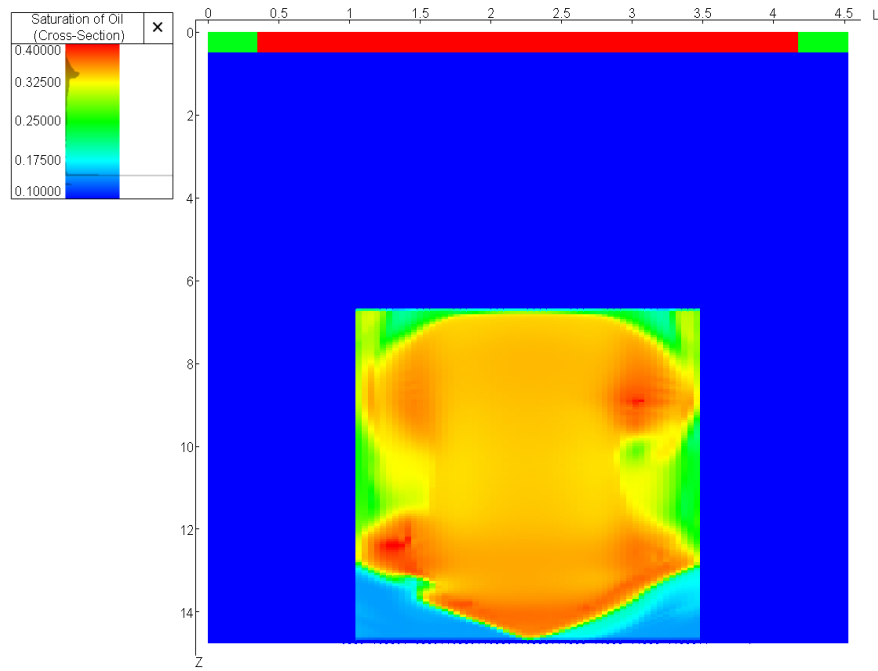


Figure 45 – The Oil Saturation Profile after 25 Hours (X Cross-Section) for the Alkali Simulation Model. Oil Saturation Scale is from 0.13 to 0.4. L:Z is 1:3.

The radial flow of the fluids is shown in the horizontal cross-section of the core at the half of the plug height (Figure 46). The oil saturation decreases from 0.35 at the centre of the plug to 0.25 at the edges of the sample. The total oil recovery is higher than for the test-water model, which is visible on the 3D view (Figure 47) as a higher number of the grid cells at the top layer of the simulation model is occupied by oil.

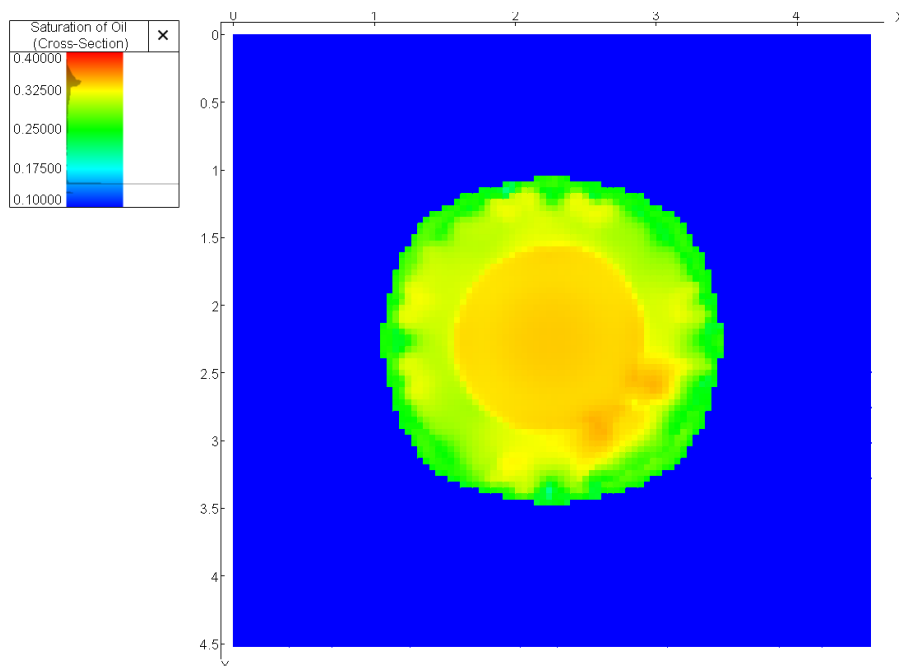


Figure 46 – The Oil Saturation Profile after 25 Hours (Z Cross-Section) for the Alkali Simulation Model. Oil Saturation Scale is from 0.3 to 0.4. X:Y is 1:1.

The alkali solution imbibes into the core region with a high speed at the first time-step. Hence, an extremely high volume of oil is displaced on the first step. As a result of the drastic drop of the oil saturation in the grid cells, the decrease of the capillary pressure of the oil-water system is observed. The capillary pressure distribution on the vertical cross-section of the model is shown in Fig. 4, Appendix C. The average capillary pressure drops from 0.73 atm to 0.0002 atm. The decrease is higher than for the test-water model, due to the reduction of IFT by alkali solution. The distribution of the capillary pressure in the grid cells with time confirms the imbibition of the chemical solution from all sides of the core plug. The maximum value of capillary pressure at the last time-step is 0.00001 atm like the value from in the test-water simulation model.

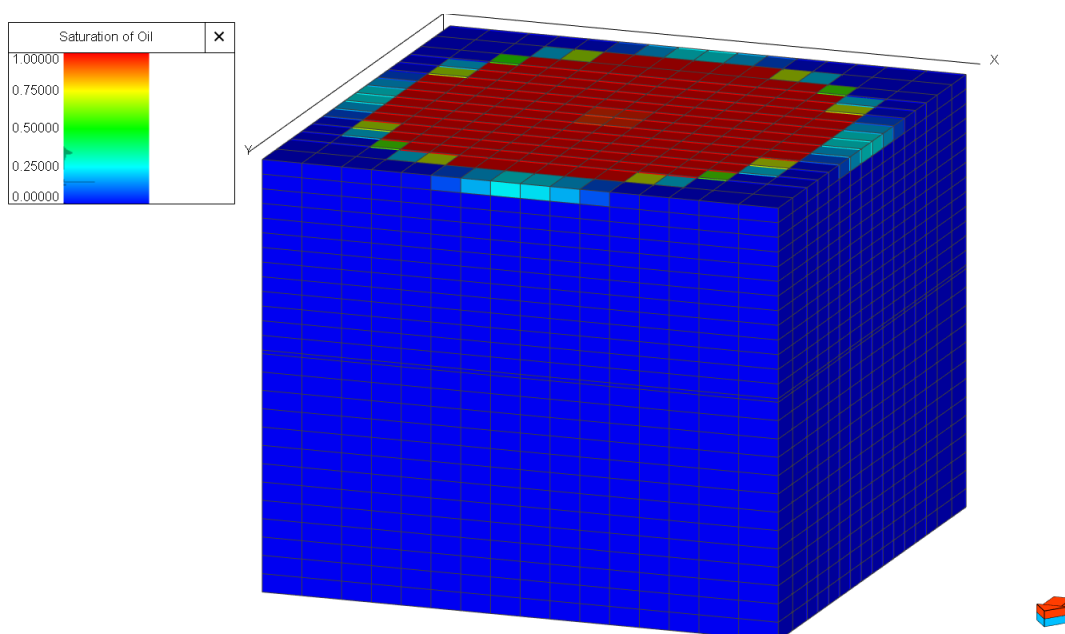


Figure 47 – 3D Oil Saturation Profile after 25 Hours for the Alkali Simulation Model. X:Y:Z is 1:1:3.

4.2.3 Simulation Model for the Alkali-Polymer Experiment

The last simulation model was created for the alkali-polymer spontaneous imbibition experiment. Polymer parameters were added in addition to the keywords used for the alkali simulation model: polymer adsorption, dead-pore volume (DPV) and a residual resistance factor (RRF).

Unfortunately, no history match was achieved in the study. Around 30 simulation runs were made using 16 variables in the history match. However, all models showed the maximum value of the cumulative oil production around 5.7 scc. In the laboratory experiment, the volume of displaced oil after 25 hours from the beginning of the experiment is 7.1 scc.

A sensitivity study was performed to understand the impact of each polymer and alkali property on oil production. DPV, RRF, Maximum Polymer Adsorption and IFT were varied individually in five different simulation cases. The values of the variables are shown in Table 15, where the first case is used as a base for the sensitivity analysis. The values of other variables, like parameters of the permeability curves and capillary curve, the ratio of vertical to horizontal permeability and the IFT were taken from case 2 of the alkali experiment.

During the trial of the history match, the residual resistance factor higher than 5 resulted in errors in the model; therefore, for the sensitivity study, the parameter was varied from 0 to 3. The lowest polymer adsorption at the maximum concentration of the polymer in the solution (2000 ppm) was used for the study. In the base case, the adsorption was neglected. The interfacial tension was set to zero in the fifth simulation case.

Table 15 – Sensitivity Study for the Alkali-Polymer Model Based on the Change of the Individual Variable for each Simulation Case (IFT, DPV, RRF, and Polymer Adsorption).

Case	DPV	RRF	Max. Adsorption	IFT (0)	IFT(Surf)
1	0	1	0	6.37	0.27
2	0.3	1	0	6.37	0.27
3	0	3	0	6.37	0.27
4	0	1	18.2e-7	6.37	0.27
5	0	1	0	2.5	0

The plots of the cumulative oil production for the sensitivity cases and the results from the laboratory experiment on the Amott cell are shown in Figure 48. According to the plot, none of the polymer keywords influences production. The change of the slope of the graph is observed for the case 5, where the interfacial tension between water and oil decrease by 2.55 times and the interfacial tension between oil and water with the presence of alkali is assumed to be zero. The reduction of the IFT affects the production rate and at the same time allows to produce a higher final amount of oil from the plug. However, the cumulative volume of oil displaced after 25 hours for the 5th sensitivity case is still 0.5 scc lower than in the laboratory experiment. More simulation cases and sensitivity studies should be performed in order to achieve a good match.

The form of the production is similar to the alkali SI. The flow is characterized as more gravity dominated, which corresponds to the low displacement rate.

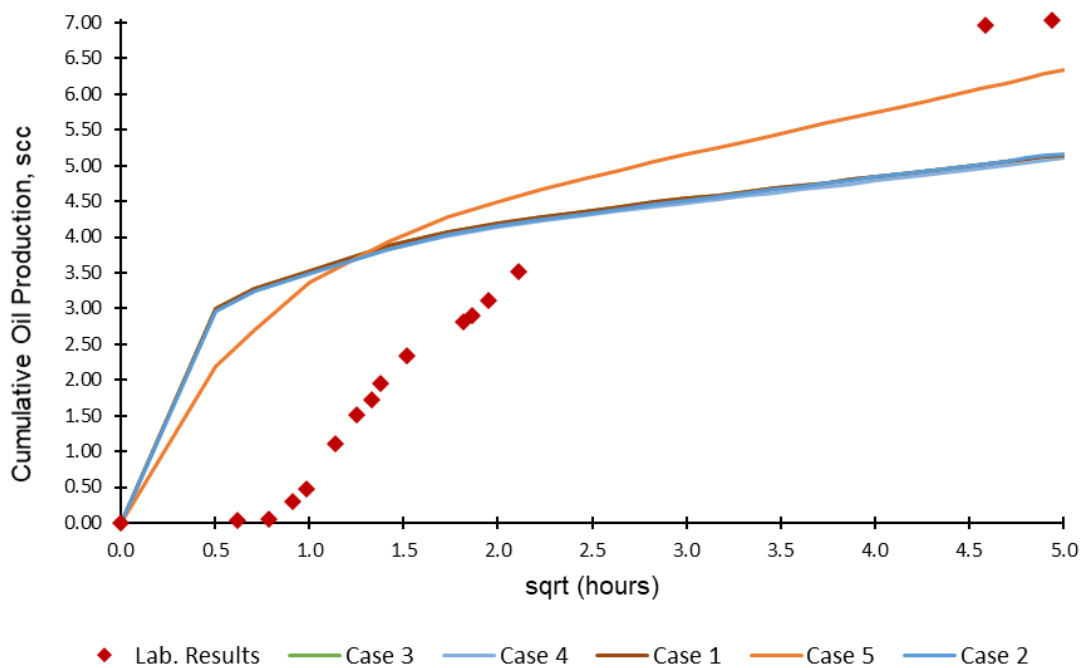


Figure 48 - Sensitivity Study for the Alkali-Polymer Model Based on the Variables IFT, DPV, RRF, and Polymer Adsorption.

The Pearson correlation coefficients for the variables over time are shown in Figure 49. The coefficients are calculated based on the five cases. The plot confirms the high influence of IFT on the production and elimination of the effect of the polymer keywords.

Among polymer parameters, the highest impact at the beginning of the production is by residual resistance factor. The residual resistance factor indicates effective water permeability reduction, which slows down the flow of the water in the core. Hence, oil production is slow as well. That is confirmed by the production curve. As RRF is connected to the adsorption, the Pearson coefficient of the adsorption has the same shape. The lowest impact is by the dead-pore volume. DPV has the opposite effect on water flow rates. Faster water breakthrough should be expected when the pores are plugged by the polymer.

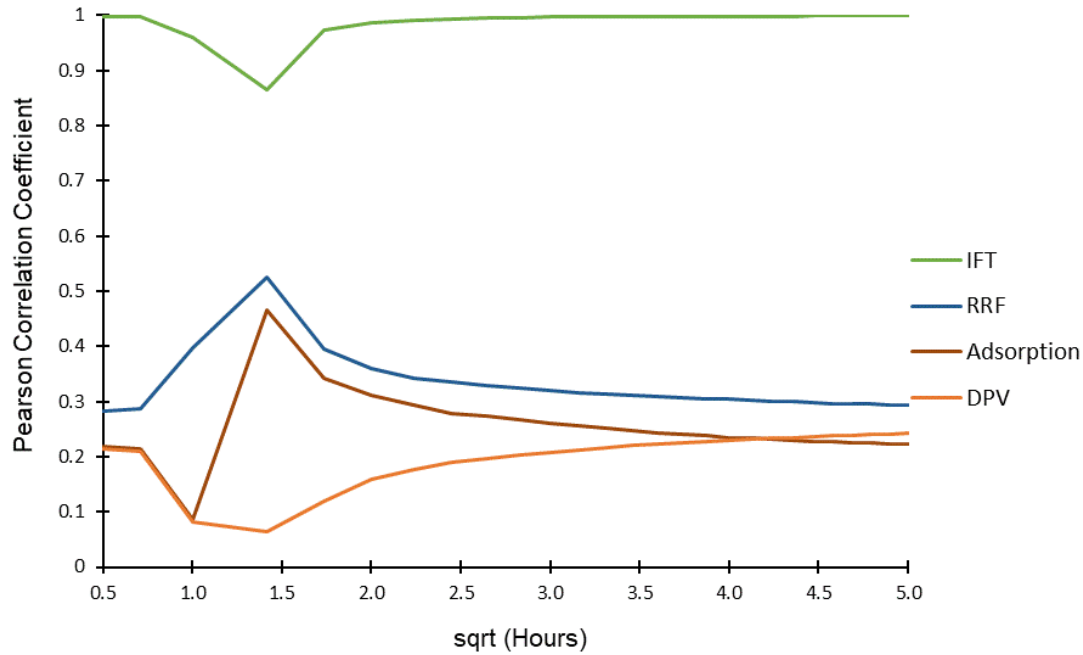


Figure 49 – Pearson Correlation Coefficient as the Function of Time for the Variables (IFT, RRF, Polymer Adsorption, DPV) Used in the Sensitivity Study for the Alkali Simulation Model.

In reality, the values of IFT for the alkali-polymer solution are lower than for the alkali only. Two possible reasons are mentioned by Arekhov (2019): 1) introduction of polymer into the solution leads to the reduction of the alkali concentration; 2) slower diffusion of sodium carbonate molecules due to high viscosity of the polymer. This means that the decrease of the IFT in the sensitivity down to a value of zero does not align with the laboratory experiments on interfacial tension evaluation. Hence, it is not correct to manipulate the production from the model by such reduction of the IFT. Other possibilities to achieve a history match in the alkali-polymer model, as well as the reasons for the absence of the effects of the polymer keywords, should be investigated.

Chapter 5

Conclusion

5.1 Summary

Three simulation models were built for spontaneous imbibition experiments in the Amott cell. The data from the laboratory experiments was used as an input for fluid and rock characterization, and the results of the oil production by SI were taken for the history matching of the models. The conclusions of the work will be presented in the chronological order separately for each model.

5.1.1 Test-Water Model Results

The first simulation model was built for the experiment with test-water as imbibing fluid. Capillary pressure curve and relative permeability curves were used as variables for the history matching. The relationship of the capillary and gravity forces was studied through sensitivity study. The controlling parameter for gravity was the relationship of vertical to horizontal absolute permeabilities. It is assumed, that with the decrease of the ratio of vertical permeability to the horizontal permeability, the flow of the fluid in the upward direction is slowed down. Therefore, the production of oil by gravity segregation is suppressed. Capillary forces were controlled by the value of the maximum capillary pressure. It is concluded from the sensitivity study, that the oil displacement on the early stage is highly dependent on the capillary pressure and the effect of the gravity forces is minor. However, it does not mean that the absence of ultra-low values of capillary forces will lead to zero oil production. In contrast, cumulative oil production for the strongly gravity dominated SI is higher after 25 hours than for the strongly capillary dominated cases. Hence, capillary forces are important at the beginning of the SI, while gravitational force plays a major role later in production.

In the main work on the test-water model, a good history match to the experimental results was achieved only for the late production. However, the production at the first time-steps is much higher in the model than in the laboratory. Two reasons for the discrepancy are offered: 1) numerical pressure equilibration problem, 2) induction time. The first one is related to the simulation model and may be solved with other types of initialization of the model. The second reason is applied for the laboratory experiment and connected to the back-capillary pressure (bubble pressure) on the faces of the core. Bubble pressure opposes to the capillary drive and slows down the production. In addition, oil bubbles that create back-capillary pressure are stuck on the surface of the core till they achieve a certain size. Hence, the volume measurements in the graduated tube of the Amott cell are lower than the amount of volume displaced in reality. The results of the capillary pressure curve and relative permeabilities should not be count as a perfect representation for the laboratory experiment due to the mismatch of the model for the low water saturations in the core region.

Different stages of the flow are observed from the saturation profile on the model cross-sections. At the early stage of the production, oil is displaced from all surfaces of the core, indicating counter-current type of spontaneous imbibition. With time shift from the counter-current to co-current SI is observed after 2 hours of production. The oil at this moment is produced in an upward direction. The oil that at the beginning was displaced downwards starts to enter the core plug, which is indicated by high oil saturation at the bottom of the core. The stages of counter-current, mixed flow and co-current imbibition are observed from the oil production plot. Obtained results of the simulation agree with the conclusions of SI simulations described in the different articles.

The change of the grid size did not show a considerable discrepancy in oil production results. However, in order to mitigate early breakthrough and ease numerical pressure distribution error, it was decided to perform further work on the smaller grid size.

5.1.2 Alkali Model Results

The second simulation model was built for the alkali SI experiment. In addition to capillary pressure and relative permeabilities, IFT between oil and water was used as a variable for the history match. The simulation results showed a sufficient history match for the laboratory data only at the late time-steps. Oil production curve at the early stage had an even bigger difference between the simulation and laboratory results than the one observed in the test-water model. In addition to the described reasons, lowering of the IFT down-to ultra-low values can give the same slope of the production curve as for the experimental outcomes, which is proved by some simulation cases.

Capillary saturation curve was one of the important outcomes of the study. The values of the capillary number after alkali imbibition are in agreement with the values reported in the articles for the same rock characteristics.

The results of the alkali model show the same SI stages as for the test-water model. The shift from the counter-current to the co-current flow is observed earlier, after 1 hour. However, the oil production curve obtained in the laboratory looks more like gravity driven flow from the beginning of the production while in the model the capillary forces still play an important role at the first stage of spontaneous imbibition. It could be that the IFT values achieved in the laboratory experiment are even lower than the ones given by the simulation model.

Saturation profiles for the alkali model differ from the test-water model. Due to the presence of three different fluids (oil, test-water and alkali), the creation of the oil bank is observed. The flow cannot be described as radial. The displacement front is propagated as a toroidal ring. However, the formation of the cones did not happen, which may be explained by the early co-current flow that does not allow cones to develop.

5.1.3 Alkali-Polymer Model Results

The third simulation model was created for the alkali-polymer experiment. Unfortunately, no history match was achieved for this model. The shape of the production obtained in the laboratory suggests the same flow behaviour as for the alkali model with the gravity segregation as the main driving force. The cumulative oil production, however, is higher for the alkali-polymer spontaneous imbibition.

Sensitivity study for the polymer parameters and the IFT was performed. The study showed the most impact of IFT on early production. With the decrease of the IFT capillary pressure decreases and the co-current SI is observed. Among polymer parameters, the most impact is by residual resistance factor. As RRF is increased, the effective water permeability is decreased. Therefore, slow water flow and oil displacement are expected. The smallest correlation coefficient with oil production is for the dead pore volume, as the increase of DPV should correspond to the fast water breakthrough, which is not the case in the outcomes.

5.2 Evaluation

The scope of the thesis was not accomplished fully, as no history match was achieved for the alkali-polymer model. Hence, it is hard to evaluate the impact of the polymer on the spontaneous imbibition and the difference of the alkali and alkali-polymer imbibition.

The mismatch of the production curves at the early stages in the alkali model questions the values of the IFT obtained by the simulation and the relative permeability curves. Therefore, it

is hard to evaluate the types of flow and capillary/gravity forces relationship in the SI from the model.

5.3 Future Work

For the future work on the simulation of the spontaneous imbibition in the Amott cell, the following recommendations can be considered:

- 1) Other methods of the model initialization other than forced pressure distribution can be applied in order to eliminate the numerical pressure equilibration problem.
- 2) Radial type of grid cells will be better for the cylindrical flow simulation.
- 3) Another AHM tool should be considered to speed up the history matching procedure.
- 4) Global sensitivity analysis (GSA) can be performed in addition to the local sensitivity studies to see the impact of the parameters on each other and for a better understanding of the influence of the parameters on the oil displacement. It will allow to decrease the amount of the variables for the history match and therefore, decrease the time need.
- 5) More runs and studies on the model should be done to fully understand the reason for the mismatch of oil production at the early time-steps between simulation models and the laboratory experiments.

Chapter 6

References

- Ahmed, T., 2019. *Reservoir Engineering Handbook*. 5 ed. Cambridge: Gulf Professional Publishing.
- Alpak, F., Lake, L. & Embid, S., 1999. *Validation of a Modified Carman-Kozeny Equation to Model Two-Phase Relative Permeabilities*. Houston, SPE Annual Technical Conference and Exhibition.
- Alzayer, H., Jahanbakhsh, A. & Sohrabi, M., 2017. *The Role of Capillary-Pressure in Improving the Numerical Simulation of Multi-Phase Flow in Porous Media*. Abu-Dhabi, SPE Reservoir Characterisation and Simulation Conference and Exhibition.
- Andersen, P. et al., 2019. Core Scale Modeling of Polymer Gel Dehydration by Spontaneous Imbibition. *SPE Journal*, 24(3), pp. 1201-1219.
- Arekhov, V., 2019. *Understanding Wettability Changes during Alkali-Polymer through Spontaneous Imbibition Data*. Leoben, Department of Petroleum Engineering, Montanuniversität.
- Babadagli, T., 2005. Analysis of Oil Recovery by Spontaneous Imbibition of Surfactant Solution. *Oil & Gas Science and Technology*, 60(4), pp. 697-710.
- Behbahani, H. & Blunt, M., 2005. Analysis of Imbibition in Mixed-Wet Rocks Using Pore-Scale Modeling. *SPE Journal*, 10(4), pp. 466-474.
- Bo, Q., Zhong, T. & Liu, Q., 2003. *Pore Scale Network Modeling of Relative Permeability in Chemical Flooding*. Kuala Lumpur, SPE International Improved Oil Recovery Conference in Asia Pacific.
- Brooks, R. & Corey, A., 1964. Hydraulic Properties of Porous Media. *Hydrology papers (Colorado State University)*, Volume 3.

- Bunge, A. & Radke, C., 1982. Migration of Alkaline Pulses in Reservoir Sands. *Society of Petroleum Engineers Journal*, 22(06), pp. 998-1012.
- Castor, T. P., Somerton, W. H. & Kelly, J. F., 1981. Recovery Mechanisms of Alkaline Flooding. In: D. Shah, ed. *Surface Phenomena in Enhanced Oil Recovery*. New York: Plenum Publishing, pp. 249-291.
- Cooke, C., Williams, R. & Kolodzie, P., 1974. Oil Recovery by Alkaline Waterflooding. *Journal of Petroleum Technology*, 26(12), pp. 1365-1374.
- Dada, A., Olalekan, A., Olatunya, A. & Dada, O., 2012. Langmuir, Freundlich, Temkin and Dubinin–Radushkevich Isotherms Studies of Equilibrium Sorption of Zn 2+ Unto Phosphoric Acid Modified Rice Husk. *IOSR Journal of Applied Chemistry*, 3(1), pp. 38-45.
- Dake, L., 1978. *Fundamentals of Reservoir Engineering*. Amsterdam: Elsevier.
- deZabala, E., Vislocky, J., Rubin, E. & Radke, C., 1982. A Chemical Theory for Linear Alkaline Flooding. *Society of Petroleum Engineers Journal*, 22(02), pp. 245-258.
- Fakher, S., Abdelaal, H., Elgahawy, Y. & Imqam, A., 2019. A Characterization of Different Alkali Chemical Agents for Alkaline Flooding Enhanced Oil Recovery Operations: an Experimental Investigation. *SN Applied Sciences*, 1(12), p. 1622.
- Fan, T. & Buckley, J., 2007. Acid Number Measurements Revisited. *SPE Journal*, 12(04), pp. 496-500.
- Fischer, H. & Morrow, N., 2005. *Spontaneous Imbibition with Matched Liquid Viscosities*. Dallas, Texas, USA, SPE Annual Technical Conference and Exhibition.
- Føyen, T. L., 2016. *Onset of Spontaneous Imbibition*. Bergen , Department of Physics and Technology, University of Bergen.
- Fulcher, R., Ertekin, T. & Stahl, C., 1985. Effect of Capillary Number and Its Constituents on Two-Phase Relative Permeability Curves. *Journal of Petroleum Technology*, 37(2), pp. 249-260.
- Garnes, J., Mathisen, A., Scheie, A. & Skauge, A., 1990. *Capillary Number Relations for Some North Sea Reservoir Sandstones*. Tulsa, SPE/DOE Enhanced Oil Recovery Symposium.
- Goda, T. & Sato, K., 2014. History Matching with Iterative Latin Hypercube Samplings and Parameterization of Reservoir Heterogeneity. *Journal of Petroleum Science and Engineering*. *Journal of Petroleum Science and Engineering*, 14(1), pp. 61-73.
- Guo, H. et al., 2017. Proper Use of Capillary Number in Chemical Flooding. *Journal of Chemistry*, pp. 1-11.

-
- Hamad, W., 2019. *Low Salinity Water Flooding by Spontaneous Imbibition*. Leoben, Department of Petroleum Engineering, Montanuniversität.
- Haugen, Å., Fernø, M., Mason, G. & Morrow, N., 2014. Capillary Pressure and Relative Permeability Estimated from a Single Spontaneous Imbibition Test. *Journal of Petroleum Science and Engineering*, 115(1), pp. 66-77.
- Hou, B., Wang, Y. & Huang, Y., 2015. Study of Spontaneous Imbibition of Water by Oil-Wet Sandstone Cores using Different Surfactants. *Journal of Dispersion Science and Technology*, 36(9), pp. 1264-1273.
- Humphry, K. et al., 2013. Impact of Wettability on Residual Oil Saturation and Capillary Desaturation Curves. *Petrophysics*, 55(4), pp. 1-11.
- Jennings, H. Y., Johnson, C. E. & McAuliffe, C. D., 1974. A Caustic Water flooding Process for Heavy Oils. *Journal of Petroleum Technology*, 26(12), pp. 1344-1352.
- Johnson, C., 1976. Status of Caustic and Emulsion Methods. *Journal of Petroleum Technology*, 28(01), pp. 85-92.
- Kalaei, M., Green, D. & Willhite, G., 2010. *Numerical Modeling of the Water Imbibition Process in Water-Wet Laboratory Cores*. Anaheim, California, USA, SPE Western Regional Meeting.
- Kang, W., 2001. Study of Chemical Interactions and Drive Mechanisms in Daqing ASP Flooding. *Petroleum Industry Press*.
- Kazempour, M., Sundstrom, E. & Alvarado, V., 2011. *Effect of Alkalinity on Oil Recovery during Polymer Floods in Sandstone*. The Woodlands, Texas, SPE International Symposium on Oilfield Chemistry.
- Krumrine, P. & Falcone Jr, J., 1983. *Surfactant, Polymer, and Alkali Interactions in Chemical Flooding Processes*. Dallas, Texas, SPE Oilfield and Geothermal Chemistry Symposium.
- Lagmuir, I., 1918. The Adsorption of Gases on Plane Surfaces of Glass, Mica and Platinum. *Journal of the American Chemical Society*, 40(9), pp. 1361-1403.
- Lake, L., 1989. *Enhanced Oil Recovery*. Englewood Cliffs, NJ: Prentice-Hall.
- Leverett, M., 1939. Flow of Oil-Water Mixtures Through Unconsolidated Sands. *Transactions of the AIME*, 132(01), pp. 149-171.
- Li, K. & Horne, R., 2001. An Experimental and Analytical Study of Steam/Water Capillary Pressure. *SPE Reservoir Evaluation & Engineering*, 4(06), pp. 477-482.

- Li, Y. R. D., Mason, G. & Morrow, N., 2006. Pressures Acting in Counter-Current Spontaneous Imbibition. *Journal of Petroleum Science and Engineering*, 52(1-4), pp. 87-89.
- Lu, H., 2005. *Improving Oil Recovery (IOR) with Polymer Flooding in A Heavy-Oil River-Channel Sandstone Reservoir*. Freiberg, Universitätsbibliothek der TU BAF.
- Mason, G. et al., 2012. Spontaneous Counter-Current Imbibition Outwards from a Hemispherical Depression. *Journal of Petroleum Science and Engineering*, Volume 90-91, pp. 131-138.
- Mason, G. et al., 2010. Oil Production by Spontaneous Imbibition from Sandstone and Chalk Cylindrical Cores with Two Ends Open. *Energy & Fuels*, 24(2), pp. 164-1169.
- Mason, G., Fischer, H., Morrow, N. & Ruth, D., 2008. Spontaneous Counter-Current Imbibition into Core Samples with All Faces Open. *Transport in Porous Media*, 78(2), pp. 199-216.
- Mason, G. & Morrow, N., 2013. Developments in Spontaneous Imbibition and Possibilities for Future Work. *Journal of Petroleum Science and Engineering*, 110(1), pp. 268-293.
- Mayer, E., Berg, R., Carmichael, J. & Weinbrandt, R., 1983. Alkaline Injection for Enhanced Oil Recovery - A Status Report. *Journal of Petroleum Technology*, 35(01), pp.209-221., 35(01), pp. 209-221.
- Meng, Q., Liu, H. & Wang, J., 2017. A Critical Review on Fundamental Mechanisms of Spontaneous Imbibition and the Impact of Boundary Condition, Fluid Viscosity and Wettability. *Advances in Geo-Energy Research*, 1(1), pp. 1-17.
- Meng, Q., Liu, H., Wang, J. & Pang, Z., 2016. Asymmetry Characteristics of Oil Production by Spontaneous Imbibition from Cores with Two Ends Open. *Transport in Porous Media*, 113(3), pp. 735-751.
- Mishra, S., Bera, A. & Mandal, A., 2014. Effect of Polymer Adsorption on Permeability Reduction in Enhanced Oil Recovery. *Journal of Petroleum Engineering*, 2014(1), pp. 1-9.
- Mohnot, S. & Bae, J., 1989. A-Study of Mineral/Alkali Reactions-Part 2. *SPE Reservoir Engineering*, 4(03), pp. 381-390.
- Mohnot, S., Bae, J. & Foley, W., 1987. A Study of Mineral/Alkali Reactions. *SPE Reservoir Engineering*, 2(04), pp. 653-663.
- Morrow, N. & Mason, G., 2001. Recovery of Oil by Spontaneous Imbibition. *Current Opinion in Colloid & Interface Science*, 6(4), pp. 321-337.
- Morrow, N. & McCaffery, F., 1978. *Displacement Studies in Uniformly Wetted Porous Media*. New York: Academic Press.

-
- Needham, R. & Doe, P., 1987. Polymer Flooding Review. *Journal of Petroleum Technology*, 39(12), pp. 1503-1507.
- Pimienta, L., Fortin, J. & Guéguen, Y., 2017. New Method for Measuring Compressibility and Poroelasticity Coefficients in Porous and Permeable Rocks. *Journal of Geophysical Research: Solid Earth*, 122(4), pp. 2670-2689.
- Potts, D. & Kuehne, D., 1998. Strategy for Alkaline/Polymer Flood Design with Berea and Reservoir-Rock Corefloods. *SPE Reservoir Engineering*, 3(04), pp. 1143-1152.
- Rangel-German, E. & Kovscek, A., 2002. Experimental and Analytical Study of Multidimensional Imbibition in Fractured Porous Media. *Journal of Petroleum Science and Engineering*, 36(1-2), pp. 45-60.
- Schechter, D., Zhou, D. & Orr, F., 1991. *Capillary Imbibition and Gravity Segregation in Low IFT Systems*. Dallas, SPE Annual Technical Conference and Exhibition.
- Schumi, B. et al., 2019. Alkali/Cosolvent/Polymer Flooding of High-TAN Oil: Using Phase Experiments, Micromodels, and Corefloods for Injection-Agent Selection. *SPE Reservoir Evaluation & Engineering*, 23(02), pp.463-478., 23(02), pp. 463-478.
- Sheng, D.-C., Yang, P.-H. & Liu, Y.-L., 1993. Alkali-Polymer Interaction and Alkali+Polymer/Crude IFT. *Oilfield Chemistry*, 10(1), pp. 46-50.
- Sheng, D.-C., Yang, P.-H. & Liu, Y.-L., 1994. Effect of Alkali-Polymer Interaction on the Solution Properties. *Petroleum Exploration and Development*, 21(2), pp. 81-85.
- Sheng, J., 2011. *Modern Chemical Enhanced Oil Recovery: Theory and Practice*. s.l.:Elsevier.
- Sheng, J., 2017. Critical Review of Alkaline-Polymer Flooding. *Journal of Petroleum Exploration and Production Technology*, 7(1), pp. 147-153.
- Sheng, J., 2019. Spontaneous Imbibition. In: *Enhanced Oil Recovery in Shale and Tight Reservoirs*. s.l.:Gulf Professional Publishing, pp. 259-307.
- Shen, M. D. & Chen, Z., 1996. Chemical Behavior of Minerals in Alkaline Solutions. In: S. Liu & Z. Lu, eds. *Advance in Petroleum Geology*. Sichuan: Sichuan Science and Technology Press, p. 144–148..
- Sorbie, K., 2013. *Polymer-Improved Oil Recovery*. Edinburgh: Springer Science & Business Media.
- Subkow, P., 1942. *Process For The Removal Of Bitumen From Bituminous Deposits*. US, Patent No. 2,288,857.

Sulaimon, A. & Adeyemi, B., 2018. Effects of Interfacial Tension Alteration on the Destabilization of Water-Oil Emulsions. *Science and Technology Behind Nanoemulsions*, pp. 83-109.

Tavassoli, Z., Zimmerman, R. & Blunt, M., 2005. Analysis of Counter-Current Imbibition with Gravity in Weakly Water-Wet Systems. *Journal of Petroleum Science and Engineering*, 48(1), pp. 94-104.

Thomas, N., Ghosh, B., AlAmeri, W. & Kilybay, A., 2016. Alkali and Hybrid-Alkali Flooding as a Tertiary Oil Recovery Mode: Prospects and Challenges. *International Journal of Petroleum and Petrochemical Engineering*, 2(02), pp. 22-31.

tNavigator 19.4, 2020. *Simulation User Manual*. Rock Flow Dynamics: s.n.

Unsal, E., Mason, G., Morrow, N. & Ruth, D., 2009. Bubble Snap-Off and Capillary-Back Pressure during Counter-Current Spontaneous Imbibition into Model Pores. *Langmuir*, 25(6), pp. 3387-3395.

Willhite, G. P. & Dominguez, J. G., 1977. Mechanisms of Polymer Retention in Porous Media. In: D. O. Shah & R. S. Sheeler, eds. *Improved Oil Recovery by Surfactant and Polymer Flooding*. New York.: Academic Press Inc., pp. 511-554.

Zaitoun, A. & Kohler, N., 1987. *The Role of Adsorption in Polymer Propagation through Reservoir Rocks*. San Antonio, Texas, USA, SPE International symposium on oilfield chemistry.

Zhang, K. & Qin, J., 2011. The Effect of Alkali and Surfactant on Polymer Molecular Structure. *Petroleum Science and Technology*, 29(2), pp. 183-191.

Appendix A

Polymer Adsorption Tables

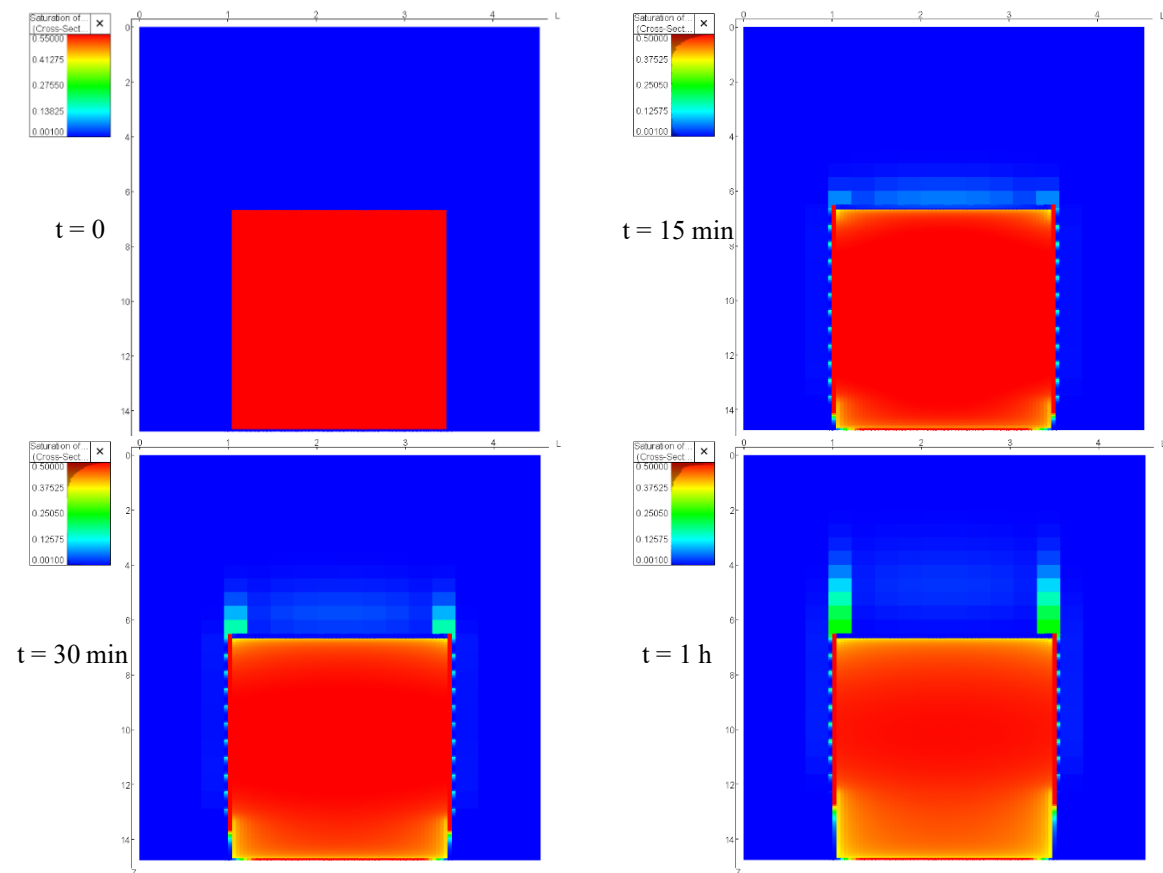
Tab. 1 – Tables of the Polymer Adsorption used in the History Match.

PLYADS_1 a=0.015, b=2		PLYADS_2 a=0.016, b=0.4	
Polymer Concentration, ppm	Adsorption, µg/g	Polymer Concentration, ppm	Adsorption, µg/g
0	0.00	0	0.00
200	3.00	200	3.20
400	6.00	400	6.40
600	8.99	600	9.60
800	11.98	800	12.80
1000	14.97	1000	15.99
1200	17.96	1200	19.19
1400	20.94	1400	22.39
1600	23.92	1600	25.58
1800	26.90	1800	28.78
2000	29.88	2000	31.97
PLYADS_3 a=0.012, b=0.8		PLYADS_4 a=0.013, b=5	
Polymer Concentration, ppm	Adsorption, µg/g	Polymer Concentration, ppm	Adsorption, µg/g
0	0.00	0	0.00
200	2.40	200	2.60
400	4.80	400	5.19
600	7.20	600	7.78
800	9.59	800	10.36
1000	11.99	1000	12.94
1200	14.39	1200	15.51
1400	16.78	1400	18.07
1600	19.18	1600	20.63
1800	21.57	1800	23.19
2000	23.96	2000	25.74

PLYADS_5 a=0.014, b=3.5		PLYADS_6 a=0.015, b=10	
Polymer Concentration, ppm	Adsorption, µg/g	Polymer Concentration, ppm	Adsorption, µg/g
0	0.00	0	0.00
200	2.80	200	2.99
400	5.59	400	5.98
600	8.38	600	8.95
800	11.17	800	11.90
1000	13.95	1000	14.85
1200	16.73	1200	17.79
1400	19.50	1400	20.71
1600	22.28	1600	23.62
1800	25.04	1800	26.52
2000	27.81	2000	29.41
PLYADS_7 a=0.017, b=3.5		PLYADS_8 a=0.018, b=3	
Polymer Concentration, ppm	Adsorption, µg/g	Polymer Concentration, ppm	Adsorption, µg/g
0	0.00	0	0.00
200	3.40	200	3.60
400	6.79	400	7.19
600	10.18	600	10.78
800	13.56	800	14.37
1000	16.94	1000	17.95
1200	20.31	1200	21.52
1400	23.68	1400	25.09
1600	27.05	1600	28.66
1800	30.41	1800	32.23
2000	33.76	2000	35.79
PLYADS_9 a=0.019, b=9		PLYADS_10 a=0.01, b=5	
Polymer Concentration, ppm	Adsorption, µg/g	Polymer Concentration, ppm	Adsorption, µg/g
0	0.00	0	0.00
200	3.79	200	2.00
400	7.57	400	3.99
600	11.34	600	5.98
800	15.09	800	7.97
1000	18.83	1000	9.95
1200	22.56	1200	11.93
1400	26.27	1400	13.90
1600	29.97	1600	15.87
1800	33.65	1800	17.84
2000	37.33	2000	19.80

Appendix B

Cross-Sections of the Test-Water Model



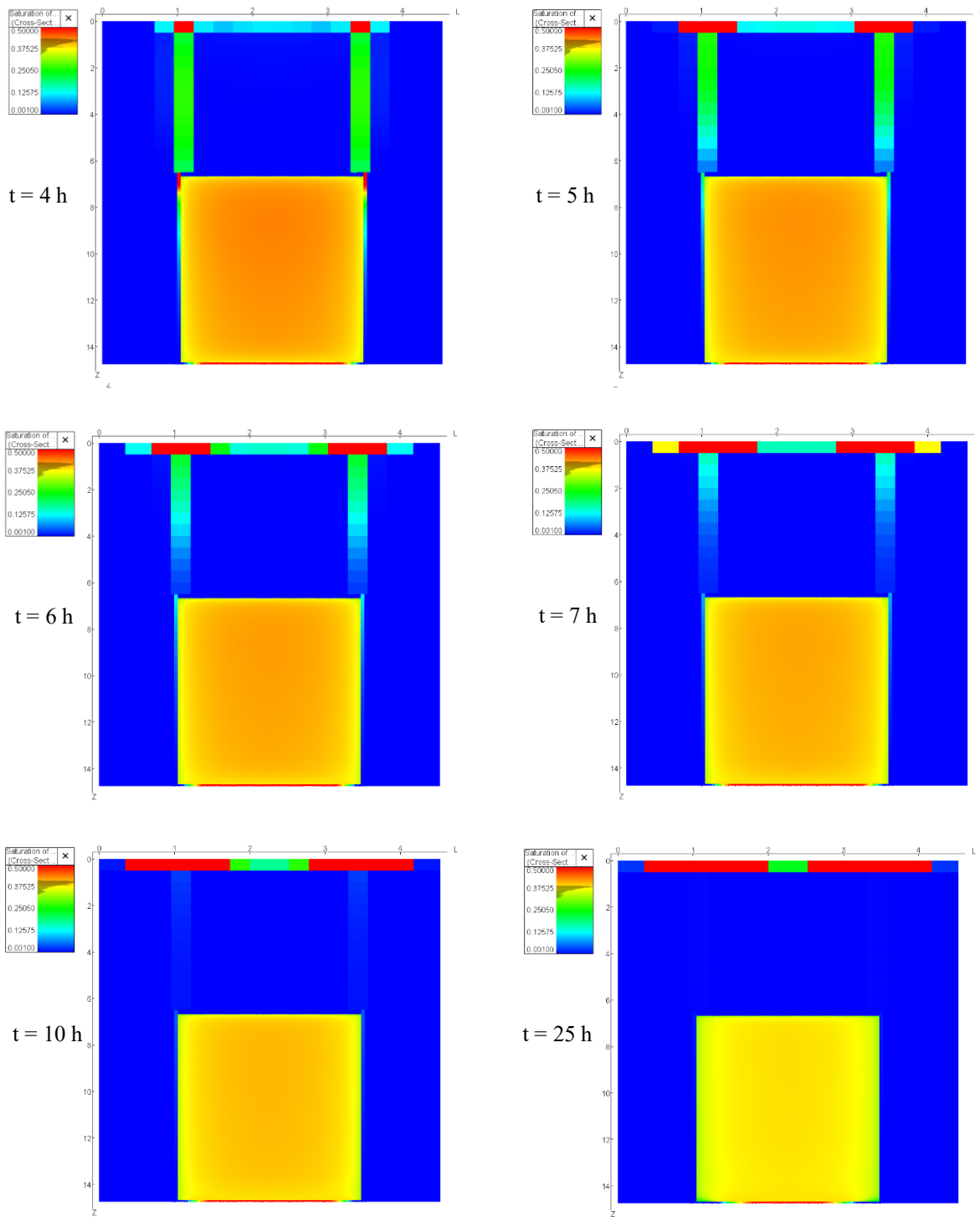
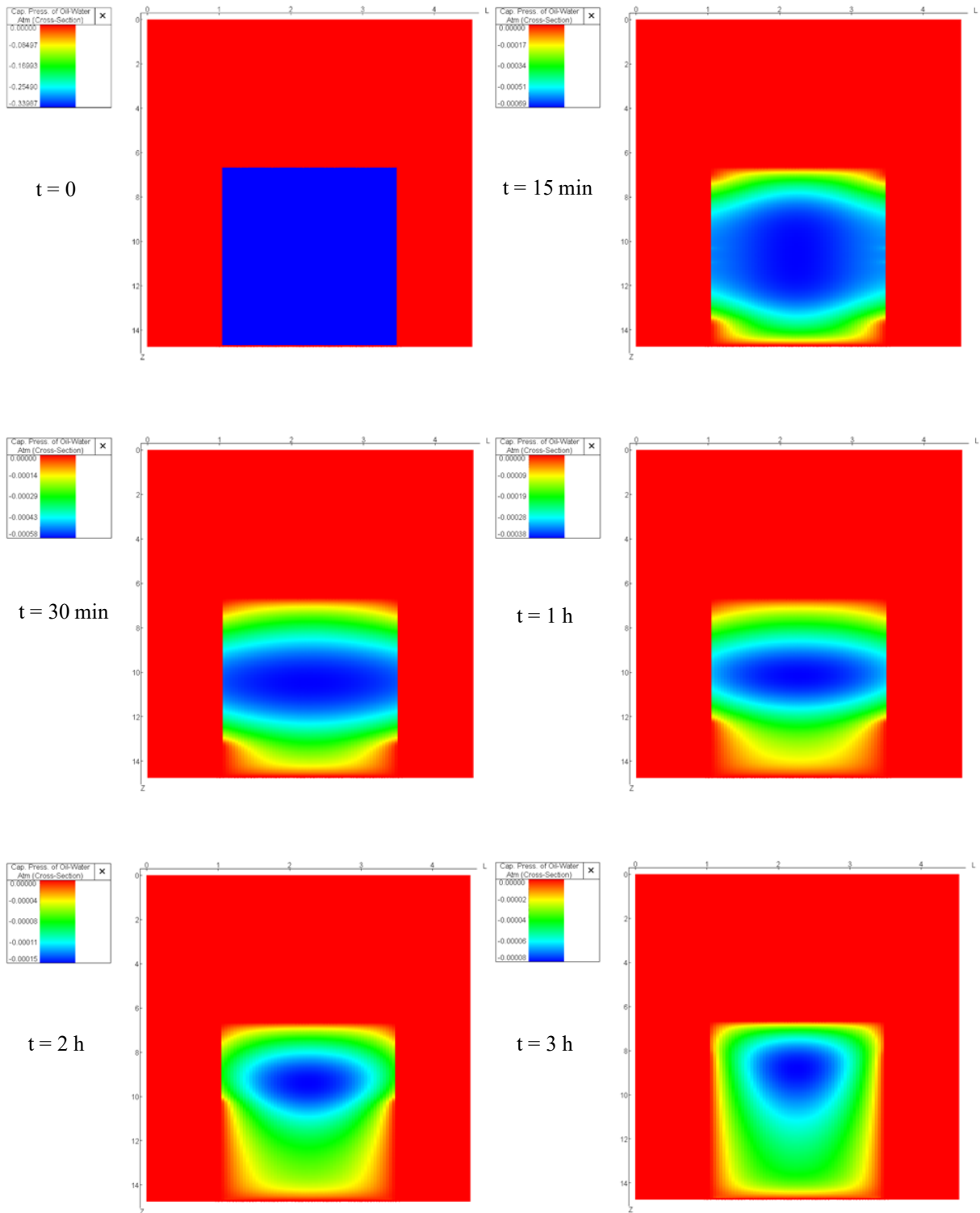


Fig. 1 – Oil Saturation Profile as a Function of Time for the Central X Cross-Section for the History-Matched Test Water Simulation Model. Picture Scale 2:3.



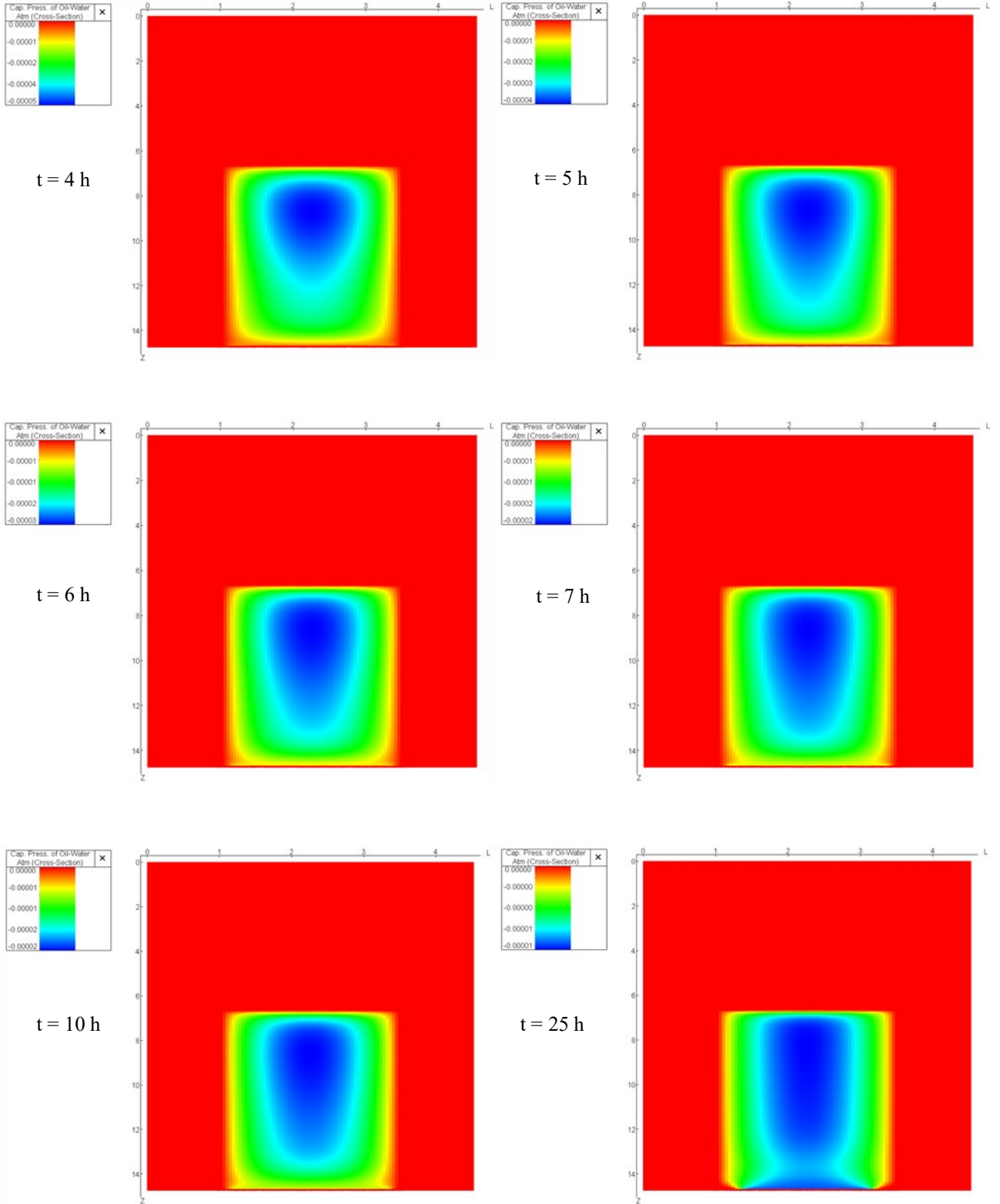
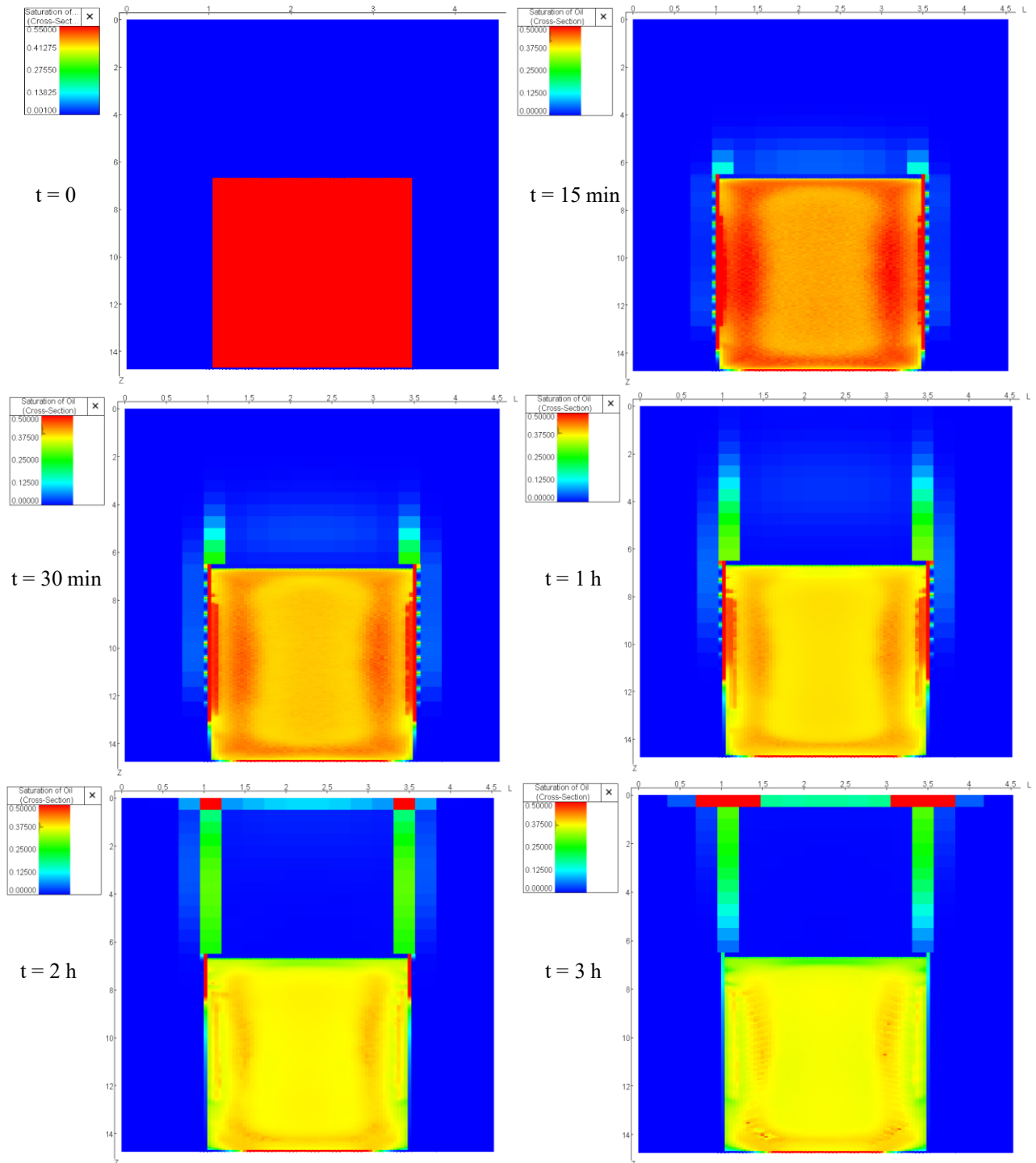


Fig. 2 – Capillary Pressure Distribution as the Function of Time for the Central X Cross-Section for the History-Matched Test-Water Simulation Model. Picture Scale 2:3.

Appendix C

Cross-Sections of the Alkali Model



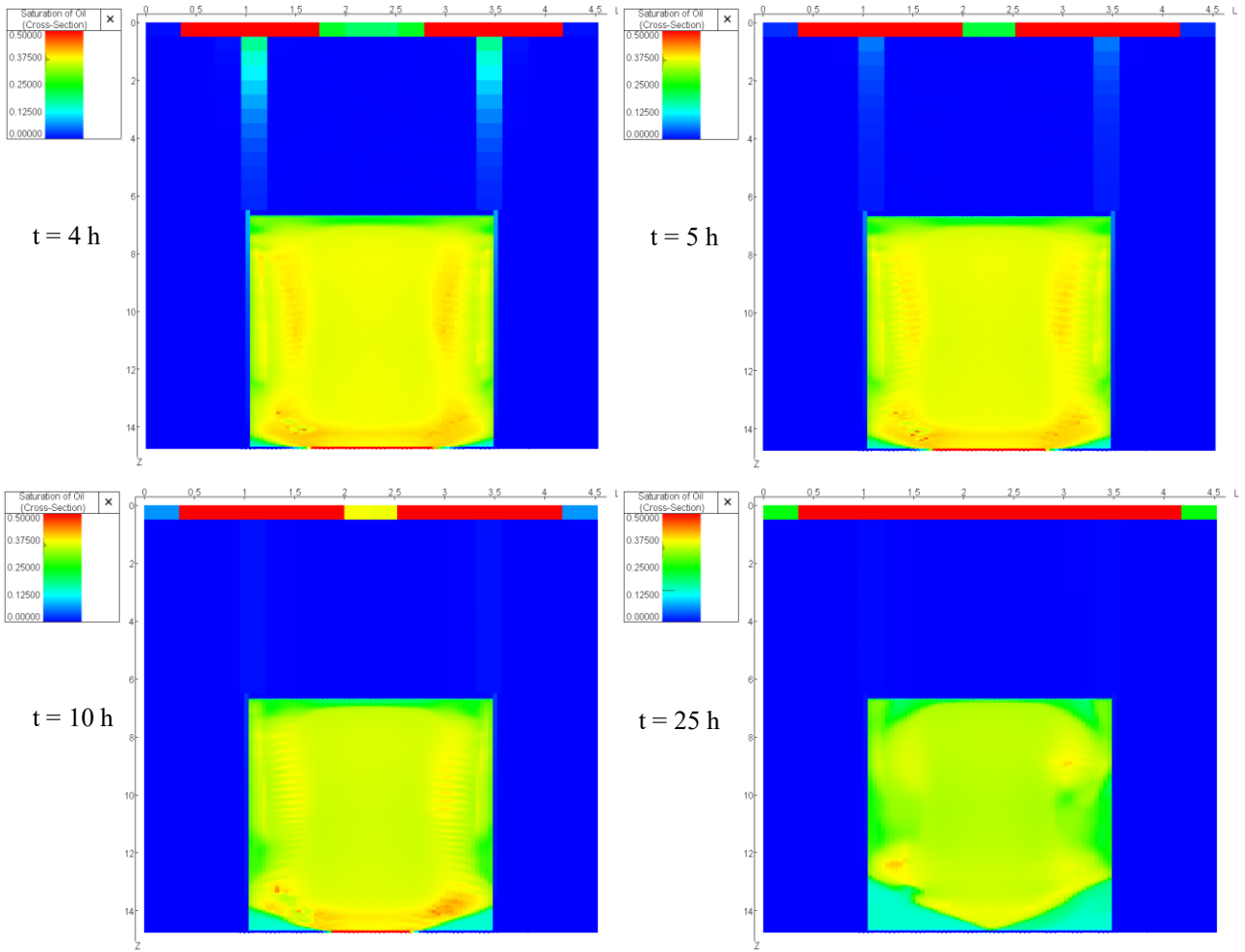
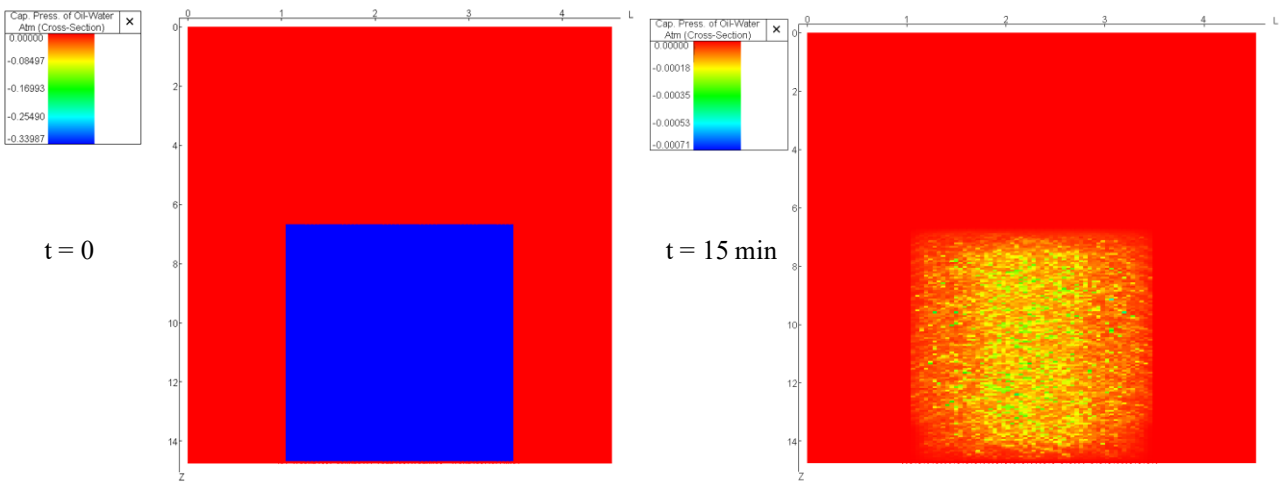


Fig. 3 – Oil Saturation Profile as the Function of Time for the Central X Cross-Section for the History-Matched Alkali Simulation Model. Picture Scale 2:3.



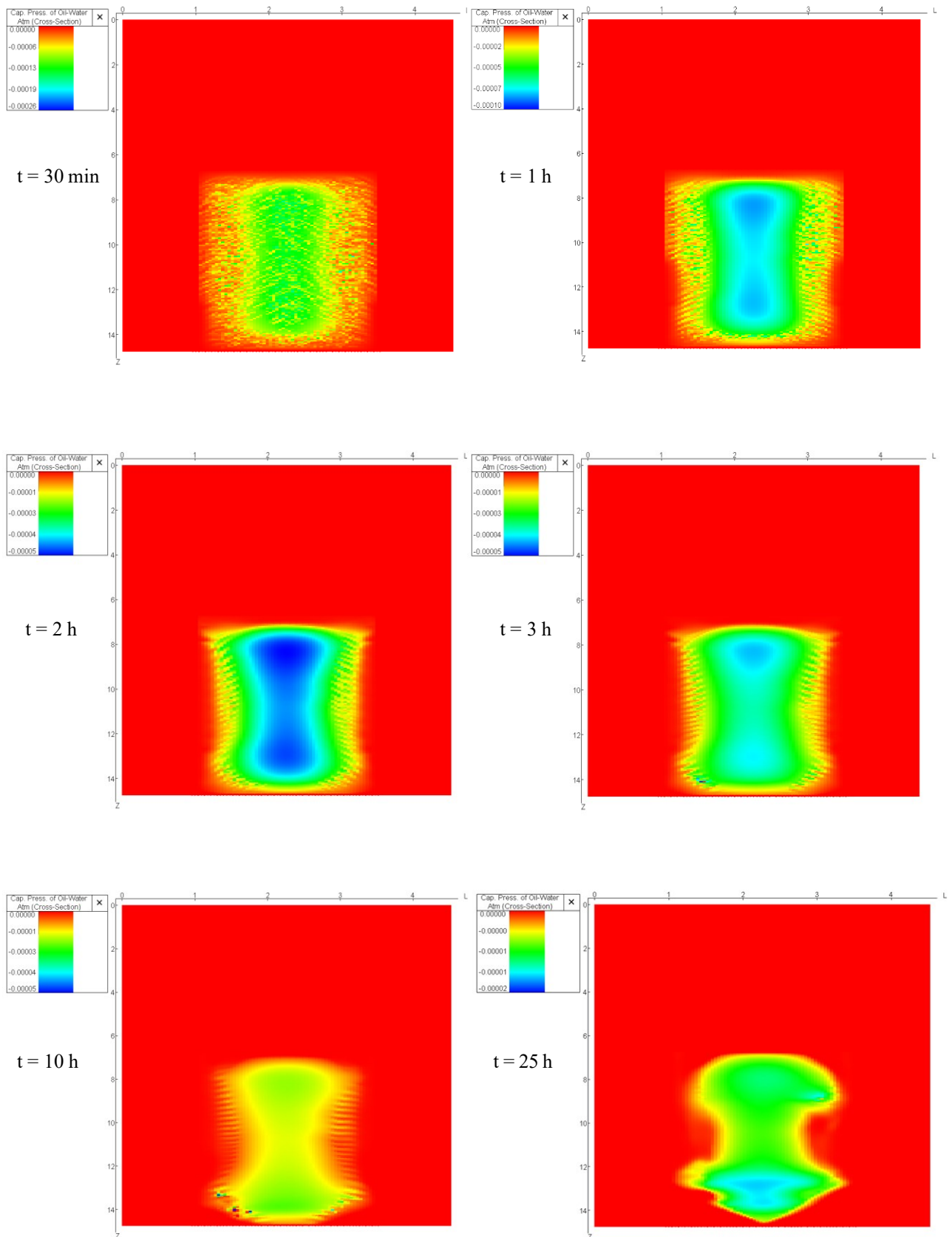


Fig. 4 – Capillary Pressure Distribution as the Function of Time for the Central X Cross-Section for the History-Matched Alkali Simulation Model. Picture Scale 2:3.

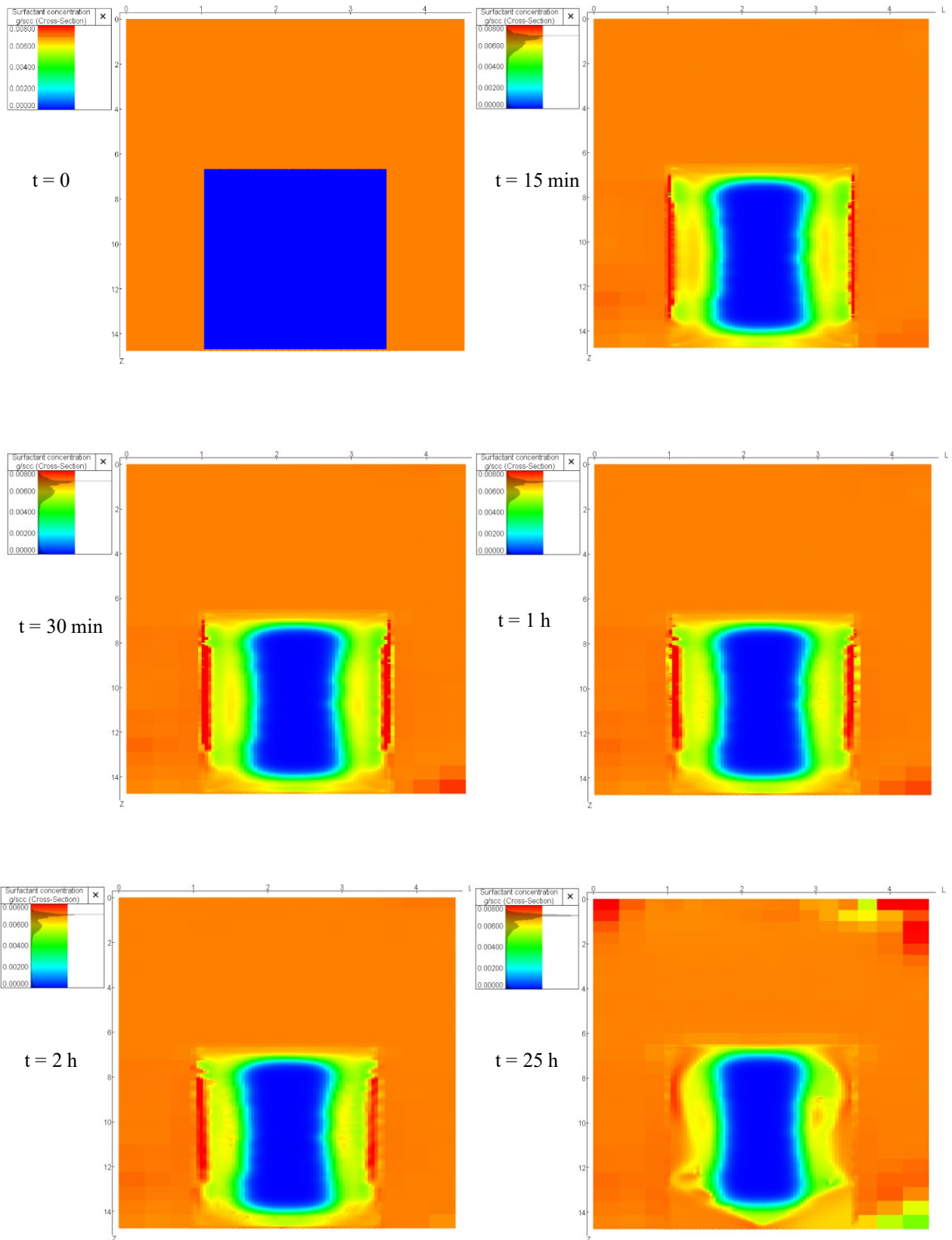


Fig. 5 – Surfactant Concentration Distribution as the Function of Time for the Central X Cross-Section for the History-Matched Alkali Simulation Model. Picture Scale 2:3